ABSTRACT

CHITRPHIROMSRI, PATIROP. Modeling of Thermal Performance of Firefighter Protective Clothing during the Intense Heat Exposure. (Under the direction of Dr. Andrey V. Kuznetsov.)

The purpose of this research is to investigate numerically the heat and moisture transport in the firefighter protective clothing under the flash fire exposure. Numerical results help in understanding the basic mechanisms of the transient heat and moisture transport through the protective clothing, air gap, and human skin in the intense thermal environments; and the effects of the moisture content on the thermo-physical properties of protective garments during the radiation heat exposure as well as during the cool-down period. Prediction of thermal performance of garment aids in designing and creating a new firefighter protective turnout gear in order to prevent and minimize tissue burns that result from the radiant energy produced by the fire as well as from the localized contact flame exposure.

During fire extinguishing, firefighters often sweat profusely, which leads to accumulation of moisture in the turnout gear. In addition, firefighters may also be exposed to the dousing water from a hose spray. Evaporation, condensation, desorption, and absorption of the moisture and energy associated with phase change can affect the temperature and energy flux to the skin. Normally, wet garments can absorb more heat than dry garments.

Traditional thermal protective garments rely passively on thermal properties of fabric and the entrapment of insulating air layers to resist heat flux from flash fire exposures. To improve the level of heat flux resistance of thermal protective garments, this research evaluates the feasibility of developing a novel garment system based on the utilization of a water-injection, which incorporates knowledge and technologies that actively raise thermal resistance in the

presence of intensive heat exposure. During the flash fire exposure, this intelligent garment will absorb a significant amount of the incident heat flux due to evaporation of injected water, thus limiting the temperature increase and the total heat flux to the firefighter's skin. For the intelligent garment investigated in this research, the liquid water will be injected in the outer layer of the garment through a capillary net composed of thin perforated tubes; the injection process will be activated by a temperature sensor embedded in the outer fabric layer. Therefore, the new turnout system augments this outer layer, by providing an active thermal barrier and acting as a thermal buffer against the high heat flux associated with the flash fire exposure while the remaining inner layers continue to efficiently provide the conventional protection based on the traditional insulation due to their small thermal conductivity.

MODELING OF THERMAL PERFORMANCE OF FIREFIGHTER PROTECTIVE CLOTHING DURING THE INTENSE HEAT EXPOSURE

by

PATIROP CHITRPHIROMSRI

A dissertation submitted to the Graduate Faculty of
North Carolina State University
in partial fulfillment of the
requirements for the Degree of
Doctor of Philosophy

MECHANICAL ENGINEERING

Raleigh
2004

APPROVED BY:

ANDREY V. KUZNETSOV
Chair of Advisory Committee

ROGER L. BARKER

WILLIAM L. ROBERTS

KEVIN M. LYONS

ZHILIN LI

To my parents, sisters, and girlfriend

BIOGRAPHY

Patirop Chitrphiromsri was born in Bangkok, Thailand in 1972. He graduated from Taweethapisek High School, Bangkok in 1990 and received a Bachelor of Engineering degree from Kasetsart University, Thailand in 1995, majoring in Electrical and Mechanical Engineering. After graduation, he went to Northern Illinois University in DeKalb, Illinois, where he worked part time as a teaching assistant towards his coursework from 1996 to 1998 and obtained his Master of Science degree in Mechanical Engineering in 2001. From 1998 to 2001, he was employed by Butler Technical Group as a design engineer for Caterpillar Inc., Aurora, Illinois. In August 2001, he enrolled as a graduate student in the Department of Mechanical and Aerospace Engineering at North Carolina State University in Raleigh, North Carolina then he began his study and got the support by the National Textile Center towards a Doctor of Philosophy degree in Mechanical Engineering.

ACKNOWLEDGEMENTS

I would like to express my sincere gratitude to Dr. Andrey V. Kuznetsov, Chair of my Advisory Committee, for his advice, guidance, and invaluable support throughout my study. He was deeply engaged with me from the formative stage, through the refining of this work to the final writing. His enthusiasm in research kept inspiring me to work harder. In addition, his great patient and deep understanding both technically and personally make me feel grateful and truly respectful to him.

I am indebted to Dr. Roger L. Barker for giving me the opportunity to work on this research. Without his instruction and help, this work would never be completed.

Appreciation is also extended to the other advisory committee members, Dr. William L. Roberts, Dr. Kevin M. Lyons, and Dr. Zhilin Li. Their time, patience, and help are greatly appreciated.

I am appreciative to Dr. Guowen Song, a research associate, for valuable help and comment on my numerical and theoretical model. His helpful discussions and advice on the experiment are also greatly appreciated. Special thanks also go to my officemates, friends, and the Friday group for their concern, support, and encouragement.

This work was sponsored in part by the National Textile Center, University Research Consortium, project F01-NS50.

Finally, deep gratitude is given to my family, especially my dad, mom, sisters, and girlfriend, for their precious love, constant support, and encouragement throughout the years. Without their help, none of this would be possible at all.

TABLE OF CONTENTS

LIST OF TABLES

LIST OF FIGURES

1. INTRODUCTION

1.1. BACKGROUND

Prediction of protective garment performance in preventing or minimizing tissue burns requires the ability to understand and model heat transfer from the incident radiant and/or convective heat sources to and through the protective clothing, through interfacial air gap, and, finally, through the skin. This project takes into account multiple modes of heat and mass transfer as well as some temperature dependent changes, which occur as the exposure progresses. There has been a considerable amount of research (ref. as [1], [2], [3], [4], [5], [6], [7]) conducted on the modeling of heat transfer through fabric layers in contact with human skin to predict burn injuries. However, intense heat exposure induces fundamental changes in fabric thermal properties that produce nonlinear thermal transfer characteristics. Consequently, heat transfer models cannot be used to predict protective clothing performance without significant enhancement to include the complex dynamics of the fabric properties altering.

Experiments were conducted to measure the effects of intense heat exposure on the performance of protective garments. These experimental data provided essential input to improve heat and moisture transfer models developed in this research. Other experiments used the Pyroman® instrumented fire manikin to understand and quantify the nature of flash fire events. Parameter estimation methods were used to characterize the flame temperature and convective heat transfer coefficient of the hot gases around the manikin. Manufacturers of fire protective clothing and materials were providing test items for the development and

validation of thermal protective models. This included manufactures of moisture barriers, thermal insulation materials, and outer shells for the multi-layer garments.

A model that predicts the thermal protective performance of the protective garments in the intense heat exposures was developed to understand the basic mechanisms of the transient heat and moisture transport through the protective clothing, air gap, and human skin in the intense thermal environments and the effects of the moisture content on the thermo-physical properties of protective garments during the radiation heat exposure.

A database of the fabric thermo-physical properties that reflect the changes that occur in a fabric as a result of the intense thermal assaults was established together with experimental determination of the effects of heat source and fabric spectral characteristics in order to enhance the accuracy of model predictions that are sensitive to input parameters used in the model developed in this research. Thus, the results of this research can evaluate thermal protective performance of the garments, guide improvements in material design and aid in the industry development of more effective garments for protecting firefighters when exposed to flash fire.

1.2. INTRODUCTION OF PARTS AND CHAPTERS

This dissertation consists of three parts and six chapters. Each one of Chapters 2 to 5 is mainly a published or submitted paper and is relatively independent of each other. Part One, which includes Chapter 2, investigates modeling the thermal protective performance of heat resistant garments in flash fire exposures. Part Two, which includes Chapter 3 to 4, investigates modeling heat and moisture transport in firefighter protective clothing during flash fire exposure. Since the complex nonlinear dynamic changes in thermal properties of

the garment (which are the density, specific heat and thermal conductivity) occur as the exposure progresses, the effect of moisture content in the fabric on the thermal protective performance is discussed in Part Two. Part Three, which includes Chapter 5, investigates the improvement of the performance of firefighter protective garment systems using evaporation of injected water to create a barrier to the incident heat flux. This innovative garment system will provide active protection by absorbing a significant amount of the incident heat and then limiting the temperature increase in the fabric and the heat flux from the garment to the firefighter's skin.

1.2.1. Modeling the Thermal Protective Performance of Heat Resistant Garments in Flash Fire Exposures

Inspired by the experimental results obtained by Song [7], Song et al. [8] utilizes a heat transfer model to investigate the performance of the thermal protective garment under highly intense heat. Chapter 2 (published as ref. [8]) experimentally and computationally investigates the thermal protective performance of heat resistant garments in flash fire exposures. Torvi's model [6] is incorporated with characteristics of the simulated flash fire generated in the chamber and the heat induced changes in fabric thermo-physical properties. Torvi's model is fairly complete in the way that it treats heat transfer in the skin, the fabric, and the air gap in between the skin and the fabric. Torvi's model relies on the assumption that no mass transfer occurs in the interstitial air inside the fabric. The penetration of thermal radiation through a thin fabric layer is also accounted for. The model is validated by comparing its predictions with an instrumented manikin fire test in terms of the predicted severity of damage to human skin when subjected to high heat fluxes.

1.2.2. Modeling Heat and Moisture Transport in Firefighter Protective Clothing during Flash Fire Exposure

Chapter 3 (published as ref. [9]) is based on the previous work by Gibson [2, 3]. Gibson's model provides a mathematically complete treatment of coupled heat and mass transport through fabric. It treats the textile material as the hygroscopic porous medium saturated with a multi-phase moisture. This chapter is restricted to accounting for the bound water and the water vapor only. The basic mechanisms of the transient heat and moisture transport through the garment, air gap and human skin in the intense thermal environments are investigated. The model predictions are in good agreement with experimental data in terms of both the sensor temperature histories and burn injury predictions.

1.2.3. Porous Medium Model for Investigating Transient Heat and Moisture Transport in Firefighter Protective Clothing under High Intensity Thermal Exposure

Chapter 4 (published as ref. [10]) continues the work reported in Chapter 3 to develop a model based on Le et al. [11] to account for all possible phases of moisture in the fabric during the flash fire exposure. The phase changes among the bound water, free liquid water and water vapor in the fabric play an important role in thermal protective performance of the firefighter garments. By introducing the free liquid water into the fabric, the thermal protective performance of the garment is significantly improved.

1.2.4. Investigation of Feasibility of Developing Intelligent Firefighter Protective Garments Based on the Utilization of a Water-Injection System

Chapter 5 (published as ref. [12]) continues Chapter 4 utilizing the heat and moisture transport model to improve the performance of firefighter protective garment by using a controlled injection of free liquid water to create a barrier to the incident heat flux. A considerable amount of research is conducted on the thermal management of textile fibers and composite materials (Kaska and Chen [13]; Colvin and Mulligan [14]; Colvin and Bryant [15]; Colvin et al. [16]; Pause [17]). In current research, the outer layer of the garment is injected with water through a capillary net of thin perforated tubes; the injection process can be activated by a temperature sensor embedded in the outer layer of the fabric.

REFERENCES

1 N. Y. Chen, "Transient heat and moisture transfer through thermally irradiated cloth", *Ph.D. Thesis, Massachusetts Institute of Technology*, Cambridge, MA, 1959.

2 P. W. Gibson, "Multiphase heat and mass transfer through hygroscopic porous media with applications to clothing materials", *Technical Report Natick/TR-97/005*, U.S. Army Natick Research, Development, and Engineering Center, Natick, MA, 1996.

3 P. W. Gibson and M. Charmchi, "Integration of a human thermal physiology control model with a numerical model for coupled heat and mass transfer through hygroscopic porous textiles", *Presented at the 1996 ASME International Mechanical Engineering Congress & Exhibition*, Atlanta, GA, November 17-22, 1996.

4 W. E. Mell and J. R. Lawson, "A heat transfer model for fire fighter's protective clothing", *National Institute of Standards and Technology, NISTIR 6299*, January, 1999.

5 H. L. Morse, J. G. Thompson, K. J. Clark, K. A. Green, and C. B. Moyer, "Analysis of the thermal response of protective fabric", *Technical Report, AFML-RT-73-17, Air Force Materials Information Service*, Springfield, VA.

6 D. A. Torvi, "Heat transfer in thin fibrous materials under high heat flux conditions", *Ph.D. Thesis, University of Alberta*, Edmonton, Alberta, Canada, 1997.

7 G. Song, "Modeling thermal protection outfits for fire exposures", *Doctoral Dissertation, North Carolina State University*, Raleigh, NC, 2002.

8 G. Song, R. L. Barker, H. Hamouda, A. V. Kuznetsov, P. Chitrphiromsri, and R. Grimes, "Modeling the thermal protective performance of heat resistant garments in flash fire exposures", *Textile Res. J.*, accepted for publication, 2004.

9 P. Chitrphiromsri and A. V. Kuznetsov, "Modeling heat and moisture transport in firefighter protective clothing during flash fire exposure", *Heat and Mass Transfer*, accepted for publication, 2004.

10 P. Chitrphiromsri and A. V. Kuznetsov, "A Porous medium model for investigating transient heat and moisture transport in firefighter protective clothing under high intensity thermal exposure", *J. Porous Media*, accepted for publication, 2004.

11 C. V. Le, N. G. Ly, and R. Postle, "Heat and mass transfer in the condensing flow of steam through an absorbing fibrous medium", *Int. J. Heat Mass Transfer*, vol. 38, pp. 81-89, 1995.

12 P. Chitrphiromsri, A. V. Kuznetsov, G. Song, and R. L. Barker, "Investigation of feasibility of developing intelligent firefighter protective garments based on the utilization of a water-injection system", *Numer. Heat Transfer, Part A*, submitted for publication, 2004.

13 K. E. Kaska and M. M. Chen, “Improvement of the performance of solar energy of waste heat utilization systems using phase change slurry as enhanced heat transfer storage fluid”, *J. Solar Energy Eng.*, vol. 107, pp. 229-236, 1985.

14 D. P. Colvin and J. C. Mulligan, “Microencapsulated phase change materials for storage of heat”, *NASA Tech Briefs*, July 1989.

15 D. P. Colvin and Y. G. Bryant, “Protective clothing containing encapsulated phase change materials”, *ASME-IMECE, HTD-Vol. 362, BED-Vol. 40*, pp. 123-132, 1998.

16 D. P. Colvin, L. J. Hayes, Y. G. Bryant, and D.R. Myers, “Thermal analysis of PCM cooling garments”, *ASME HTD-Vol. 268, Advances in Bioheat and Mass Transfer*, 1993.

17 B. H. Pause, “New heat protective garment with phase change material”, *Performance of Protective Clothing: Issues and Priorities for the 21st Century: Seventh Volume, ASTM STP 1386*, 2000.

PART ONE:

HEAT TRANSFER MODEL

2. MODELING THE THERMAL PROTECTIVE PERFORMANCE OF HEAT RESISTANT GARMENTS IN FLASH FIRE EXPOSURES

ABSTRACT

This chapter develops a numerical model to predict skin burn injury resulting from heat transfer through a protective garment worn by an instrumented manikin exposed to laboratory-controlled flash fire exposures. This model incorporates characteristics of the simulated flash fire generated in the chamber and the heat induced changes in fabric thermo-physical properties. The model also accounts for clothing air layers between the garment and the manikin. The model is validated using an instrumented manikin fire test system [1]. Results from the numerical model helped to develop a better understanding of the heat transfer process in protective garments exposed to intense flash fires, and to establish systematic methods for the engineering of materials and garments to produce optimum thermal protective performance.

2.1. INTRODUCTION

A considerable amount of research has been conducted on modeling the heat transfer through fabric layers and predicting the resulting skin burn injury [2, 3, 4, 5, 6, 7]. All these models were developed based on laboratory bench top tests. They do not consider clothing spatial effects, which may be vital in predicting the protective performance of clothing worn on the human body. They also do not consider the effects of the garment design and construction, the role of seams, closures, pockets, and vents to thermal protective performance of clothing

in actual wear. Additionally fundamental changes in fabric thermal, optical, and spatial properties through pyrolysis, char formation, and shrinkage were not included. Intense heat exposures generally produce nonlinear changes in fabric thermal physical properties and fabric optical characteristics [8, 9, 10]. Consequently, a heat transfer model cannot accurately predict clothing protective performance without also accounting for the complex changes in clothing material properties when exposed to these intense high heat exposures.

This research developed a numerical model that is capable of predicting the heat transfer through clothing materials and garments when exposed to intense heat environments. The primary objective was to construct a model to simulate heat transfer through a single layer of a protective garment worn by a manikin exposed to a flash fire condition. This approach uses the fabric thermo-physical properties as a function of fabric temperature, accounts for the air layer distribution between the garment and manikin, and incorporates characteristics of the flash fire generated in the chamber. The integrated generalized model was validated using the Pyroman® Thermal Protective Clothing Analysis System [1]. This model helped to develop an understanding of the heat transfer process in protective garments exposed to intense flash fires, and to establish a systematic method and basis for the engineering of materials and garments to produce optimum thermal protective performance.

2.2. MODELING THE MANIKIN FIRE TESTING SYSTEM

The Pyroman® manikin fire test system utilizes a fully instrumented, life-sized manikin capable of measuring the performance of thermal protective clothing. The system uses a size 40 regular manikin made from a flame resistant polyester resin reinforced with fiberglass. The manikin is suspended from the ceiling of an 11′ × 18′ fire resistant burn chamber and

surrounded by eight industrial burners capable of producing a large volume, simulated, flash fire capable of fully engulfing the manikin in flames. The manikin is instrumented with 122 individual heat flux sensors distributed over the surface of his body. In addition to measuring the heat transfer to the manikin with exposure of the test garment or protective clothing ensemble, these sensors also set the exposure level by directly exposing the manikin to the flames in a test without the garment. The test specimen is placed on the manikin at ambient atmospheric conditions and exposed to the flash fire simulation with controlled heat flux, duration, and flame distribution. The incident heat flux measured by the sensors, during and after the exposure, is used to calculate the changing temperature of human tissue at two skin depths, one representing a second degree burn injury point and the other a third degree burn injury point. A computer system controls data acquisition, calculation of surface heat flux, calculates skin temperature distribution histories, and predicts skin burn damage for each sensor location. The computer produces a full report of the test including a contour mapping of burn locations.

Figure 2-1 shows a schematic of the existed manikin test. The left section of the diagram contains the physical event that transpires in the test chamber. Heat flows from left to right in the diagram. The flash fire combustion front is generated in the chamber and strikes the surface of the garment. Heat is transferred through the garment, through an air gap located between the garment and the manikin surface, and finally to the manikin surface and to the heat flux sensor. Data from the sensor are collected by the computer and translated into a surface heat flux history, skin temperature distribution history, and finally a skin burn damage prediction. Creating a model for the flash fire boundary condition, the heat transfer

through the protective garment, and the heat transfer through the insulating air layer remains to be developed and are the focus of this research.

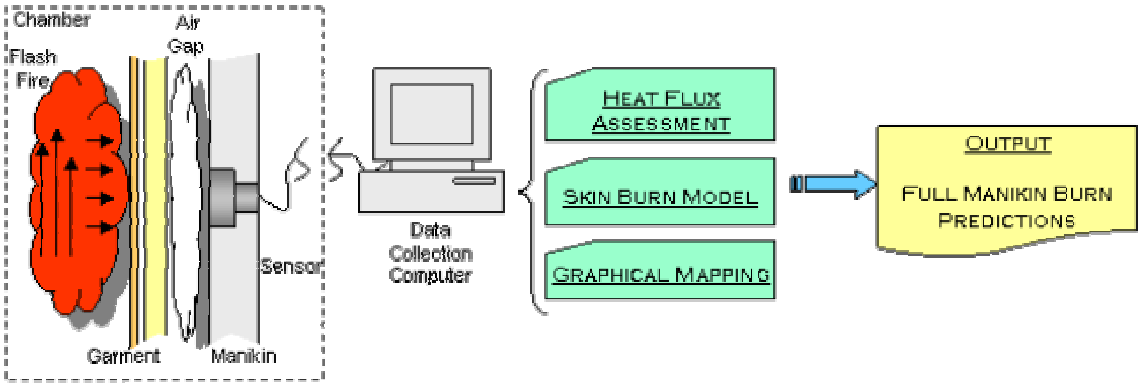

Figure 2-1 Block diagram of instrumented manikin test

To simulate the flash fire test, a numerical model was designed in the following manner: first, the presence of the sensor and the manikin can be discarded since they are measurement instruments of the test and not germane to the ultimate goal of predicting burn damage in human skin. Human skin can be numerically substituted directly for these devices. A time dependant numerical model can be written to calculate the rate of heat conduction in the garment being evaluated, through the variably sized air gap located between the garment and human skin, and in human skin. As in the manikin test system, the software can also calculate the amount of burn damage to human skin and produce a graphical mapping of burn damage. To properly execute the simulation model, information on the thermodynamic character of the simulated flash fire, the variation of the fabric thermo-physical properties under flash fire conditions, and the size, distribution and variation of air gaps between the garment and human skin must be available. To resolve this issue, empirical estimations of

the flash fire boundary condition, fabric thermo-physical properties and the size and distribution of insulating air gaps can be made and used as inputs to the numerical model. A diagram of the entire simulation model is described in Figure 2-2.

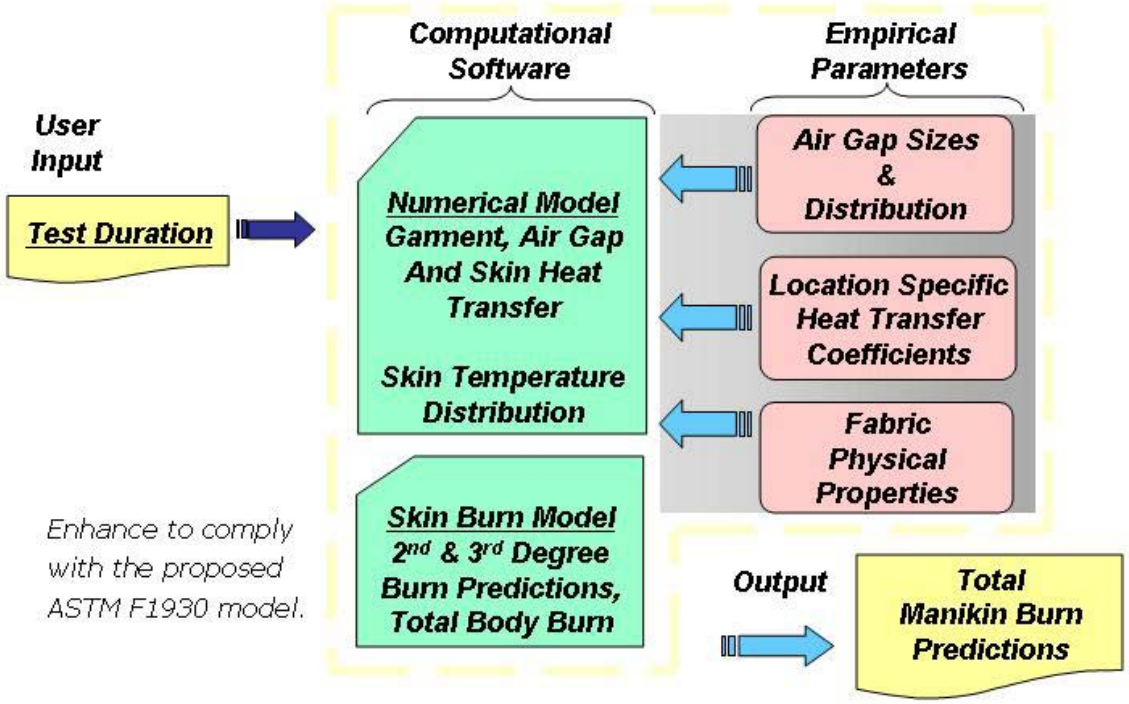

Figure 2-2 Manikin simulation model block diagram

The following sections detail the construction of the computer simulation model and the empirical estimation of the fire boundary condition, fabric dynamic thermo-physical properties, and air gap data.

2.3. *Heat Transfer Model for Fabric, Air Gap, and Human Skin*

To simulate the transfer of heat through the protective garment, the intermediate insulating air gap, and human skin, a one dimensional finite difference model was constructed. The model consisted of three separate sections to accommodate the unique boundary conditions associated with garment, the air gaps, and human skin. The model addresses as many of the variables associated with the manikin test as possible and to provide computational improvements where relevant. A general schematic of the heat transfer model is shown in Figure 2-3.

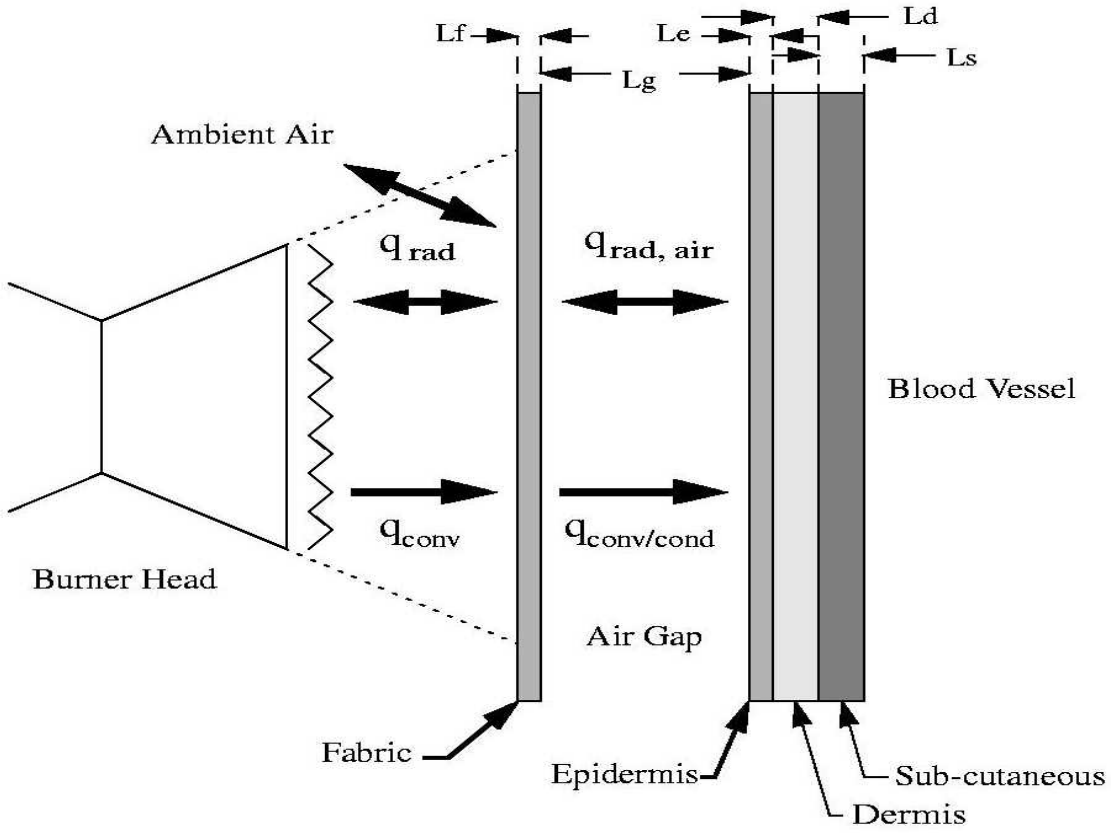

Figure 2-3 Schematic for a one-dimensional heat transfer model

The schematic establishes how energy is transferred to the protective fabric in both the radiative and convective modes. Energy is conducted through the fabric simultaneously by conduction and radiation. At the skin surface, thermal energy is transferred through radiation from the protective garment and conduction/convection from the trapped air. The energy is then conducted through three layers of human skin to an isothermal boundary at the base of the subcutaneous layer.

The differential equation proposed by Torvi [7] as:

$$\rho_f(T)c_{p_f}(T)\frac{\partial T}{\partial t} = \frac{\partial}{\partial x}\left(k_f(T)\frac{\partial T}{\partial x}\right) + \gamma \cdot q''_{rad}\, e^{-\gamma x}, \text{ for } t > 0 \qquad (2.1)$$

where T is fabric temperature and ρ_f, c_{p_f}, and k_f are the temperature dependant density, specific heat, and thermal conductivity of the fabric, respectively. The term $\gamma \cdot q''_{rad} e^{-\gamma x}$ represents internal heat generated by thermal radiation transferred to the internal region of the fabric by the transmissibility of the fabric τ. The extinction coefficient of the fabric γ is evaluated as:

$$\gamma = -\ln(\tau)/L_f \qquad (2.2)$$

where L_f is the thickness of the fabric. The boundary conditions at the external surface of the protective fabric ($x = 0$) are:

$$q''_{rad} = \sigma\varepsilon_g(T_g^4 - T_f^4) - \sigma\varepsilon_f F_{fab-amb}(1-\varepsilon_g)(T_f^4 - T_{amb}^4) \qquad (2.3a)$$

and

$$q''_{conv} = h_s(T_g - T_f), \text{ for } x = 0,\ t > 0 \qquad (2.3b)$$

where σ is the Stefan-Boltzman constant; ε_g and ε_f are the emissivities of the hot gases and the fabric, T_g is the gas temperature, T_f is the fabric surface temperature, h_s is the heat transfer coefficient, T_{amb} is the ambient air temperature, and $F_{fab-amb}$ is a view factor. The radiation boundary condition, however, is nonlinear and complicates the solution process. To simplify this boundary condition, the total amount of energy transferred to the garment, both radiant and convected, was estimated using nude burn test results from the actual manikin system. The resulting boundary condition at the external surface of the garment is reduced to

$$(q''_{conv} + q''_{rad}) = h_{fl}(T_g - T_f), \text{ for } x = 0,\ t > 0 \qquad (2.4)$$

where h_{fl} is the empirically estimated total heat transfer coefficient between the flame and the garment. Heat transfer by conduction/convection through the trapped air located between the internal surface of the fabric and human skin was modeled as a resistance to heat flow between the two surfaces. A value for the heat transfer coefficient between the fabric and skin was modeled as a function of the size of the air gap and the temperature of the trapped air as:

$$h_{gap} = Nu \frac{k_{air}(T)}{L_{airgap}} \qquad (2.5)$$

where Nu is the Nusselt number, $k_{air}(T)$ is the thermal conductivity of the air, and L_{airgap} is the size of the air gap. L_{airgap} is taken from garment air gap measurements described later in the chapter. The boundary at the interface between the fabric and skin can be expressed as:

$$q''_{conv} = h_{gap}(T_f - T_s), \text{ for } x = L_f,\ t > 0 \qquad (2.6)$$

Radiation heat transfer from the fabric to human skin was also considered. The radiation couple is modeled simply, for the one-dimensional case, as radiation exchange between two infinitely tall parallel plates. Taking the emissivities of the fabric and human skin to be the average values of 0.9 and 0.94 respectively [7, 9], the radiation boundary condition between the fabric and skin can be expressed as:

$$q''_{rad} = 0.85\sigma\left(T_f^4 - T_s^4\right), \text{ for } x = L_f,\ t > 0 \qquad (2.7)$$

This research adopted Pennes' approach [11] to model heat conduction in human skin. The model consists of three tissue layers: the epidermis, dermis, and subcutaneous layers, which accounts for cooling blood perfusion in the subcutaneous layer. Therefore,

$$\rho_s c_{p_s} \frac{\partial T}{\partial t} = \nabla \cdot (k_s \nabla T) + (\rho c_p)_b \omega_b (T_a - T), \text{ for } t > 0 \qquad (2.8)$$

In equation (2.8), ρ_s, c_{p_s}, and k_s are the density, specific heat and thermal conductivity of human tissue and ρ_b and c_{p_b} are the density and the specific heat of blood. ω_b is the rate of blood perfusion and is taken to be 0.00125 $m^3/s/m^3$. The boundary condition at the base of the subcutaneous layer is set at a constant basal temperature of 37ºC. As an initial condition, linear distribution of skin temperature is assumed between a surface temperature of 34ºC and the basal temperature of 37ºC.

A finite difference method was used to solve the differential equations [12, 13] at each of the sensor locations on the manikin surface. Due to the nonlinear radiation terms, the Gauss-Seidel point-by-point iterative scheme was employed to solve these equations. To avoid divergence associated with iterative methods, an underrelaxation process was utilized. The Crank-Nicholson implicit scheme was used to solve the resulting ordinary differential equations. With the model for the manikin fire test formulated, values must be determined for

the fabric's temperature dependant thermo-physical properties, the total heat transfer coefficients between the simulated flash fire and the garment, and the size and distribution of air gaps for the protective garment.

2.4. EXPERIMENTAL

2.4.1. CHARACTERIZING THE LAB FIRE ENVIRONMENT

The flash fire simulation is produced by eight propane burning industrial torches. If complete combustion of the propane fuel occurs, adiabatic flame temperatures between 1997ºC and 2127ºC are to be expected, although actual flame temperatures are lower due to environmental heat losses and incomplete combustion of the propane gas [14, 15]. The flame temperatures measured around the manikin body ranged from 800ºC to 1400ºC during a 4-second simulated flash fire exposure with controlled average heat flux of 2.0 cal/cm^2·sec. The overall heat flux (2.0 cal/cm^2·sec) is the average of 122 heat sensor measurements over the surface of manikin body. As illustrated in Figure 2-4, the intensity of the incident thermal energy was found to be normally distributed over the surface of the manikin. Sensors located at different positions on the manikin body measure different heat flux values depending on the location on the manikin body (e.g. arm, leg, shoulder). Variations in heat flux over the manikin surface can be attributed to the three-dimensional shape of the manikin body and to the dynamic nature of the flame column surrounding the manikin.

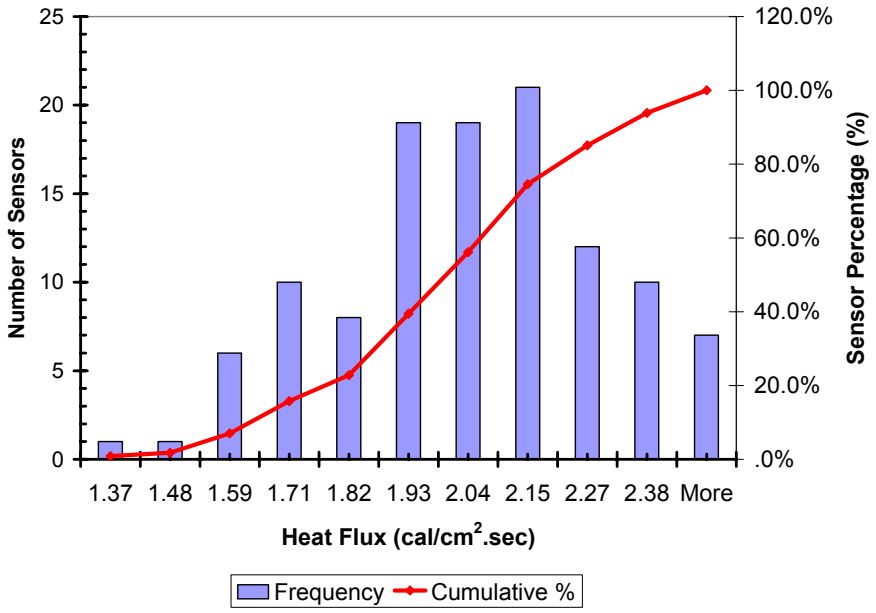

Figure 2-4 Histogram and cumulative curve of heat fluxes measured by 122 sensors in Pyroman® manikin for a 4-second exposure

To estimate heat transfer from the fire to the manikin, it is necessary to determine heat transfer coefficients at each of the 122 thermal sensor locations. To estimate the heat transfer coefficient between the flames of the simulated flash fire and the clothed manikin, a series of experiments were conducted using the manikin test system. These experiments were conducted on a nude manikin to facilitate instrumentation. For these experiments, a special sensor was constructed that simultaneously measured surface temperature, surface heat flux, and gas temperature at a location 1 cm above the surface of the manikin body. The sensor was placed in each of the 122 manikin sensor locations and exposed to a nominal 2.0 cal/cm^2·sec (84 kW/m^2) simulated flash fire. Using this experimental data for total heat flux, the surface temperature of the manikin, and gas temperature, the following relationship [16] can be used to estimate the total heat transfer coefficient at each thermal sensor location:

$$\hat{h}_M = \frac{\hat{q}_M}{T_{fl}(t_M) - 0.5(\hat{T}_{OM} - \hat{T}_{OM-1})} \tag{2.9}$$

where $\hat{h}_M$ is estimated heat transfer coefficient, $\hat{q}_M$ is calculated heat flux, T_{fl} is flame temperature, and $\hat{T}_{OM}$ is estimated surface temperature at time t_M. An example of typical results, for a specific sensor location, is shown in Figure 2-5. These experiments confirm that the flash fire generated by the torches produces a highly dynamic fire environment. Measured heat transfer coefficients ranged from 80-140 W/m^2 $^\circ$C for a 4-second fire exposure. Our studies show that the value of the heat transfer coefficients depends on the flame temperature and the specific location of the sensor on the manikin body [17]. Locations at the manikin that encounter higher flame temperatures produce higher heat transfer coefficients. Heat transfer coefficients measured in the chest, back, and middle leg areas are higher compared to sensors located in the shoulder, thigh, and upper arms of the manikin body.

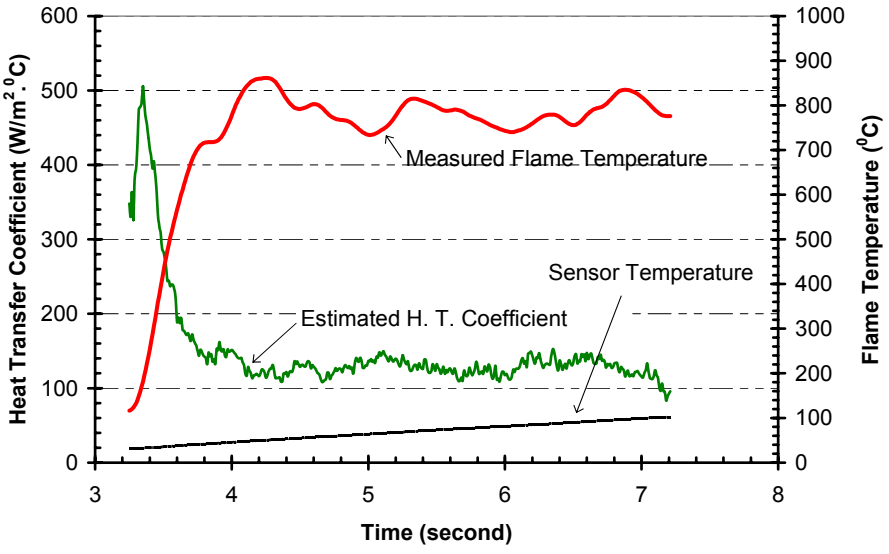

Figure 2-5 Estimated heat transfer coefficient using measured flame temperature and Pyrocal sensor

2.4.2. *Estimation of Heat-Induced Change in Fabric Thermo-Physical Properties*

Fabric thermal conductivity and volumetric heat capacity change considerably during exposing to intense heat. This is an under-determined problem. An experimental parameter estimation method proposed by Beck and Arnold [18] was employed to determine the variation in these properties with temperature in the fabrics of interest for the simulated flash fire used in the manikin test. An experiment was devised wherein a skin simulant sensor was used to measure the heat flux transferred through a fabric sample when exposed to the flash fire. A separate thermocouple simultaneously measured fabric surface temperature during the exposure. Heat flux and temperature history data were then submitted to a licensed software program [19] from Beck where instantaneous values for the fabric's thermal conductivity and volumetric heat capacity were calculated to minimize the sum of the least squares error as:

$$S = \sum_{j=1}^{J_t} \sum_{i=1}^{n} (Y_{ji} - T(\beta)_{ji})^2 \qquad (2.10)$$

where $T(\beta)_{ji}$ is a function of the estimated thermal parameters, the thermal conductivity, and volumetric heat capacity. The vector β contains the "true" parameter values, and the estimated values of the parameters are estimated by minimizing S through the use of a modified Gauss linearization method [18], which introduces larger error and less stable than single-value decomposition technique (Mandrel [20]; Lawson and Hanson [21]), but the Guess method is reasonably and sufficiently accurate. J_t is the number of the thermocouples, Y_{ji} represents the measured temperature at location i. Estimates for the thermal conductivity and volumetric heat capacity for a 254 g/m^2 Kevlar®/PBI fabric under flash fire conditions is shown in Figure 2-6. These results illustrate both fabric thermal conductivity and volumetric heat capacity decrease during the exposure. Since the differences in thermal conductivity and

volumetric heat capacity of Nomex® IIIA and Kevlar®/PBI is very small, estimates for thermo-physical properties of Kevlar®/PBI were used for both materials [7].

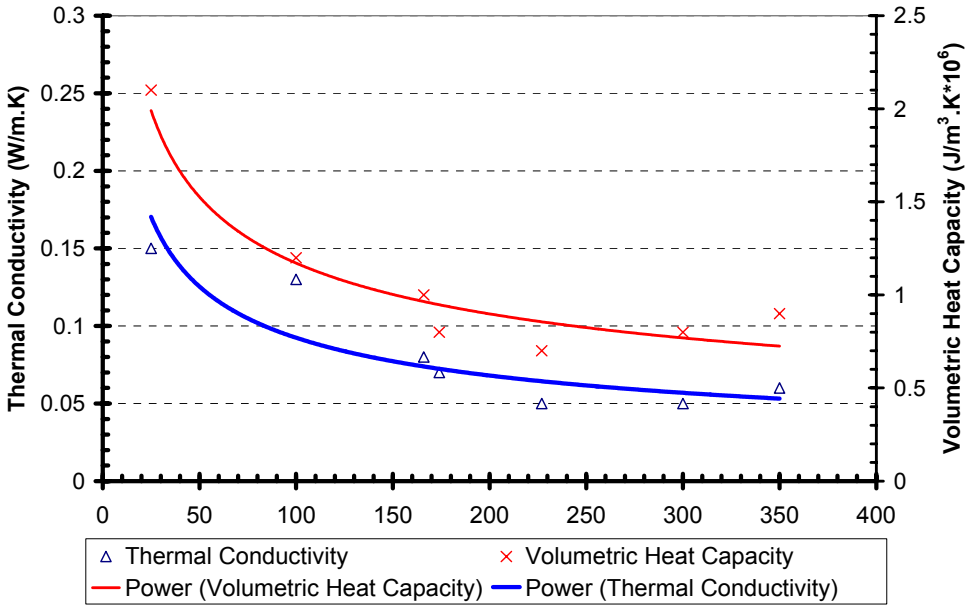

Figure 2-6 Estimated transient thermal properties of Kevlar®/PBI under flash fire conditions

2.4.3. Determination of Garment Air Gap Size and Distribution

Three-dimensional body scanning technology was used to measure air gap sizes and distribution between the manikin body and different sized protective garments for both pre and post exposure conditions. The process used data taken from a dressed manikin superimposed on data taken from a nude manikin. Figure 2-7 presents quantitative results for the various sizes of Kevlar®/PBI protective coveralls measured prior to exposure. The data show that air layers are not similarly sized or evenly distributed over the manikin body. Examining garments, which have been exposed to the simulated flash fire shows, thermally induced fabric shrinkage plays a significant role in determining air gap dimensions. Nomex® IIIA coveralls (size 42, 'deluxe' style, 203 g/m^2) shrink significantly when subjected to a 4-

second, 2.0 cal/cm^{2}sec exposure, thereby reducing the insulating air layer by 50% on average, and as much as 90% in areas around the legs of the manikin as shown in Figure 2-8.

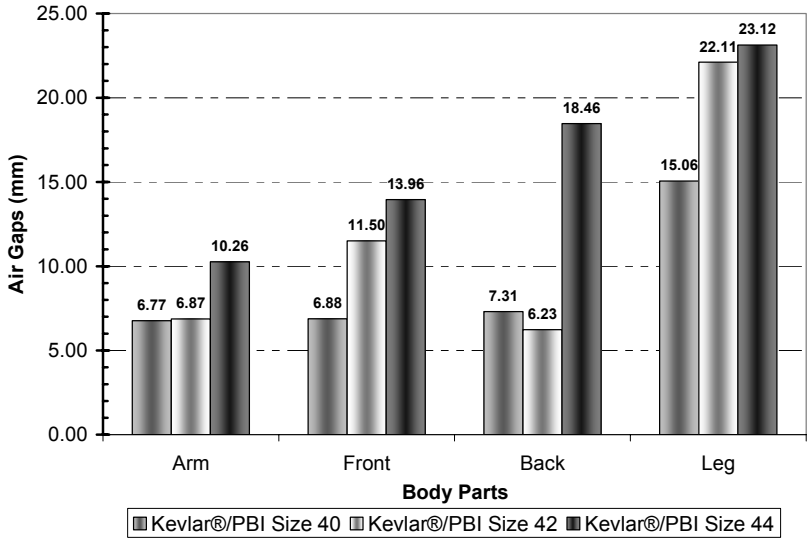

Figure 2-7 Different sized garments and their average air gap distribution in Pyroman® body

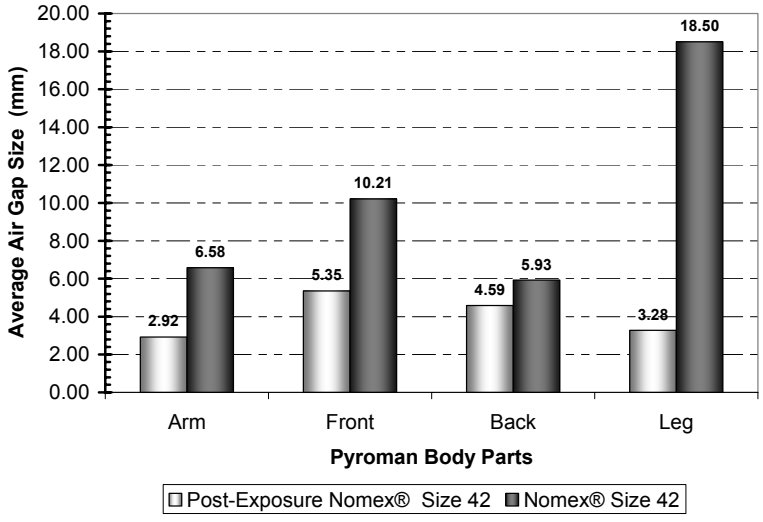

Figure 2-8 Comparisons of air gaps for Nomex® IIIA (203 g/m^2) coverall before and after a 4-second exposure

2.5. *MODEL PREDICTIONS AND COMPARISON WITH MANIKIN TESTS*

Two protective garments were selected to demonstrate the model developed by this research: a Kevlar®/PBI coverall and a Nomex® IIIA coverall. These coveralls are typical industrial thermal protective coveralls having standard pocketing in a "Deluxe" style. All garments used in this research were laundered 5 times using an industrial laundering procedure before manikin testing. This laundering procedure is similar to ASTM 1449-92, but for this research both temperature and detergents were modified to AATCC 135 requirements. The major parameters used in the numerical model are summarized in Table 2-1. Test garments were conditioned at 21 ± 3°C, 65 ± 5% relative humidity prior to testing. The garment fabric thickness was measured on a KES compression test. The thermal conductivity and volumetric heat capacity of these two protective fabrics were estimated using the parameter estimation method [17]. Based upon data in the literature [15, 19], an emissivity of 0.9 and a transmissivity of 0.01 were chosen for each of the two fabrics.

Table 2-1 Parameters used in numerical model

	Kevlar®/PBI Coverall	Nomex® IIIA coverall
Fire Boundary condition	2.0 cal/cm^2·sec (83.72 kW/m^2)	2.0 cal/cm^2·sec (83.72 kW/m^2)
Heat Flux Standard Deviation	0.28	0.28
Fabric Weight	153 g/m^2	203 g/m^2
Garment Air Gap Sizes	Size 42 [17]	Size 42 [17]
Garment Size	42	42
Burning Time	3 and 4 (seconds)	3 and 4 (seconds)

Tests were performed according to the ASTM 1930, Standard test method for evaluation of flame resistant clothing for protection against flash fire simulations using an instrumented manikin. These manikin tests for Kevlar®/PBI and Nomex® IIIA coveralls covered a period

of six days. The average heat flux values obtained from these six-day calibrations for each individual sensor were used as the fire boundary conditions in the numerical model. Table 2-2 provides a comparison of the manikin system experimental and numerical model results for one layer protective coveralls made from Kevlar®/PBI and Nomex® IIIA for three- and four-second exposures.

Table 2-2 Manikin test results and numerical model predictions

Kevlar®/PBI Coverall for a 3-second Exposure						
Skin Burn	Manikin Test					Model Prediction
	Rep. 1	Rep. 2	Rep. 3	S.D.	Avg.	
2nd %	19.6	15.6	18	2.0	17.7	15.7
3rd %	6.6	6.6	6.6	0.0	6.6	6.6
Total %	26.2	22.2	24.6	2.0	24.3	22.2
Kevlar®/PBI Coverall for a 4-second Exposure						
Skin Burn	Manikin Test					Model Prediction
	Rep. 1	Rep. 2	Rep. 3	S.D.	Avg.	
2nd %	48.4	51.6	52.5	2.2	50.8	52.5
3rd %	7.4	8.2	8.2	0.5	7.9	8.2
Total %	55.8	59.8	60.7	2.6	58.8	60.7
Nomex® IIIA Coverall for a 3-second Exposure						
Skin Burn	Manikin Test					Model Prediction
	Rep. 1	Rep. 2	Rep. 3	S.D.	Avg.	
2nd %	26.2	22.9	22.9	1.9	24.0	22.1
3rd %	6.6	6.6	6.6	0.0	6.6	7.4
Total %	32.8	29.5	29.5	1.9	30.6	29.5
Nomex® IIIA Coverall for a 4-second Exposure						
Skin Burn	Manikin Test					Model Prediction
	Rep. 1	Rep. 2	Rep. 3	S.D.	Avg.	
2nd %	45.9	46.7	52.5	3.6	48.3	48.4
3rd %	14.8	12.3	9.8	2.5	12.3	13.1
Total %	60.7	59	62.3	1.7	60.7	61.5

These experiments demonstrate that the numerical model reasonably simulates the results of actual manikin tests in total burn results for a single layer garment in both 3- and 4-second exposures. Distribution of burn injury predicted by the model consists with the manikin tests.

Figure 2-9 illustrates an example body burn distribution of Kevlar®/PBI coverall exposed to 3-second flash fire. The distribution consistency indicates a reasonable simulation of heat transfer coefficient at each sensor location and measurement of overall garment air gap size and its distribution. The comparison between the established burn distribution provided by the experimental and model simulation is particularly good for close fitting areas. In loose fitting areas, such as the leg, the model prediction and manikin test shows a larger amount of variation. Additionally the numerical model over-predicted third degree burns for Nomex® IIIA coverall in 4-second exposure in the leg area. The over prediction is mainly due to the variation of the existing air gap in loose areas. The numerical model generally is more accurate for Kevlar®/PBI than Nomex® IIIA coveralls; and provides better predictions for 3-second exposures than for 4-second fire exposures. This finding can be attributed to thermally induced shrinkage of Nomex® IIIA coverall, which reduces the air layer sizes and producing an increase in heat transfer to the manikin. In order to simulate shrinkage, a one-step air gap change is established into the numerical model based on the actual measurements of the air gap before and after exposure, while in the manikin test, the shrinkage process is gradual and much more complicated. This can be demonstrated by comparing the heat flux history of the numerical model with manikin tests of Kevlar®/PBI and Nomex® IIIA in a 4-second exposure as illustrated in Figures 2-10 and 2-11. Figure 2-11 shows the heat flux sudden change at about 1.5 seconds as result of the onset of shrinkage. As the result of the shrinkage, the air gap size is dramatically reduced, and therefore increases the heat transfer rate to skin. This change lowers the garment thermal protective performance. Additionally, the heat flux history measured by manikin test sensors in both cases (Kevlar®/PBI and Nomex® IIIA) correlates very well with the one predicted in the model as shown in Figures

2-10 and 2-11. We note that the fire boundary condition and air gap size used in the numerical model for specific sensor locations are not necessarily the same as in the actual manikin test. The change in fire boundary condition and air gap size at each specific sensor locations among the replicates of garment manikin test is one of the features in instrumented manikin fire test.

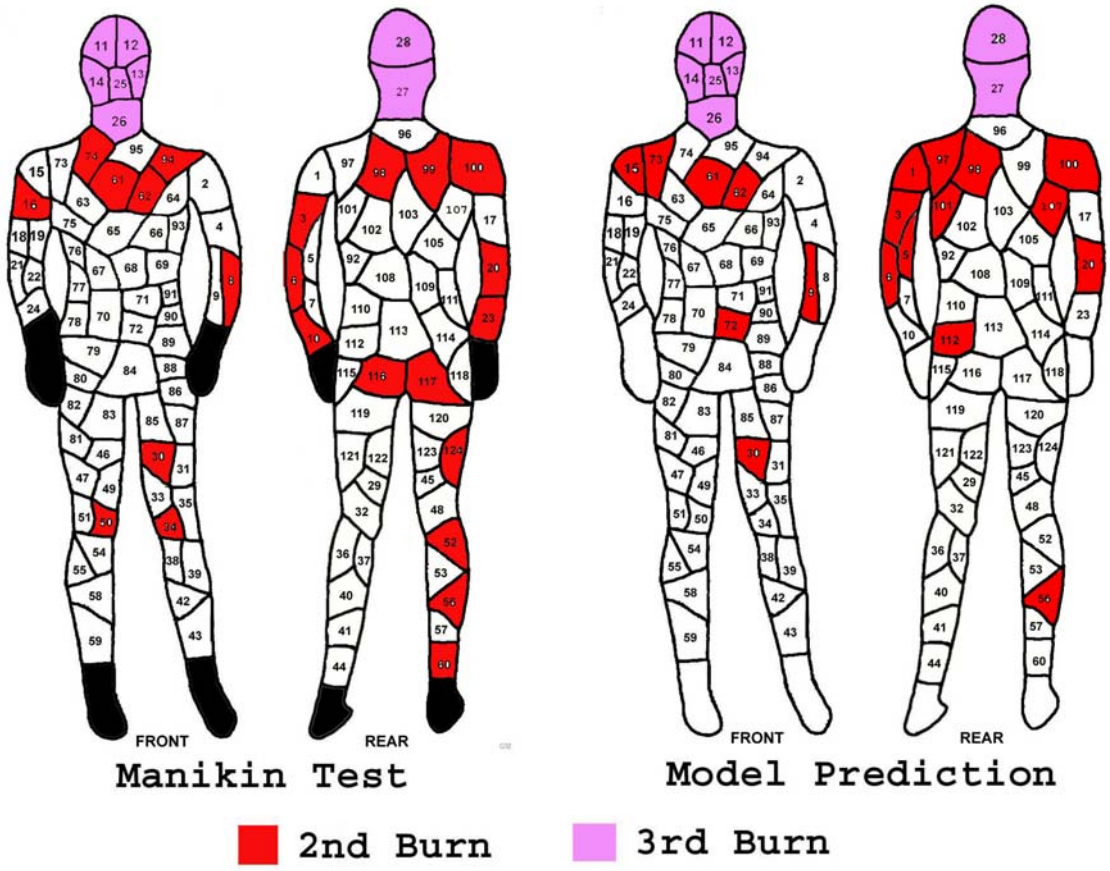

Figure 2-9 A comparison of burn distribution of manikin test and model prediction for a 3-second exposure

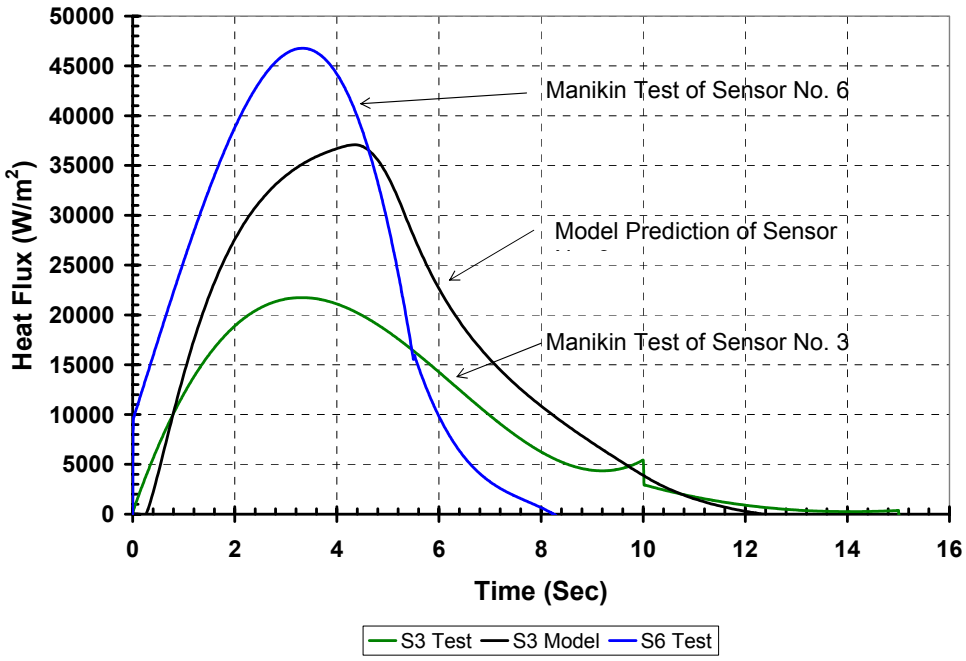

Figure 2-10 Heat flux histories of manikin test and model prediction

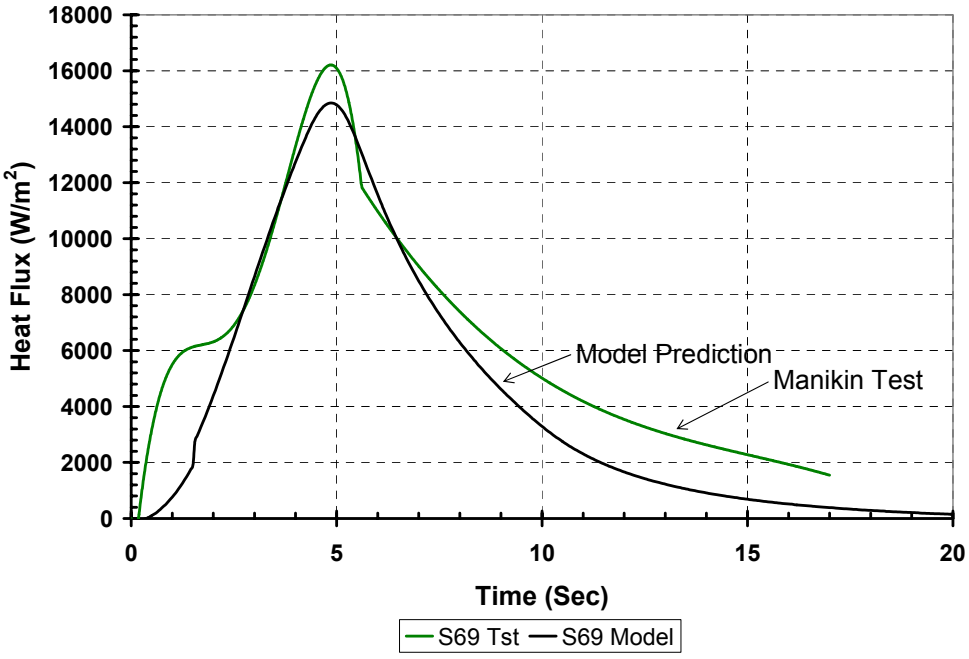

Figure 2-11 Heat flux histories of manikin test and model prediction

2.6. CONCLUSIONS

The manikin simulation model reproduced surface heat flux and skin damage results very well for the single layer protective garments considered. Garment shrinkage during exposure can be taken into account by considering the changes of air gap size between the garment and manikin body. Based on these results, we conclude that the numerical model is capable of predicting heat transfer through one layer protective clothing and the resulting human skin burn damages in flash fire conditions with good accuracy. The simulation model does not include many variables considered essential to fully simulate actual use conditions, such as multiple layer garments and moisture contained in the fabric. It should be noted that as an extensive amount of garment specific experimental data was required in order to execute the program, the model can prove to be a powerful tool for engineering more protective, efficient garments.

ACKNOWLEDGEMENTS

This research was funded by the National Textile Center. We wish to thank to David Bruner and Mike King in Textile/Clothing Technology Corporation (TC^2) for help in conducting the three-dimensional body scanning. Thanks also to James Beck and R. McMasters in Michigan State University who helped with parameter estimation method and codes. The author also would like to take this opportunity to thank Jon Porter, research technician at T-PACC, for helping us to perform the measurements of fabric thickness on a Kawabata's instrument.

AUTHOR'S NOTE

Caution should be taken in drawing conclusions about the safety benefits from these results. The data described in this work are taken from laboratory tests and controlled exposures. They are not presented to predict the actual field conditions where the nature of the thermal exposure can be physically complicated and unqualified. We wish to emphasize that it is not our intention to recommend, exclude, or predict the suitability of any commercial product for a particular end-use.

REFERENCES

1 M. Pawar and R. L. Barker, "Analyzing the performance of protective garments in manikin fire tests", *in Proceedings of the Fifth Scandinavian Symposium on Protective Clothing*, Elsinore, Denmark, 1997.

2 N. Y. Chen, "Transient heat and moisture transfer through thermally irradiated cloth", *Ph.D. Thesis, Massachusetts Institute of Technology*, Cambridge, MA, 1959.

3 P. W. Gibson, "Multiphase heat and mass transfer through hygroscopic porous media with applications to clothing materials", *Technical Report Natick/TR-97/005*, U.S. Army Natick Research, Development, and Engineering Center, Natick, MA, 1996.

4 P. W. Gibson and M. Charmchi, "Integration of a human thermal physiology control model with a numerical model for coupled heat and mass transfer through hygroscopic porous textiles", *Presented at the 1996 ASME International Mechanical Engineering Congress & Exhibition*, Atlanta, GA, November 17-22, 1996.

5 W. E. Mell and J. R. Lawson, "A heat transfer model for fire fighter's protective clothing", *National Institute of Standards and Technology, NISTIR 6299*, January, 1999.

6 H. L. Morse, J. G. Thompson, K. J. Clark, K. A. Green, and C. B. Moyer, "Analysis of the thermal response of protective fabric", *Technical Report, AFML-RT-73-17, Air Force Materials Information Service*, Springfield, VA.

7 D. A. Torvi, "Heat transfer in thin fibrous materials under high heat flux conditions", *Ph.D. Thesis, University of Alberta*, Edmonton, Alberta, Canada, 1997.

8 R. L. Barker and Y. M. Lee, "Analyzing the transient thermophysical properties of heat-resistant fabrics in TPP exposures", *Textile Res. J.*, vol. 57 (6), pp. 331-338, 1987.

9 I. Shalev, "Transient thermo-physical properties thermally degrading fabrics and their effect on thermal protection", *Doctoral Dissertation, North Carolina State University*, Raleigh, NC, 1984.

10 I. Shalev and R. L. Barker, "Predicting the thermal protective performance of heat-protective fabrics from basic properties", *Special Technical Testing Publication 900*, *American Society for Testing and Materials*, 1986.

11 H. H. Pennes, "Analysis of tissue and arterial blood temperatures in resting human forearm", *J. Appl. Physiol.*, vol. 1, pp. 93-122, 1948.

12 S. V. Patankar, *Numerical Heat Transfer and Fluid Flow*, Taylor & Francis, Philadelphia, PA, 1980.

13 J. C. Tannehill, D. A. Anderson, and R. H. Pletcher, *Computational Fluid Mechanics and Heat Transfer*, 2nd Ed., Taylor & Francis, Philadelphia, PA, 1997.

14 N. J. Abbott and S. Schulman, "Protection from fire: nonflammable clothing – A review", *Fire Technol*., vol. 12, pp. 204-218, 1976.

15 D. Drysdale, *An Introduction to Fire Dynamics*, 2nd Ed., John Wiley & Sons Ltd., Chichester, England, 1998.

16 J. V. Beck, B. Blackwell, and C. R. Jr. St. Clair, *Inverse Heat Conduction: Ill-Posed Problems*, John Wiley & Sons, Inc., New York, NY, 1985.

17 G. Song, "Modeling thermal protection outfits for fire exposures", *Doctoral Dissertation, North Carolina State University*, Raleigh, NC, 2002.

18 J. V. Beck and K. Arnold, *Parameter Estimation in Engineering and Science*, John Wiley & Sons, Inc., New York, NY, 1977.

19 J. V. Beck and R. McMasters, *Users Manual for Prop1D—Program for Estimating Thermal Properties from Transient Temperature and Heat Flux Measurements, Version 7.0*, Beck Engineering Consultants Company, 2000.

20 J. Mandrel, "Use of the singular value decomposition in regression analysis", *Am. Stat.*, vol. 36, pp. 15-24, 1982.

21 C. L. Lawson and R. J. Hanson, *Solving Least Squares Problems*, Prentice-Hall, Englewood Cliffs, NJ, 1974.

PART TWO:

HEAT AND MOISTURE TRANSPORT MODEL

3. MODELING HEAT AND MOISTURE TRANSPORT IN FIREFIGHTER PROTECTIVE CLOTHING DURING FLASH FIRE EXPOSURE

ABSTRACT

In this chapter, a model of heat and moisture transport in firefighter protective clothing during a flash fire exposure is presented. The aim of this study is to investigate the effect of coupled heat and moisture transport on the protective performance of the garment. Computational results show the distribution of temperature and moisture content in the fabric during the exposure to the flash fire as well as during the cool-down period. Moreover, the duration of the exposure during which the garment protects the firefighter from getting second and third degree burns from the flash fire exposure is numerically predicted. A complete model for the fire-fabric-air gap-skin system is presented.

NOMENCLATURE

A surface area [m^2]

c_p specific heat at constant pressure [J kg^{-1} K^{-1}]

D_a diffusivity of water vapor in the air [m^2 s^{-1}]

D_{eff} effective diffusivity of the gas phase in the fabric [m^2 s^{-1}]

D_{solid} effective diffusivity of bound water in the solid phase [m^2 s^{-1}]

d_f average fiber diameter [m]

F view factor

g gravitational acceleration [9.81 m s^{-2}]

h_c convective heat transfer coefficient [W m^{-2} K^{-1}]

h_m convective mass transfer coefficient [m s^{-1}]

k thermal conductivity [W m^{-1} K^{-1}]

L thickness [m]

$\dot{m}_{sv}$ water vapor mass flux out of the fiber [kg m^{-3} s^{-1}]

M molecular weight [kg $kmol^{-1}$]

Nu Nusselt number

p pressure [Pa]

P frequency factor (pre-exponential factor) [s^{-1}]

$q''_{air,cond/conv}$ heat flux by conduction/convection from the fabric to the human skin across the air gap [W m^{-2}]

$q''_{air,rad}$ heat flux by radiation from the fabric to the human skin across the air gap [W m^{-2}]

q''_{conv} convective heat flux from the flame to the fabric [W m^{-2}]

q''_{rad} incident radiation heat flux from the flame onto the fabric [W m^{-2}]

R universal gas constant [8.315×10^3 J $kmol^{-1}$ K^{-1}]

$R_{f,\phi=0.65}$ fabric regain at 65% relative humidity

$R_{f,skin}$ equilibrium regain at the fiber surface

$R_{f,total}$ total fiber regain

Ra Rayleigh number

T temperature [K]

t time [s]

x linear horizontal coordinate [m]

Greek symbols

α thermal diffusivity of the air [$m^2\ s^{-1}$]

β thermal expansion coefficient of the air [K^{-1}]

ΔE activation energy for skin [J $kmol^{-1}$]

Δh_l enthalpy of transition from bound water to free liquid water [J kg^{-1}]

Δh_{vap} enthalpy of evaporation per unit mass [J kg^{-1}]

ΔT temperature difference across the air gap [K]

δ thickness of the air gap [m]

ε volume fraction

$\tilde{\varepsilon}$ emissivity

ϕ relative humidity

γ extinction coefficient of the fabric [m^{-1}]

ν kinematic viscosity of the air [$m^2\ s^{-1}$]

ρ density [kg m^{-3}]

σ Stefan-Boltzman constant [5.670×10^{-8} W $m^{-2}\ K^{-4}$]

$\tilde{\tau}$ transmissivity of the fabric

τ fabric tortuosity

Ω quantitative measure of burn damage

ω_b blood perfusion [0.00125 $m^3\ s^{-1}\ m^{-3}$ tissue]

Subscripts

0	initial state
a	dry air
art	arterial
amb	ambient air
blood	blood
bw	bound water
ds	dry solid
eff	effective
eq	equilibrium
fab	fabric
fl	flame
g	hot gases
gap	air gap
s	saturation
sens	sensor
skin	human skin
v	water vapor
w	water
γ	gas phase
σ	solid phase

3.1. INTRODUCTION

Every year many firefighters are injured as a result of exposure to a flash fire. In order to prevent or minimize the burn injuries, thermal protective clothing must be properly designed. In developing thermal protective materials, such as firefighter garments, researchers traditionally focus on heat transfer in fabrics subjected to flash fire conditions. However, moisture transport in fabrics and its effect on protective performance of the garment has not been studied in sufficient detail. In this chapter, a model that couples heat and moisture transport is developed.

Protective fabric can be treated as a porous medium. There are many existing models for the analysis of multiphase transport in porous media. Vafai and Sözen [1] summarized and compared these models. One of the models, which is suitable for fabrics subjected to intensive heat, is Gibson's model [2]. However, Gibson's model does not account for radiation heat transfer within the fabric layer. Torvi [3] developed a heat transfer model, which accounts for the radiative heat transfer through a fabric.

The present study is aimed at developing a model to analyze heat and moisture transport in protective clothing. Combining Gibson and Torvi's models makes it possible to account for the thermal response of the fabric. The skin model developed by Pennes [4] is utilized to predict tissue burn injuries, which are evaluated based on the approach suggested by Henriques and Moritz [5].

3.2. PROBLEM DESCRIPTION

A schematic diagram of heat and moisture transport in firefighter garments as well as heat transfer in human skin and tissue is displayed in Figure 3-1. The garment consists of three

fabric layers, which are the outer shell, the moisture barrier, and the thermal liner. The configuration of each garment layer is shown in Figure 3-1. The human skin can also be divided into three layers, such as epidermis, dermis, and subcutaneous, as shown in Figure 3-1.

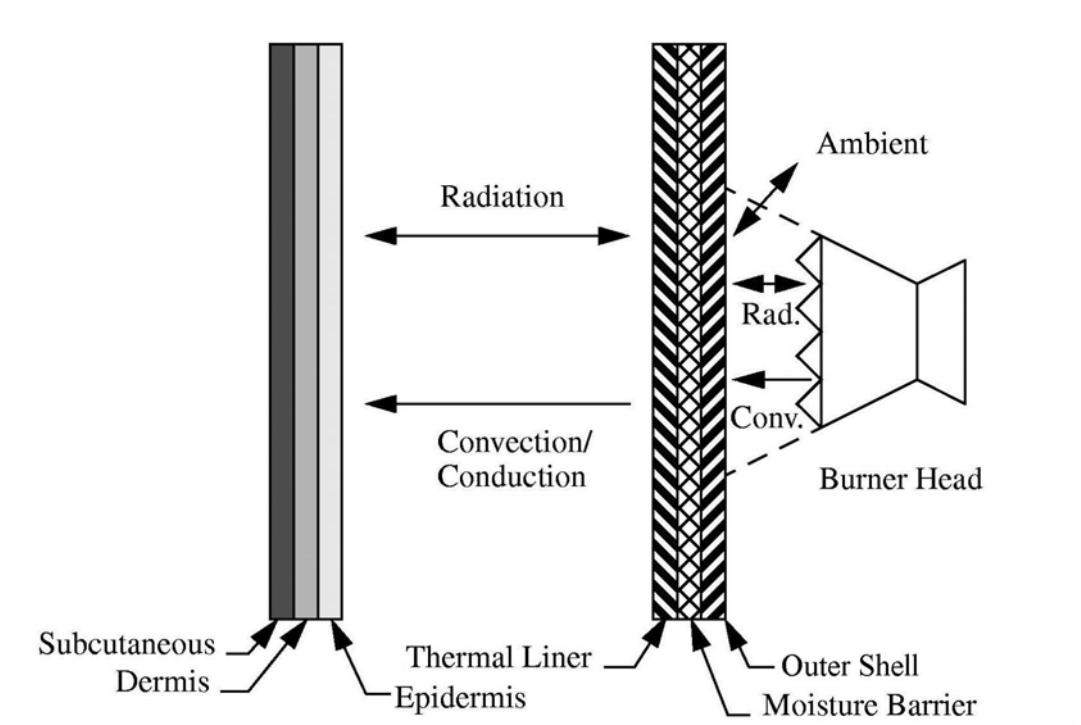

Figure 3-1 Schematic diagram of heat and moisture transport in the protective clothing and the human skin

3.2.1. HEAT TRANSFER MODEL IN FABRIC

Gibson [2] applied Whitaker's theory [6] of coupled heat and mass transfer through porous media to derive a set of equations for modeling heat and mass transfer through textile materials. He assumed that fabric can be modeled as a hygroscopic porous media. He modeled the material as a mixture of a solid phase consisting of solid (e.g., polymer or cotton) fibers plus bound water absorbed by the polymer matrix, a liquid phase consisting of

free liquid water, and a gaseous phase consisting of water vapor plus dry air. The model accounts for heat transfer by conduction in all phases, convection in the gas and liquid phases, and latent heat release due to phase change from liquid to vapor phase.

For simplicity, the gas phase convection contributions due to pressure differences, which can arise either due to body movement or due to external air movement (wind), are neglected. Moreover, it is assumed that if there is any extra liquid sweat which builds up on the skin surface, it will either drip off or wick into the fabric and then will be absorbed by the fabric fibers and become bound water. In the other words, free liquid water exists neither on the surface of the skin nor in the fabric layer. A schematic diagram of porous textile structure is illustrated in Figure 3-2.

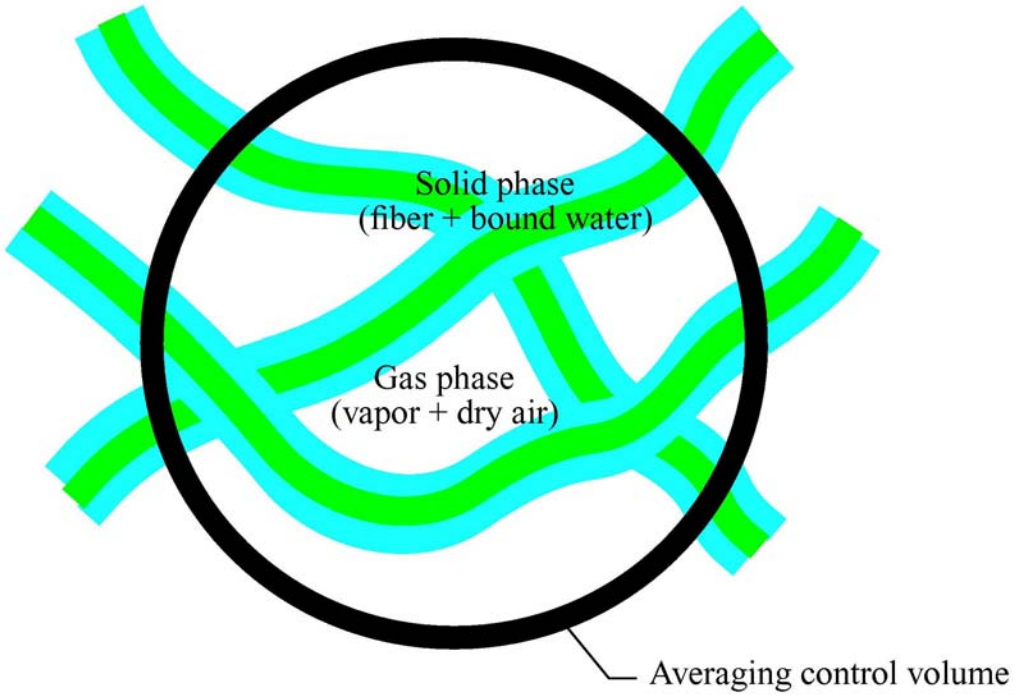

Figure 3-2 Schematic diagram of two-phase structure of porous textile media in the averaging control volume

Torvi [3] assumed that convective heat flux only applies to the surface of the fabric but radiative heat flux can penetrate through the fabric up to a certain depth. Based on the above assumptions, the energy balance in the infinitesimal element of fabric can be written in the form of a differential equation. The partial differential equation is developed for the temperature distribution in a composite fabric layer by combining Gibson and Torvi's models. Therefore, the energy equation is modeled based on Gibson's model plus the penetrating radiation term, which is described by Torvi's model [3]. Thermal properties of all phases are accounted for in the model based on the relations given by Gibson [2]. Radiative heat transfer in the fabric is accounted for by introducing in the energy equation a source term similar to that of Torvi's model [3].

3.2.1.1. Energy Equation

$$\rho c_p \frac{\partial T}{\partial t} + \left(\Delta h_l + \Delta h_{vap}\right)\dot{m}_{sv} = \frac{\partial}{\partial x}\left(k_{eff}\frac{\partial T}{\partial x}\right) + \gamma \cdot q''_{rad} e^{-\gamma x} \qquad (3.1)$$

where ρ is the effective density of the fabric, c_p is the effective specific heat of the fabric, T is the temperature, t is the time, Δh_l is the enthalpy of transition from the bound water to the free liquid water, Δh_{vap} is the enthalpy of evaporation per unit mass, $\dot{m}_{sv}$ is the mass flux of vapor out of the fiber (or into the fiber if $\dot{m}_{sv}$ is negative), x is the linear horizontal coordinate, k_{eff} is the effective thermal conductivity of the fabric, γ is the extinction coefficient of the fabric, and q''_{rad} is the incident radiation heat flux from the flame onto the fabric.

The effective density of the fabric, ρ, can be calculated [2] as:

$$\rho = \varepsilon_{bw}\rho_w + \varepsilon_{ds}\rho_{ds} + \varepsilon_\gamma(\rho_v + \rho_a) \tag{3.2}$$

where ε_{bw} is the volume fraction of the water dissolved in the solid phase, ρ_w is the density of the liquid water, ε_{ds} is the volume fraction of the dry solid fiber (assumed to be constant), ρ_{ds} is the density of the dry solid, ε_γ is the volume fraction of the gas phase, ρ_v is the intrinsic density of the water vapor, and ρ_a is the intrinsic density of the dry air.

The effective specific heat of the fabric, c_p, can be calculated [2] as:

$$c_p = \frac{\varepsilon_{bw}\rho_w(c_p)_w + \varepsilon_{ds}\rho_{ds}(c_p)_{ds} + \varepsilon_\gamma[\rho_v(c_p)_v + \rho_a(c_p)_a]}{\rho} \tag{3.3}$$

where $(c_p)_w$ is the specific heat of the liquid water, $(c_p)_{ds}$ is the specific heat of the dry solid, $(c_p)_v$ is the specific heat of the water vapor, and $(c_p)_a$ is the specific heat of the dry air.

The enthalpy of transition from the bound water to the free liquid water state, Δh_l, can be presented [2] as:

$$\Delta h_l = 1.95\times10^5(1-\phi)\times\left[\frac{1}{(0.2+\phi)} + \frac{1}{(1.05-\phi)}\right] \tag{3.4}$$

where ϕ is the relative humidity defined as:

$$\phi = \frac{p_v}{p_s} \tag{3.5}$$

In equation (3.5), p_v is the partial pressure of the water vapor and p_s is the saturation vapor pressure, which is a function of T only.

The saturation vapor pressure, p_s, is calculated [2] as:

$$p_s = 614.3 \exp\left\{17.06\left[\frac{(T-273.15)}{(T-40.25)}\right]\right\} \tag{3.6}$$

The enthalpy of vaporization per unit mass, Δh_{vap}, can be calculated [2] as:

$$\Delta h_{vap} = 2.792\times10^{6} - 160T - 3.43T^{2} \tag{3.7}$$

The mass flux of the vapor out of the fiber, $\dot{m}_{sv}$, is calculated [2] as:

$$\dot{m}_{sv} = \frac{8D_{solid}\rho_{ds}}{d_f^2}(R_{f,total} - R_{f,skin}) \tag{3.8}$$

where D_{solid} is the effective diffusivity of bound water in the solid phase, d_f is the average fiber diameter, $R_{f,total}$ is the total fiber regain, and $R_{f,skin}$ is the equilibrium regain at the fiber surface.

Definitions of the physical properties of the fabric are given in Morton and Hearle's work [7]. The fiber regain, R_f, can be represented as:

$$R_f = \frac{\varepsilon_{bw}\rho_w}{\varepsilon_{ds}\rho_{ds}} \tag{3.9}$$

The total fiber regain, $R_{f,total}$, is calculated by using the volume fraction of the bound water, ε_{bw}, obtained from the solid phase continuity equation, which will be discussed later on in this chapter. In the same manner, the equilibrium regain at the fiber surface, $R_{f,skin}$, can be calculated by using the equilibrium volume fraction of bound water, $\varepsilon_{bw,eq}$, obtained from the sorption relation, which will be provided later on in this chapter.

The effective thermal conductivity of the fabric, k_{eff}, can be calculated [2] as:

$$k_{eff} = k_{\gamma}\left\{\frac{[1+(\varepsilon_{bw}+\varepsilon_{ds})]k_{\sigma}+\varepsilon_{\gamma}k_{\gamma}}{\varepsilon_{\gamma}k_{\sigma}+[1+(\varepsilon_{bw}+\varepsilon_{ds})]k_{\gamma}}\right\} \tag{3.10}$$

where k_{γ} is the thermal conductivity of the gas phase and k_{σ} is the thermal conductivity of the solid phase.

The thermal conductivity of the gas phase, k_{γ}, can be calculated [2] as:

$$k_{\gamma} = \left(\frac{k_v\rho_v + k_a\rho_a}{\rho_v + \rho_a}\right) \tag{3.11}$$

where k_v is the thermal conductivity of the saturated water vapor and k_a is the thermal conductivity of the dry air.

The thermal conductivity of the solid phase, k_{σ}, can be calculated [2] as:

$$k_{\sigma} = \left(\frac{k_w\rho_w\varepsilon_{bw} + k_{ds}\rho_{ds}\varepsilon_{ds}}{\rho_w\varepsilon_{bw} + \rho_{ds}\varepsilon_{ds}}\right) \tag{3.12}$$

where k_w is the thermal conductivity of the liquid water and k_{ds} is the thermal conductivity of the dry solid.

The extinction coefficient, γ, that characterizes the decrease of thermal radiation as it penetrates deeper into the fabric, is given [3] as:

$$\gamma = \frac{-\ln(\widetilde{\tau})}{L_{fab}} \tag{3.13}$$

where $\widetilde{\tau}$ is the transmissivity of the fabric and L_{fab} is the fabric thickness. It is assumed that radiation penetrates through the outer layer of the fabric only.

The incident radiation heat flux coming from the flame to the fabric, q''_{rad}, is found [3] as:

$$q''_{rad} = \sigma\,\widetilde{\varepsilon}_g(T_g^4 - T_{fab}^4) - \sigma\,\widetilde{\varepsilon}_{fab}F_{fab-amb}(1-\widetilde{\varepsilon}_g)(T_{fab}^4 - T_{amb}^4) \tag{3.14}$$

where σ is the Stefan-Boltzman constant, $\widetilde{\varepsilon}_g$ is the emissivity of the hot gases, T_g is the temperature of the hot gases, T_{fab} is the temperature at the outside surface of the fabric, $\widetilde{\varepsilon}_{fab}$ is the emissivity of the fabric, $F_{fab-amb}$ is the view factor accounting for the geometry of the fabric with respect to the ambient, and T_{amb} is the temperature of the ambient air. Since this work considers a 1D model, the view factor, $F_{fab-amb}$, is set to unity.

3.2.1.2. Solid Phase Continuity Equation

$$\rho_w \frac{\partial}{\partial t}\left(\varepsilon_{bw}\right) + \dot{m}_{sv} = 0 \tag{3.15}$$

3.2.1.3. Gas Phase Diffusivity Equation

$$\frac{\partial}{\partial t}\left(\varepsilon_\gamma \rho_v\right) - \dot{m}_{sv} = \frac{\partial}{\partial x}\left(D_{eff} \frac{\partial \rho_v}{\partial x} \right) \tag{3.16}$$

where D_{eff} is the effective diffusivity of the gas phase in the fabric, which is defined [2] as:

$$D_{eff} = \frac{D_a \varepsilon_\gamma}{\tau} \tag{3.17}$$

In equation (3.17), D_a is the diffusivity of water vapor in the air and τ is the fabric tortuosity.

The diffusivity of the water vapor in the air, D_a, is calculated [2] as:

$$D_a = 2.23 \times 10^{-5} \left(\frac{T}{273.15} \right)^{1.75} \tag{3.18}$$

3.2.1.4. Volume Fraction Constraint

$$\varepsilon_\gamma + \varepsilon_{bw} + \varepsilon_{ds} = 1 \tag{3.19}$$

3.2.1.5. Sorption Relation

$$\varepsilon_{bw,eq} = 0.578 R_{f,\phi=0.65}\left(\varepsilon_{ds}\frac{\rho_{ds}}{\rho_w}\phi\right)\left[\frac{1}{(0.321+\phi)}+\frac{1}{(1.262-\phi)}\right] \tag{3.20}$$

where $R_{f,\phi=0.65}$ is the fabric regain at 65% relative humidity. This relation is given in Gibson [2].

3.2.1.6. Thermodynamic Relations

$$p_a = p_\gamma - p_v \tag{3.21}$$

$$p_a = \rho_a \frac{R}{M_a} T \tag{3.22}$$

$$p_v = \rho_v \frac{R}{M_v} T \tag{3.23}$$

where p_a is the partial pressure of the air, p_γ is the total gas pressure, R is the universal gas constant, M_a is the molecular weight of the air, and M_v is the molecular weight of the water vapor.

3.2.1.7. Initial Conditions

$$T(x,t=0) = T_0(x) \tag{3.24}$$

$$\phi(x,t=0) = \phi_0(x) \tag{3.25}$$

$$\varepsilon_{bw}(x,t=0) = \varepsilon_{bw0}(x) \tag{3.26}$$

where T_0 is the initial temperature, ϕ_0 is the initial relative humidity, and ε_{bw0} is the initial volume fraction of the bound water.

3.2.1.8. Boundary Conditions for the Fabric

$$-k_{eff}\left.\frac{\partial T}{\partial x}\right|_{x=0} = \left(q''_{conv} + q''_{rad}\right)_{x=0} \tag{3.27}$$

$$-k_{eff}\left.\frac{\partial T}{\partial x}\right|_{x=L_{fab}} = \left(q''_{air,rad} + q''_{air,cond/conv}\right)_{x=L_{fab}} \tag{3.28}$$

$$h_m(\rho_{v,amb} - \rho_v)_{x=0} = -D_{eff}\left.\frac{\partial \rho_v}{\partial x}\right|_{x=0} \tag{3.29}$$

$$h_m(\rho_v - \rho_{v,air})_{x=L_{fab}} = -D_{eff}\left.\frac{\partial \rho_v}{\partial x}\right|_{x=L_{fab}} \tag{3.30}$$

where q''_{conv} is the convective heat flux from the flame to the fabric, $q''_{air,rad}$ is the heat flux by radiation from the fabric to the human skin across the air gap, $q''_{air,cond/conv}$ is the heat flux by conduction/convection from the fabric to the human skin across the air gap, h_m is the convective mass transfer coefficient, $\rho_{v,amb}$ is the density of water vapor in the ambient air, and $\rho_{v,air}$ is the density of water vapor in the air gap.

The radiation and convection heat fluxes can be found [3] as:

$$(q''_{conv} + q''_{rad})_{x=0} = h_{c,fl}(T_g - T_{fab}) \tag{3.31}$$

where $h_{c,fl}$ is the convective heat transfer coefficient between the flame and the outer surface of the fabric.

The heat flux by radiation from the fabric to the human skin across the air gap is given by [3]:

$$q''_{air,rad}\Big|_{x=L_{fab}} = \frac{\sigma\left(T_{fab}{}^4 - T_{skin}{}^4\right)}{\left(\frac{A_{skin}}{A_{fab}}\left(\frac{1-\widetilde{\varepsilon}_{fab}}{\widetilde{\varepsilon}_{fab}} + \frac{1}{F_{fab-skin}}\right) + \frac{1-\widetilde{\varepsilon}_{skin}}{\widetilde{\varepsilon}_{skin}}\right)} \tag{3.32}$$

where T_{skin} is the temperature at the outside surface of the human skin, A_{skin} is the surface area of the human skin, A_{fab} is the surface area of the fabric, $F_{fab-skin}$ is the view factor accounting for the geometry of the fabric with respect to the human skin (set to unity because the model is one-dimensional), and $\widetilde{\varepsilon}_{skin}$ is the emissivity of the human skin.

The heat flux by conduction/convection from the fabric to the human skin across the air gap is given by [3]:

$$q''_{air,cond/conv}\Big|_{x=L_{fab}} = h_{c,gap}(T_{fab} - T_{skin}) \tag{3.33}$$

where $h_{c,gap}$ is the convective heat transfer coefficient of the air due to conduction and natural convection in the air gap. $h_{c,gap}$ can be found [3] as:

$$h_{c,gap} = Nu\frac{k_{air}(T)}{L_{gap}} \tag{3.34}$$

where Nu is the Nusselt number; $k_{air}(T)$ is the thermal conductivity of the air, which is a function of T only; and L_{gap} is the thickness of the air gap.

3.2.2. HEAT TRANSFER MODEL IN THE SKIN

The Pennes model [4] is used to model heat transfer in the living tissue. The skin is divided into three layers, namely, the epidermis, the dermis, and the subcutaneous region. Blood perfusion applies only to the latter two regions. The model is based on the assumption that there is an energy exchange between the blood vessels and the surrounding tissue. According

to the Pennes model, the total heat transfer by the flowing blood is proportional to its volumetric flow rate and the temperature difference between the blood and the tissue.

3.2.2.1. Bio-Heat Transfer Equation

$$(\rho c_p)_{skin}\frac{\partial T}{\partial t} = \nabla\cdot(k_{skin}\nabla T) + (\rho c_p)_{blood}\omega_b(T_{art} - T) \tag{3.35}$$

where ρ_{skin} is the density of the human skin, $(c_p)_{skin}$ is the specific heat of the human skin, k_{skin} is the thermal conductivity of the human skin, ρ_{blood} is the density of the human blood, $(c_p)_{blood}$ is the specific heat of the human blood, ω_b is the blood perfusion, and T_{art} is the arterial temperature.

3.2.2.2. Boundary Conditions for the Skin

$$-k_{skin}\left.\frac{\partial T}{\partial x}\right|_{x=L_{fab}+L_{gap}} = \left(q''_{air,rad} + q''_{air,cond/conv}\right)_{x=L_{fab}+L_{gap}} \tag{3.36}$$

$$T\big|_{x=L_{fab}+L_{gap}+L_{skin}} = T_{art} \tag{3.37}$$

where L_{skin} is the thickness of the human skin.

3.2.3. NATURAL CONVECTION IN THE AIR GAP BETWEEN THE FABRIC AND THE SKIN

For modeling the thermal response of firefighter protective clothing exposed to flash fire, the convective heat transfer in the air gap between the fabric and the skin is simulated as a natural convection in a vertical enclosure, which is heated from one side. Catton [8] summarized the Nusselt number correlations for the air in a long vertical enclosure heated from one side. The relation based on Denny and Clever's work [9] is given as:

$$Nu = \begin{cases} 1.0 & , Ra \le 1713 \\ 0.112 Ra^{0.294} & , Ra > 1713 \end{cases} \tag{3.38}$$

where Ra is the Rayleigh number defined as:

$$Ra = \frac{g\beta \Delta T \delta^3}{\alpha \nu} \tag{3.39}$$

In equation (3.39), g is the gravitational acceleration, β is the thermal expansion coefficient of the air, ΔT is the temperature difference across the air gap, δ is the thickness of the air gap, α is the thermal diffusivity of the air, and ν is the kinematic viscosity of the air.

From the above expression, natural convection will contribute to heat transfer across the enclosure when the Rayleigh number is greater than 1713. The maximum Rayleigh number, Ra, for all computed cases of the Thermal Protective Performance (TPP) test was 1123. Therefore, for the case computed in this work, the Rayleigh number is always smaller than 1713, which means that natural convection is negligible. Therefore, radiation and conduction heat transfer will be dominating heat transfer mechanisms across the air gap.

3.2.4. TISSUE BURN INJURY MODEL

The tissue burn injury model is based on the work by Henriques and Moritz [5]. Thermal damage occurs when the temperature at the interface between the epidermis and dermis in the human skin (called the basal layer, cf. Fig. 3-1) rises above 44ºC. The destruction rate of the growing layer can be modeled by a first order chemical reaction. Arrhenius rate equation can be used to estimate the rate of tissue damage:

$$\frac{d\Omega}{dt} = P \exp\left(-\frac{\Delta E}{RT}\right) \tag{3.40}$$

where Ω is a quantitative measure of the burn damage at the interface or at any depth in the dermis, P is the frequency factor or pre-exponential factor, and ΔE is the activation energy for skin.

The above equation can be integrated over the time interval when the temperature at the interface is above 44ºC:

$$\Omega = \int_0^t P \exp\left(-\frac{\Delta E}{RT}\right) dt \qquad (3.41)$$

For predicting the first and second-degree burns, the temperature at the interface between the epidermis and dermis in the human skin must be used as T in equation (3.41). First-degree burn occurs when the value of the burn integral, Ω, reaches 0.53 at this interface, while second-degree burn happens when Ω attains 1.0 at the same interface. For predicting third degree burns, the temperature at the interface between the dermis and the subcutaneous layer (called the dermal base, cf. Fig. 3-1) must be used as T in equation (3.41). The third degree burn occurs when Ω attains 1.0 at this interface. These tissue burn damage criteria can be used once appropriate values of P and ΔE are provided. These values were suggested by Weaver and Stoll [10] for the basal layer and by Takata et al. [11] for the dermal base.

3.3. NUMERICAL PROCEDURE

In this work, the finite difference method (Patankar [12]; Tannehill et al. [13]) is used to solve the differential equations (equations (3.1), (3.15), (3.16), and (3.35)), which are the energy equation for the fabric, the solid phase continuity equation, the gas phase diffusivity equation, and the bio-heat transfer equation for the skin, respectively. The Crank-Nicholson scheme is used to discretize the transient partial differential equations. Due to non-linearities

in this system, the iterative scheme is used to solve these equations. In order to avoid divergence of the iteration method, the underrelaxation procedure is also utilized. The value of the underrelaxation parameter is 0.8. In addition, the properties of the fabric at the interfaces between the fabric layers abruptly change, which may occur in the composite materials. The harmonic averaging is more accurate rather than the arithmetic averaging (Patankar [12]; Li [14, 15]). The solution procedure is as follows. All variables are known at the initial state, then the program marches forward in given time increments. The new values of variables are computed by solving the set of algebraic equations. Then the iterations are repeated until the changes in the solutions become smaller than 10^{-6}. Next, after the temperature profile in multiple layers of skin is obtained, Henriques' burn integral (equation (3.41)) is used to calculate the maximum durations of the flash fire exposure before the human skin can get second and third degree burns.

3.4. RESULTS AND DISCUSSION

The thermo-physical/geometrical properties of the fabric utilized in the computations are listed in Table 3-1. The radiation parameters used in the computations, which are given by Torvi [3], are listed in Table 3-2. The thermo-physical/geometrical properties of the human skin, which are given by Torvi and Dale [16], are listed in Table 3-3. Thermal properties of the flame and the ambient air, and the initial data of the fabric and the air gap are listed in Table 3-4.

Table 3-1 Thermo-physical/geometrical properties of the fabric

Property	Outer Shell: Kombat™ 7.5 oz/yd^2	Moisture Barrier: ComfortZone™	Thermal Liner: Aralite®
ρ_{ds} [kg m^{-3}]	1384	1295	1380
$(c_p)_{ds}$ [J kg^{-1} K^{-1}]	1420	1325	1200
k_{ds} [W m^{-1} K^{-1}]	0.179	0.144	0.130
L [m]	0.56×10^{-3}	0.73×10^{-3}	1.66×10^{-3}
ε_{ds}	0.334	0.186	0.115
R_f	0.084	0.038	0.045
τ	1.50	1.25	1.00
D_{solid} / d_f^2 [s^{-1}]	2.34×10^{-2}	2.34×10^{-2}	2.34×10^{-2}

Table 3-2 Radiation parameters

Property	Fabric	Flame	Skin
$\widetilde{\varepsilon}$	0.9	0.02	0.94
$\widetilde{\tau}$	0.01	-	-

Table 3-3 Thermo-physical/geometrical properties of the human skin and blood

Property	Epidermis	Dermis	Subcutaneous	Blood
ρ [kg m^{-3}]	1200	1200	1000	1060
c_p [J kg^{-1} K^{-1}]	3600	3400	3060	3770
k [W m^{-1} K^{-1}]	0.255	0.523	0.167	-
L [m]	8×10^{-5}	2×10^{-3}	1×10^{-2}	-
ω_b [m^3 s^{-1} m^{-3}]	-	-	-	1.25×10^{-3}
T_{art} [°C]	-	-	-	37.0
$T_{skin}\big\|_{x=L_{fab}+L_{gap}}$ [°C]	34.0	-	-	-

Table 3-4 The initial conditions for the fabric and the air gap of the TPP test, and the thermal properties of the flame and the ambient air

$T_{0,fab}$ [°C]	40.0
$\phi_{0,fab}$	0.65
$\phi_{0,gap}$	0.65
ϕ_{amb}	0.65
T_g [°C]	1000
$h_{m,gap}$ [m s^{-1}]	0.021
$h_{m,amb}$ [m s^{-1}]	0.021
T_{amb} [°C]	30.0
p_γ [N m^{-2}]	1.01325×10^5
L_{gap} [m]	6.35×10^{-3}
$h_{c,fl}$ [W m^{-2} K^{-1}]	120.0

3.4.1. Model Validation and Comparison with TPP Tests

Consider a multi-layer protective garment subjected to a high intensity flash fire exposure in the Thermal Protective Performance (TPP), ASTM D 4108-87, test configuration [17] shown in the Figure 3-3. This garment consists of three different fabric layers, which are the outer shell, the moisture barrier, and the thermal liner, respectively from the exterior to the interior of the clothing ensembles. The shell fabric of the garment system is Kevlar®/PBI 7.5 oz/yd^2, moisture barrier is ComfortZone™ and thermal liner is Aralite®. The tests were performed with and without air gap. An air gap between the fabric inner surface and the temperature sensor can exist. The nominal thickness of the air gap for the standard TPP test is 0.00635 m (1/4"). The flame temperature, T_g, is 1500°C and the heat transfer coefficient between the flame and fabric, $h_{c,fl}$, is 54 W m^{-2} K^{-1}. The initial temperatures of the ambient (T_{amb}), fabric ($T_{0,fab}$), and sensor ($T_{0,sens}$) are 26°C, 26°C, and 28°C, respectively. The initial relative

humidities of the ambient (ϕ_{amb}), fabric ($\phi_{0,fab}$), and air gap ($\phi_{0,gap}$) are 68%. The interfacial conductance between the thermal line (Aralite®) and a sensor is 40 W m^{-2} K^{-1}.

For modeling the thermal response of firefighter protective clothing exposed to flash fire in TPP tests, the convective heat transfer in the air gap between the fabric and the sensor is simulated as a natural convection in a horizontal enclosure, which is heated from below. Hollands et al. [18] gave the correlation for air in a horizontal enclosure heated from below as:

$$Nu = 1 + 1.44\left[1 - \frac{1708}{Ra}\right]^{\circ} + \left[\left(\frac{Ra}{5830}\right)^{\frac{1}{3}} - 1\right]^{\circ} \qquad (3.42)$$

The notation $[\ \ ]^{\circ}$ in the above equation indicates that if the argument in the square brackets is negative, the quantity should be taken as zero.

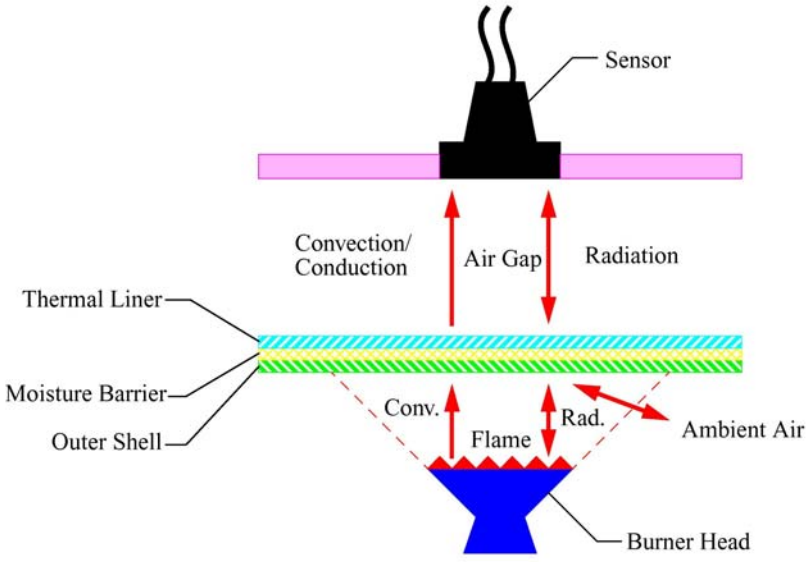

Figure 3-3 Schematic diagram of heat and moisture transport in the protective clothing and the sensor for TPP test configuration

Figure 3-4(a) and (b) show the comparisons of computational and experimental results of the temperature and heat flux histories at the surface of the sensor for 3-layer clothing systems with air gap configuration, respectively.

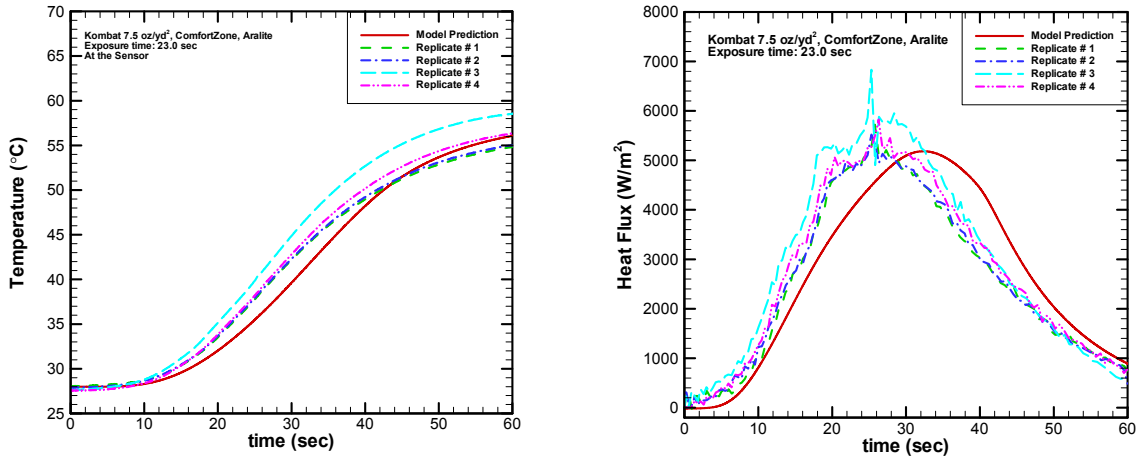

(a) (b)

Figure 3-4 (a) Comparison of computational and experimental results of the temperature histories at the surface of the sensor for 3-layer system with air gap, (b) Comparison of computational and experimental results of the heat flux histories at the surface of the sensor for 3-layer system with air gap

Figure 3-5(a) and (b) show the comparisons of computational and experimental results of the temperature and heat flux histories at the surface of the sensor for 3-layer clothing systems with air gap configuration, respectively. Both computational temperature and heat flux histories at the surface of the sensor demonstrate a good agreement with the experimental data.

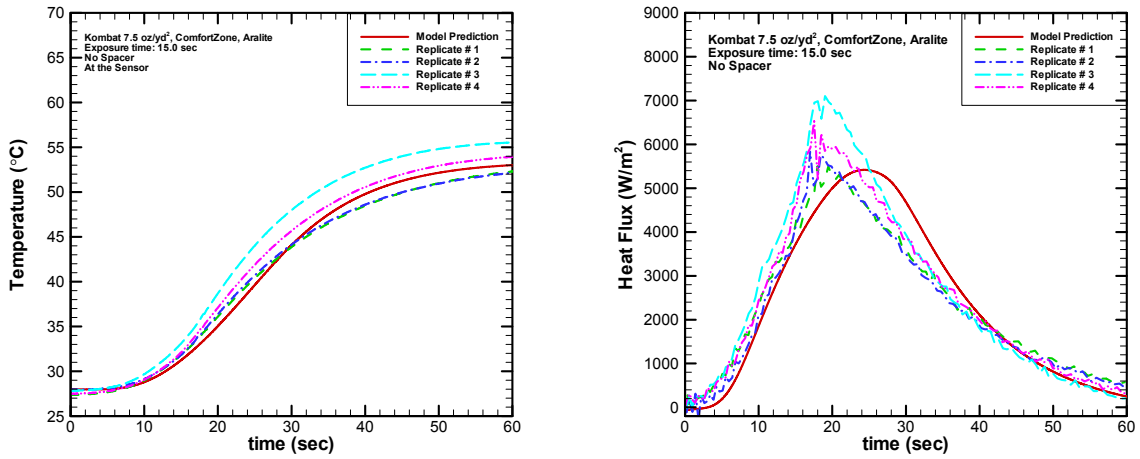

(a) (b)

Figure 3-5 (a) Comparison of computational and experimental results of the temperature histories at the surface of the sensor for 3-layer system with air gap, (b) Comparison of computational and experimental results of the heat flux histories at the surface of the sensor for 3-layer system without air gap

3.4.2. Model Prediction of Thermal Protective Clothing and Skin under Fire Exposure

Computations are performed for the duration of a flash fire exposure of 4 seconds. After the fire is off, computations continue until the time reaches 60 seconds. The temperature of the hot gas and the ambient temperature gradually decrease after 4 seconds of burning. Figure 3-6 depicts the temperature distributions in the fabric at different moments of time. The x coordinate in this figure (and in Figs. 3-7 to 3-11) shows the distance from the outer surface of the fabric (the surface that is exposed to fire). The temperature at the outer surface of the fabric increases very fast compared to that at the inner surface of the fabric while the garment is exposed to the intensive flash fire. In the same manner, the temperature at the outside surface of the fabric reduces very fast compared to that at the inside surface of the fabric during the cool-down phase of the process (after the burn).

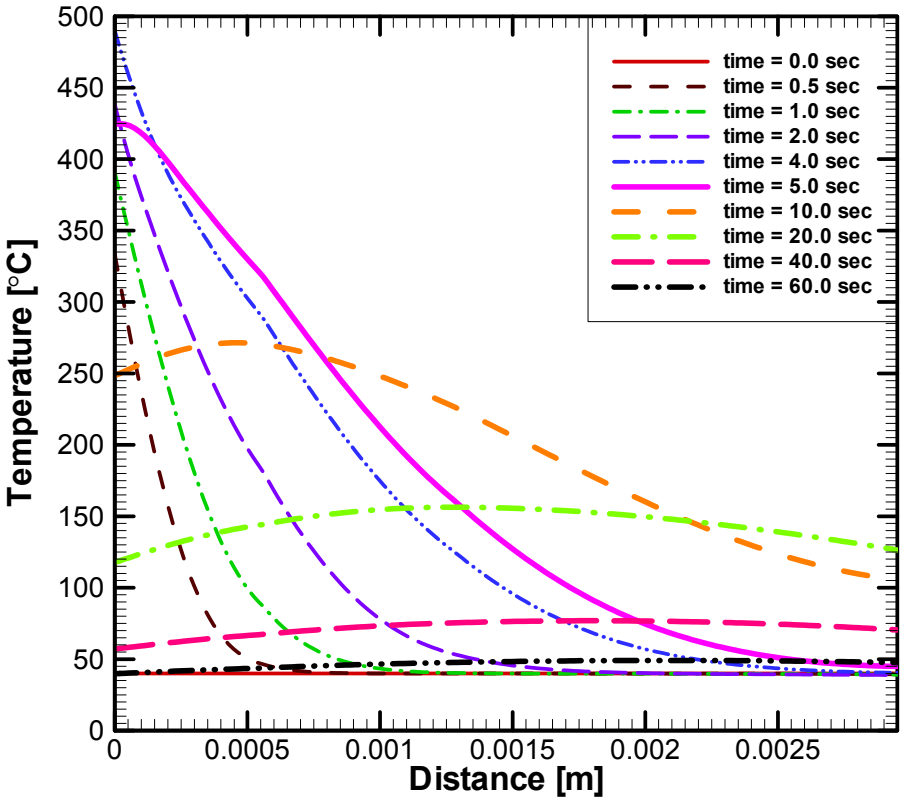

Figure 3-6 Temperature distributions in the fabric at different moments of time

Figure 3-7 displays the temperature distributions in the human skin and tissue at different moments of time. The origination point of the *x*-axis is at the outer surface of the fabric, the *x*-axis is directed inside the human tissue. According to Tables 3-1 and 3-4, the first skin layer begins at the distance of 0.0093 m from the outer surface of the fabric. The skin temperature keeps increasing even when the fire is off. This is because of the energy accumulated within the fabric and the air gap during the fire exposure. Therefore, skin burns may occur not only during the flash fire exposure, but also after the exposure because of the heat accumulated in the garment.

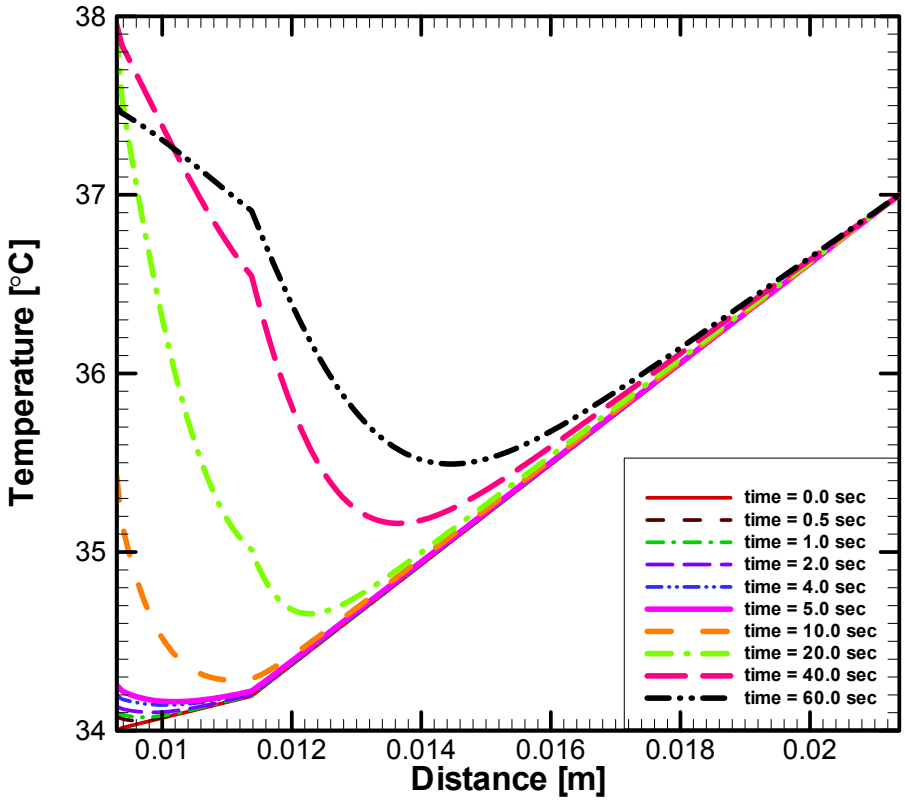

Figure 3-7 Temperature distributions in the human skin and tissue at different moments of time

Figure 3-8 shows distributions of the fiber regain in the fabric at different moments of time. Figure 3-9 illustrates distributions of the moisture content in the fabric at different moments of time. The regain is defined as the ratio of the mass of absorbed water in the fabric to the mass of dry fabric. Similarly, the moisture content is defined as the ratio of the mass of absorbed water in the fabric to the mass of wet fabric. Therefore, by their definitions, both the fiber regain and the moisture content are related, hence both graphs have the same trend. The garment is in the equilibrium state at the beginning. However, the difference in properties of the three fabric layers may cause the jumps in the fiber regain and the moisture

content at the interfaces and these may be seen in Figs. 3-8 and 3-9. Both the fiber regain and the moisture content in the fabric decrease during the 4-second flash fire exposure and they still keep decreasing until they reach their minimum values, which correspond to an equilibrium state at those temperature and humidity conditions. If the cooling time is long enough, both fiber regain and moisture content in the fabric will go back to what they were at the initial state.

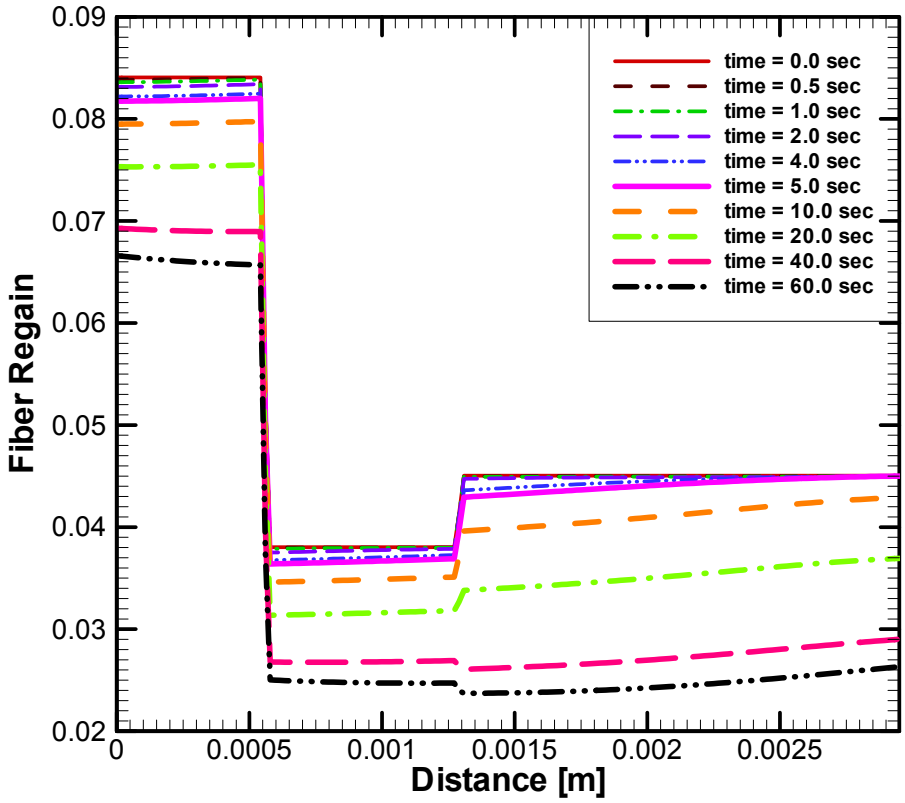

Figure 3-8 Distributions of the fiber regain in the fabric at different moments of time

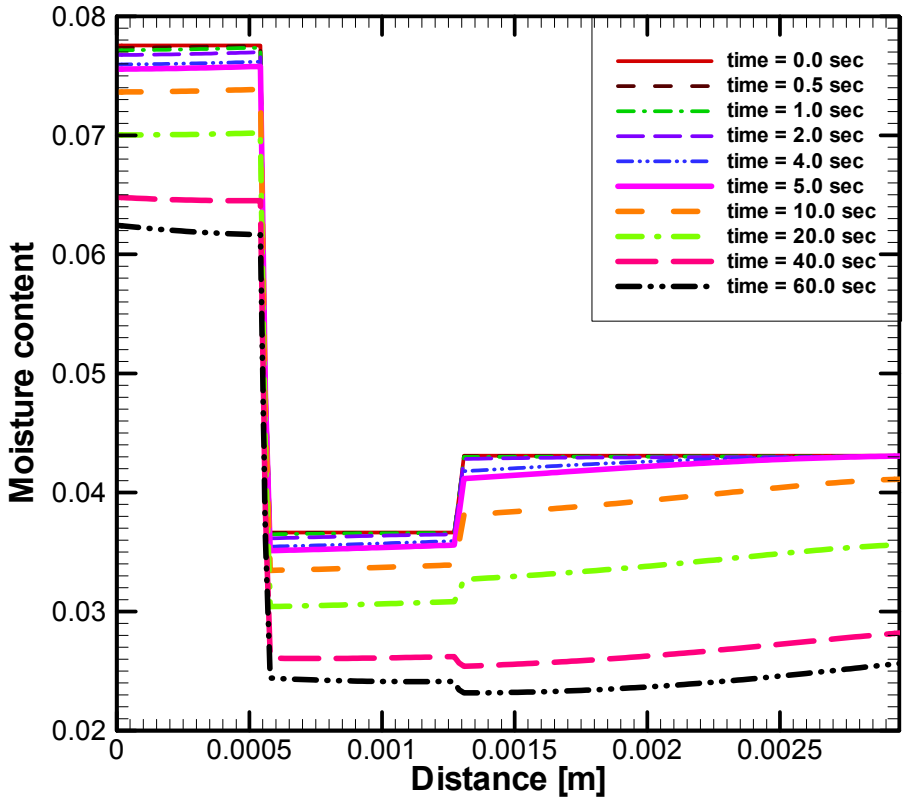

Figure 3-9 Distributions of the moisture content in the fabric at different moments of time

Figure 3-10 shows distributions of the relative humidity in the fabric at different moments of time. The relative humidity in the outer layer of garment drops very fast when it is exposed to the flash fire. In the latter layers of the garment, the relative humidity increases. This means that the moisture is pushed from the outside fabric layer to the inside fabric layer and then into the air gap because of the temperature gradient. After the temperatures at the outer surface and the inner surface of the fabric become low enough, the relative humidity starts growing back to its initial distribution.

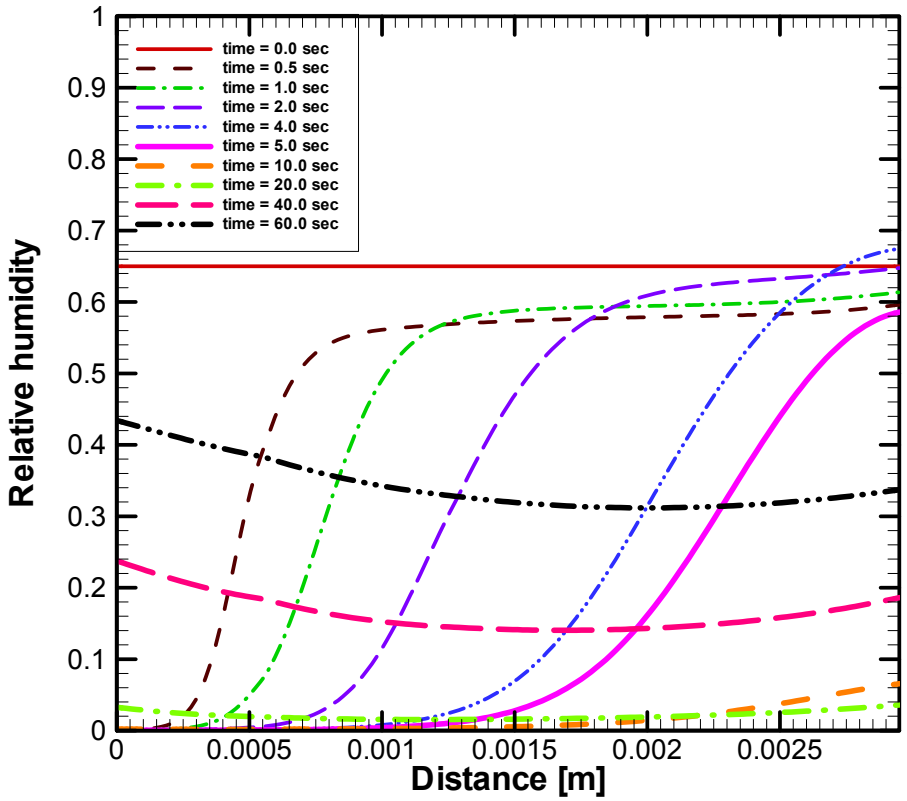

Figure 3-10 Distributions of the relative humidity in the fabric at different moments of time

Figure 3-11 depicts distribution of the vapor density in the fabric at different moments of time. The vapor density increases because the temperature increases and causes the phase transition from the bound water to the free water and then to the water vapor. In addition, Fig. 3-11 shows that the moisture moves from the outer shell to the moisture barrier and then to the thermal liner (cf. Fig. 3-1) because of the temperature gradient.

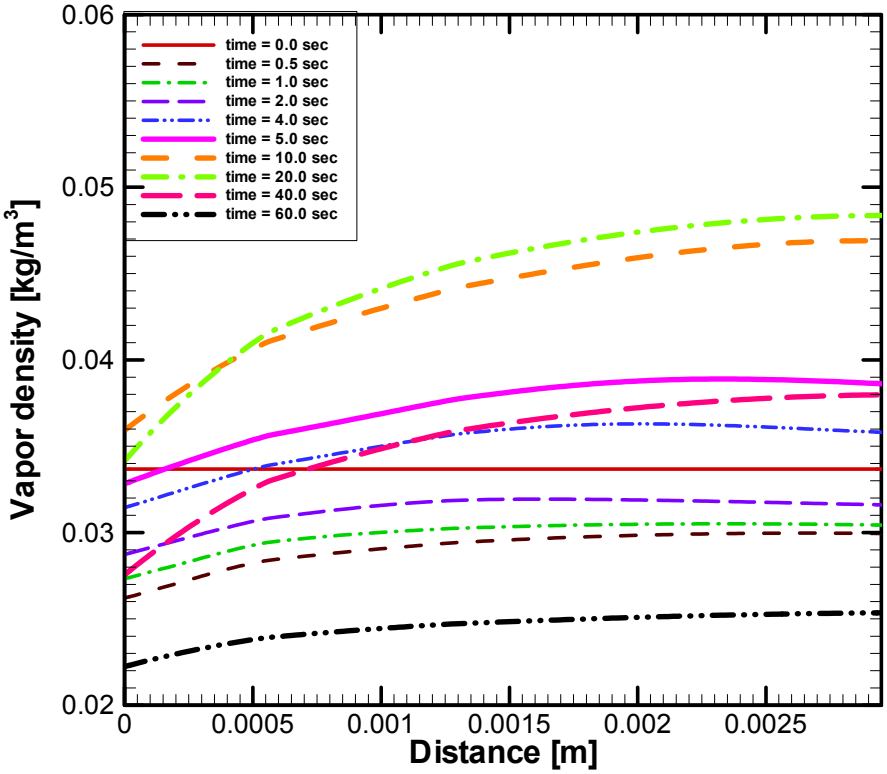

Figure 3-11 Distributions of the vapor density in the fabric at different moments of time

Figure 3-12 shows the calculated fabric weight per unit area versus time. The fabric weight decreases because the fabric loses the moisture to the air gap. Figure 3-13 displays the calculated vapor density in the air gap versus time. The vapor density in the air gap increases because the air gap gains the moisture from the fabric. However, the vapor density will decrease and the fabric weight will increase when the temperature in the garment is again low enough, which will cause the moisture transport to go backwards. Figure 3-14 presents the calculated relative humidity in the air gap versus time. Because the relative temperature increase is slower than the relative moisture density increase, one can see that the relative humidity in the air gap increases slightly and then drops rapidly. When the temperature

increases, the saturation pressure also increases. Therefore, the relative humidity in the air gap reduces even though the moisture content in the air gap increases.

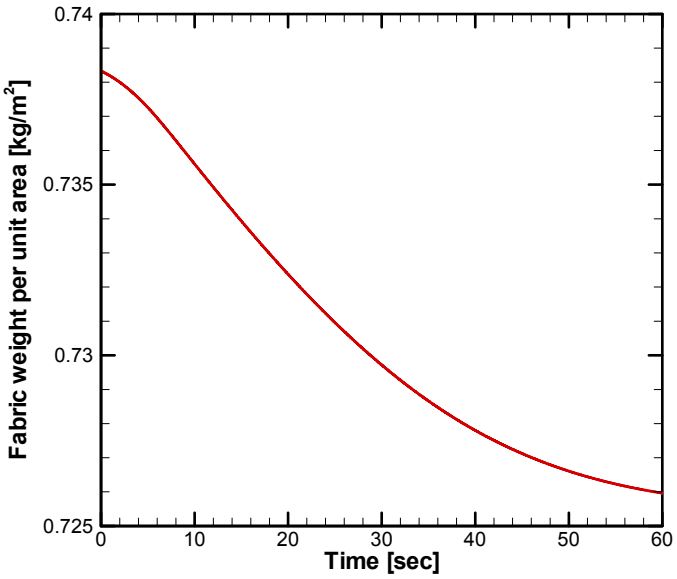

Figure 3-12 Calculated fabric weight per unit area versus time

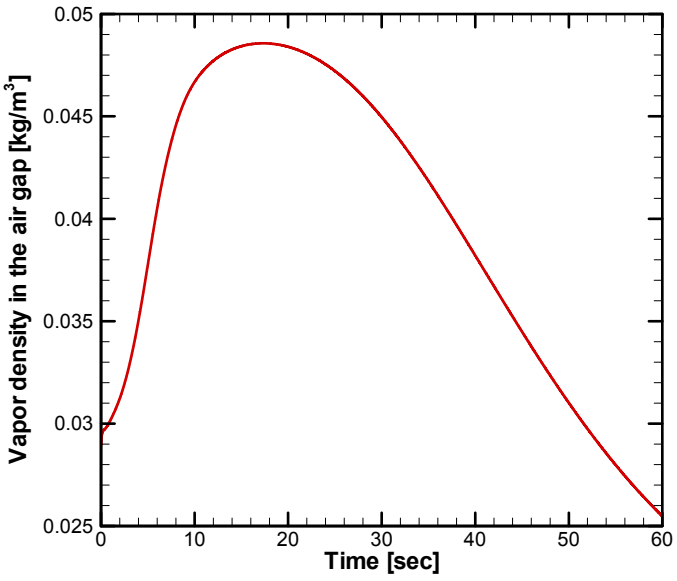

Figure 3-13 Calculated vapor density in the air gap versus time

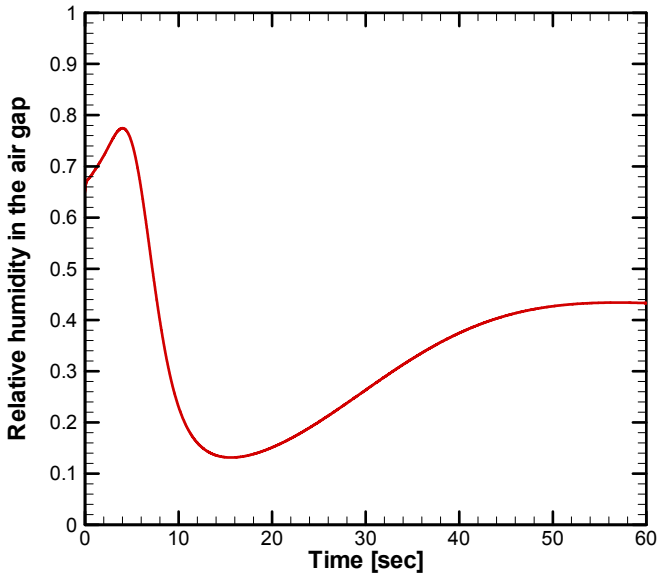

Figure 3-14 Calculated relative humidity in the air gap versus time

The thickness of the air gap between the garment and the body depends on the particular location on the human body. Table 3-5 shows that the maximum air gap occurs for the leg and the minimum air gap occurs for the shoulder. These values of the air gaps are based on representative scans performed by Song [19]. The maximum durations of the flash fire exposure before the human skin gets second and third degree burns at different locations on the human body are given in Table 3-5. This table shows that the distribution of the air gap thickness affects the maximum durations of the flash fire exposure before getting the second and third degree burns.

Table 3-5 Maximum durations of the flash fire exposure before getting the second and third degree burns at different locations on the human body

Location	Air gap thickness (mm)	Maximum exposure time for second degree burn (sec)	Maximum exposure time for third degree burn (sec)
TPP test	6.35 (or 1/4")	19.13	36.45
Arm	6.58	19.21	36.58
Front	10.21	19.63	37.31
Back	5.93	18.97	36.20
Leg	18.50	19.78	37.51
Shoulder	1.60	14.92	29.83

3.5. CONCLUSIONS

The coupled heat and moisture transport in firefighter protective clothing during flash fire exposure is investigated numerically. It is shown that the obtained comprehensive model of heat and moisture transport can be used to estimate the thermal response of protective fabric. The distributions of temperature and moisture content in the fabric and the human skin during flash fire exposure can be obtained. Maximum durations of the flash fire exposure exceeding, which would result in the second-degree burn and the third degree burn, can also be predicted.

ACKNOWLEDGEMENTS

The support provided by the National Textile Center is gratefully acknowledged. Helpful discussions with Profs. R. L. Barker, H. Hamouda, and Drs. D. B. Thomson and G. Song are greatly appreciated.

REFERENCES

1 K. Vafai and M. Sözen, "A comparative analysis of multiphase transport models in porous media", *Ann. Rev. Heat Transfer*, vol. 3, pp. 145-162, 1990.

2 P. W. Gibson, "Multiphase heat and mass transfer through hygroscopic porous media with applications to clothing materials", *Technical Report Natick/TR-97/005*, U.S. Army Natick Research, Development, and Engineering Center, Natick, MA, 1996.

3 D. A. Torvi, "Heat transfer in thin fibrous materials under high heat flux conditions", *Ph.D. Thesis. University of Alberta*, Edmonton, Alberta, Canada, 1997.

4 H. H. Pennes, "Analysis of tissue and arterial blood temperatures in resting human forearm", *J. Appl. Physiol.*, vol. 1, pp. 93-122, 1948.

5 F. C. Jr. Henriques and A. R. Moritz, "Studies of thermal injuries I: The conduction of heat to and through skin and the temperatures attained therein. A theoretical and experimental investigation", *Am. J. Pathol.*, vol. 23, pp. 531-549, 1947.

6 S. Whitaker, "Simultaneous heat, mass, and momentum transfer in porous media: A theory of drying", *Adv. Heat Transfer*, vol. 13, pp. 119-203, 1977.

7 W. Morton and J. Hearle, *Physical Properties of Textile Fibres*. The Textile Institute, Manchester, UK, 1993.

8 I. Catton, "Natural convection in enclosures", *Proceedings of the 6th International Heat Transfer Conference, Toronto*, vol. 6, pp. 13-31, 1978.

9 V. E. Denny and R. M. Clever, "Comparisons of Galerkin and finite difference methods for solving highly nonlinear thermally driven flows", *J. Comput. Phys.*, vol. 16, pp. 271-284, 1974.

10 J. A. Weaver and A. M. Stoll, "Mathematical model of skin exposed to thermal radiation", *Aerospace Medicine*, vol. 40, pp. 24-30, 1969.

11 A. N. Takata, J. Rouse, and T. Stanley, "Thermal analysis program", *I.I.T. Research Institute Report IITRI-J6286*, Illinois Institute of Technology, Chicago, IL, 1973.

12 S. V. Patankar, *Numerical Heat Transfer and Fluid Flow*, Taylor & Francis, Philadelphia, PA, 1980.

13 J. C. Tannehill, D. A. Anderson, and R. H. Pletcher, *Computational Fluid Mechanics and Heat Transfer*, 2nd Ed., Taylor & Francis, Philadelphia, PA, 1997.

14 Z. Li, "The immersed interface method – A numerical approach for partial differential equations with interfaces", *Ph.D. Thesis, University of Washington*, Seattle, WA, 1994.

15 Z. Li, "An overview of the immersed interface method and its applications", *Taiwanese J. Mathematics*, vol. 7, pp. 1-49, 2003.

16 D. A. Torvi, and J. D. Dale, "A finite element model of skin subjected to flash fire", *J. Biomech. Eng.*, vol. 116, pp. 250-256, 1994.

17 American Society for Testing and Materials, *ASTM D 4108-87, Standard Test Method for Thermal Protective Performance of Materials for Clothing by Open-Flame Method*, West Conshohocken, PA, 1987.

18 K. G. T. Hollands, T. E. Unny, G. D. Raithby, and L. Konicek, "Free convective heat transfer across inclined air layers", *J. Heat Transfer*, vol. 98, pp. 189-193, 1976.

19 G. Song, "Modeling thermal protective outfits for fire exposures", *Doctoral Dissertation, North Carolina State University*, Raleigh, NC, 2002.

4. A POROUS MEDIUM MODEL FOR INVESTIGATING TRANSIENT HEAT AND MOISTURE TRANSPORT IN FIREFIGHTER PROTECTIVE CLOTHING UNDER HIGH INTENSITY THERMAL EXPOSURE

ABSTRACT

The aim of this study is to understand the performance of firefighter protective clothing in preventing thermal injury of skin that may result from exposure to high intensity thermal radiation. A mathematical model is developed to study transient heat and moisture transport through multi-layer fabric assemblies. The model accounts for changes in thermo-physical and transport properties of the fabric due to the presence of moisture. Numerical simulations are performed to study heat and moisture transport in wet fabrics that are subjected to intensive flash fire exposure. The numerical solutions are further analyzed to provide a detailed physical understanding of the transport processes. Moisture in the fabric tends to vaporize starting from the outside surface of the fabric to the inside surface of the fabric during heating, and then part of it recondenses in the interior of the fabric during the cool-down. It is observed that the temperature distribution in the fabric layers and the total heat flux to the skin are significantly influenced by the amount of moisture and the distribution of the moisture in the protective clothing.

NOMENCLATURE

A surface area [m^2]

a empirical coefficient for the capillary pressure defined in Eq. (4.25) [Pa]

a_s specific surface area per unit volume [m^{-1}]

b empirical constant for the capillary pressure defined in Eq. (4.25)

c_p specific heat at constant pressure [J kg^{-1} K^{-1}]

D_a diffusivity of the water vapor in the air [m^2 s^{-1}]

D_{eff} effective diffusivity of the gaseous phase in the fabric [m^2 s^{-1}]

D_f diffusivity of the bound water in the solid phase [m^2 s^{-1}]

d_f average fiber diameter [m]

F view factor

g gravitational acceleration [9.81 m s^{-2}]

h_c convective heat transfer coefficient [W m^{-2} K^{-1}]

h_m convective mass transfer coefficient of the water vapor [m s^{-1}]

K Darcian permeability coefficient [m^2]

k thermal conductivity [W m^{-1} K^{-1}]

L thickness [m]

Le Lewis number, $Le = \alpha_{eff} / D_{eff}$

M_w molecular weight [kg $kmol^{-1}$]

$\dot{m}_{gl}$ mass transfer rate from the gaseous phase to the liquid phase [kg m^{-3} s^{-1}]

$\dot{m}_{gs}$ mass transfer rate from the gaseous phase to the solid phase [kg m^{-3} s^{-1}]

$\dot{m}_{ls}$ mass transfer rate from the liquid phase to the solid phase [kg m^{-3} s^{-1}]

Nu Nusselt number, $Nu = h_c L / k$

P pressure [Pa]

$q''_{cond/conv,airgap}$ heat flux by conduction/convection from the inner surface of the fabric to the human skin across the air gap [W m^{-2}]

$q''_{conv,fl}$ convective heat flux from the flame to the outer surface of the fabric [W m^{-2}]

$q''_{rad,airgap}$ heat flux by radiation from the inner surface of the fabric to the human skin across the air gap [W m^{-2}]

$q''_{rad,fl}$ incident radiation heat flux from the flame onto the outer fabric surface [W m^{-2}]

R_f fiber regain

R_u universal gas constant [8.315×10^3 J $kmol^{-1}$ K^{-1}]

Ra Rayleigh number, $Ra = g\beta\Delta TL^3/\alpha\nu$

s saturation defined in Eq. (4.24)

T temperature [K]

t time [s]

v velocity [m s^{-1}]

x linear coordinate across the fabric [m]

Greek symbols

α thermal diffusivity [m^2 s^{-1}]

β thermal expansion coefficient [K^{-1}]

Δh_{diff} enthalpy of transition from the bound water to the free liquid water [J kg^{-1}]

Δh_{vap} enthalpy of evaporation per unit mass [J kg^{-1}]

ε volume fraction

$\tilde{\varepsilon}$ emissivity

ϕ relative humidity

γ radiative extinction coefficient of the fabric [m^{-1}]

γ_{ls} proportionality constant related to the rate of absorption of the liquid water by a fiber [kg m^{-3}]

μ dynamic viscosity [kg m^{-1} s^{-1}]

ν kinematic viscosity [m^2 s^{-1}]

ρ density [kg m^{-3}]

σ Stefan-Boltzman constant [5.670×10^{-8} W m^{-2} K^{-4}]

τ fabric tortuosity

$\tilde{\tau}$ transmissivity of the fabric

ω_{blood} blood perfusion [0.00125 m^3 s^{-1} m^{-3} tissue]

Subscripts

0 initial state

a dry air

airgap air gap

amb ambient air

arterial arterial

b bound water

blood blood

c capillary

cond condensation

eff effective

eq equilibrium

evap evaporation

f dry fiber

fab fabric

fl flame

g gaseous phase

ir irreducible

l free liquid water

s solid phase

sat saturation

skin skin

tissue tissue

v water vapor

Superscript

cr critical

4.1. INTRODUCTION

During fire extinguishing, firefighters are subjected to a variety of fire conditions. Firefighters can get burns that result from the radiant energy that is produced by the fire as well as from the localized contact flame exposure. Firefighters working in these conditions, often sweat profusely, which leads to accumulation of moisture in the turnout gear. In

addition, firefighters may also be exposed to the dousing water from a hose spray. The presence of moisture in the protective clothing can significantly change the fabrics' protective performance. Normally, wet garments can absorb more heat than dry garments. Evaporation, condensation, and absorption of the moisture and the energy associated with phase change can affect the temperature and energy flux to the skin. A numerical analysis is a valuable tool for studying heat and moisture transport through the thermal protective clothing of a firefighter, because it may help in preventing skin burn injuries and in designing a new protective turnout gear.

Vafai [1] investigated thermal performance of fibrous insulations subjected to different types of humid environments. The energy equation, equations of motion for the liquid and gas phases, continuity equations for the liquid and gas phases, the gas phase diffusion equation, and the pertinent thermodynamic relations were used to analyze the multiphase transport through the porous insulation slab accounting for heat conduction, natural convection, phase change, and gas infiltration. In addition, the humidity, temperature, and pressure differences across the insulation, and the thickness of the insulation matrix were parametrically studied.

A protective fabric can be treated as a porous medium. Heat and mass transport in wet porous media are coupled in a complicated way. Energy transport in such a medium occurs by radiation and conduction in all phases as well as by convection within the liquid and gas phases. The structure of the solid matrix varies widely. In general, there is a distribution of void sizes. In an unsaturated state, these voids are partly filled with liquid, whereas the rest of the voids contain air and water vapor. Evaporation or condensation occurs at the interface between the liquid water and air; the moisture content affects the effective thermal conductivity and volumetric heat capacity of the fabric. The vapor can move in the gas phase

by diffusion from regions where the partial pressure of the vapor is higher to those where it is lower. Moreover, the liquid can also move due to the capillary force.

A significant amount of work has been done in the area of multiphase transport in porous media. Vafai and Sözen [2] summarized and compared different published models. Vafai and Whitaker [3] used the local volume-averaging technique to obtain a fundamental formulation of heat and mass transfer processes accompanied by phase change in an insulation material. Gibson [4] performed the analysis of multiphase transport in hygroscopic porous textiles. Le et al. [5] developed a comprehensive model of heat and mass transfer during the steaming of fabric beds made of different fiber types. Vafai and Sarkar [6] analyzed the moisture accumulation and the effective thermal conductivity of a fibrous insulation slab due to moisture migration based on the assumption that there is no absorbed liquid water. The problem was modeled as a transient multiphase flow with variable properties in a porous slab. The influences of different humidity levels, condensation rate, temperature, liquid content, and vapor density were investigated. Sözen and Vafai [7] developed the two-phase model of the transient flow of a vapor and a non-condensable gas through a porous medium assuming thermal non-equilibrium between the solid and the gas phases.

Torvi [8] suggested a one-dimensional transient heat transfer model, which accounts for the radiation penetrating into a fabric up to a certain depth (this approach assumes that the fabric is semi-transparent to thermal radiation). Prasad et al. [9] performed a numerical study of transient heat and water vapor transport through wet thermal liners and turnout coat ensemble when subjected to a radiative heat flux. Results were compared with experimental data and were found to be in good agreement. Barry et al. [10] developed models based on computational fluid dynamics to predict the performance of protective clothing materials.

Chitrphiromsri and Kuznetsov [11] investigated the effect of coupled heat and moisture transport on the protective performance of the firefighter protective garment during a flash fire exposure. The major limitation of Chitrphiromsri and Kuznetsov's previous work is the assumption that there is no free water; Chitrphiromsri and Kuznetsov [11] assumed that if there is any extra liquid, it is immediately absorbed by the fabric fibers and becomes the bound water.

The purpose of this work is to lift this limitation and develop a comprehensive model that accounts for the moisture transport in all three possible phases, namely, the bound water, free liquid, and water vapor. Simulations of heat and moisture transport are performed for a realistic multi-layer protective clothing configuration subjected to a high intensity thermal radiation. The effect of moisture transport on thermal protective performance is investigated in detail in this paper. The skin model (Pennes [12]) is used to predict the skin burn injury. The burn injury evaluation is based on the work by Henriques and Moritz [13].

4.2. FORMULATION OF THE PROBLEM

Consider a multi-layer protective garment subjected to high intensity radiation from a flash fire exposure. This garment consists of three different fabric layers, which are the outer shell, the moisture barrier, and the thermal liner, respectively, counting from the exterior to the interior of the clothing garment. The human skin can also be divided into three different layers, namely, the epidermis, dermis, and subcutaneous. The air gap between the fabric inner surface and the surface of the skin is usually present and it plays an important role in insulating the skin from the intensive thermal exposure. A schematic diagram of this problem is shown in Figure 4-1(a). The fabric can be modeled as a hygroscopic porous media. The

porous textile material is a mixture of a solid phase consisting of solid fibers plus the bound water absorbed by the solid polymer matrix, a liquid phase consisting of a free liquid water, and a gaseous phase consisting of the water vapor and the dry air. A schematic diagram of porous textile structure is illustrated in Figure 4-1(b).

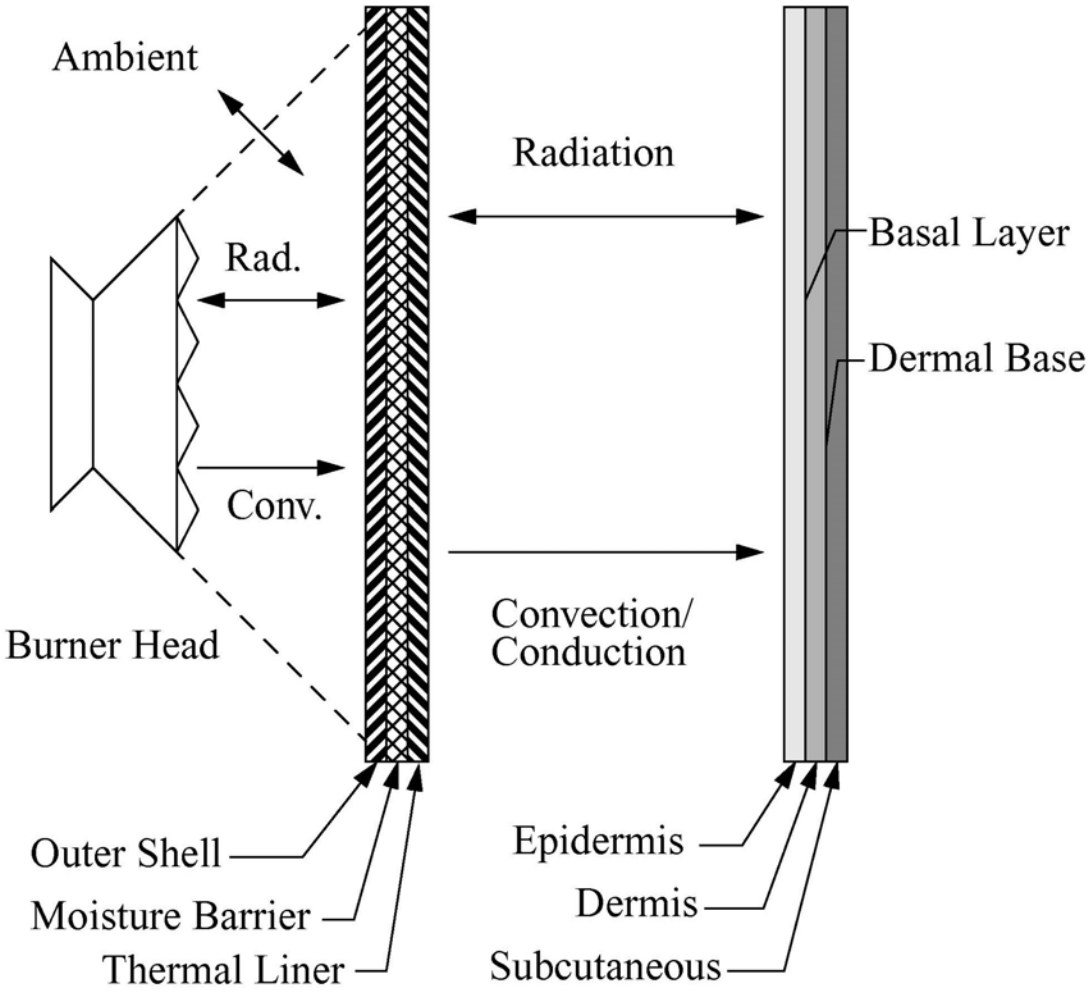

(a)

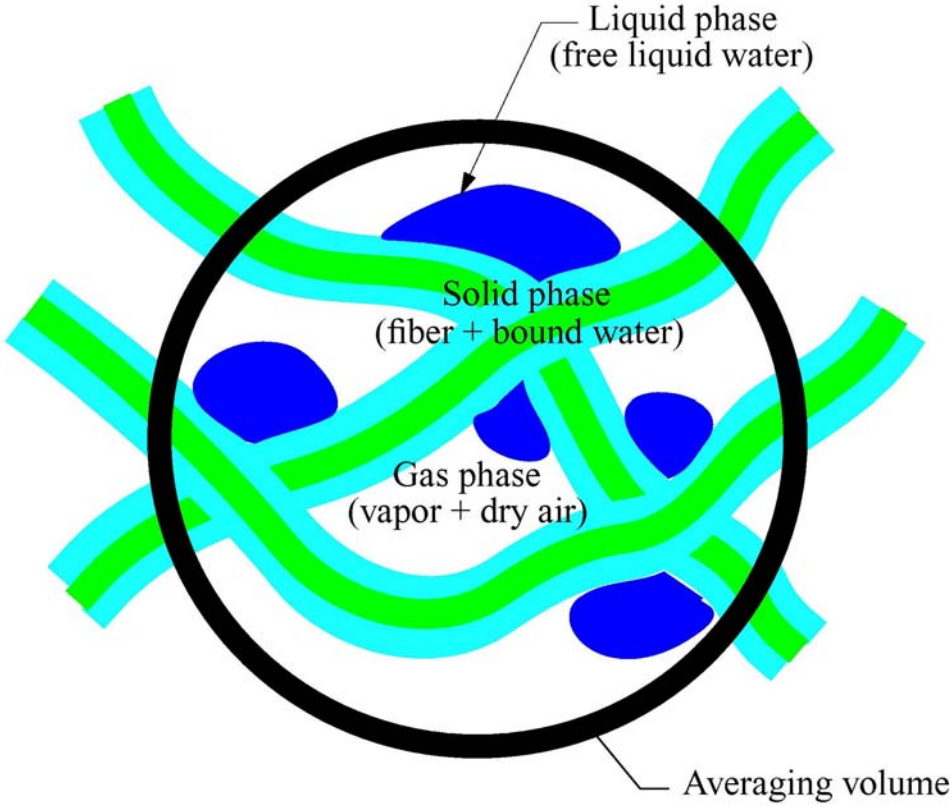

(b)

Figure 4-1 (a) Schematic diagram of heat and moisture transport in the protective clothing and the human skin, (b) Schematic diagram of a porous textile structure

The gas phase is assumed to obey the ideal gas equation. The flow is assumed to be one-dimensional. The natural convection and gravitational effects are ignored. All phases are assumed to be in thermal and phase equilibrium. The mathematical formulation of this work is based on the method of local volume averaging described in Whitaker [14]. Whitaker's theory is utilized to derive the set of governing equations for modeling coupled heat and moisture transport through a hygroscopic porous textile material. In addition, Torvi's work [8] is used to estimate radiative heat flux that penetrates through the fabric up to a certain depth.

In order to account for the variation in fiber properties with the amount of moisture in the fabric, the fibers and bound water are assumed to form a homogenous medium. The intrinsic density and volume fraction of dry fibers do not vary; therefore, the continuity equation for the solid phase can simply be expressed as:

$$\frac{\partial}{\partial t}\left(\rho_b \varepsilon_b\right) = \dot{m}_{ls} + \dot{m}_{gs} \tag{4.1}$$

where t is the time, ρ_b is the density of the bound water, ε_b is the volume fraction of the bound water, $\dot{m}_{ls}$ is the rate of mass transfer from the liquid phase to the solid phase, and $\dot{m}_{gs}$ is the rate of mass transfer from the gaseous phase to the solid phase.

The mass transfer rate of the liquid water to the absorbing fiber, $\dot{m}_{ls}$, is given by Le et al. [5] as:

$$\dot{m}_{ls} = h_m a_s \gamma_{ls} \frac{\varepsilon_l}{\varepsilon_l^{cr}} \left(\frac{R_{f,eq}}{R_f} - 1 \right) \tag{4.2}$$

where h_m is the convective mass transfer coefficient of the water vapor, a_s is the specific surface area per unit volume, γ_{ls} is a proportionality constant related to the rate of absorption of the liquid water by a fiber, ε_l is the volume fraction of the free liquid water, ε_l^{cr} is the critical value of the liquid fraction at which the liquid phase becomes mobile, $R_{f,eq}$ is the equilibrium fiber regain at the fiber surface, and R_f is the instantaneous fiber regain.

The convective mass transfer coefficient of the water vapor, h_m, is related to the convective heat transfer coefficient, h_c, utilizing the Chilton-Colburn analogy (Holman [15]; Cussler [16]):

$$h_m = \frac{h_c}{\left(\rho c_p\right)_g Le^{\frac{2}{3}}} \tag{4.3}$$

where h_c is the convective heat transfer coefficient, ρ_g is the density of the gaseous phase, $\left(c_p\right)_g$ is the specific heat of the gas phase, and Le is the Lewis number.

The density of the gaseous phase, ρ_g, is given as:

$$\rho_g = \rho_v + \rho_a \tag{4.4}$$

where ρ_v is the density of the water vapor and ρ_a is the density of the dry air.

The specific heat of the gas phase, $\left(c_p\right)_g$, is calculated as:

$$\left(c_p\right)_g = \frac{\left[\rho_v\left(c_p\right)_v + \rho_a\left(c_p\right)_a\right]}{\rho_g} \tag{4.5}$$

where $\left(c_p\right)_v$ is the specific heat of the water vapor and $\left(c_p\right)_a$ is the specific heat of the dry air.

The Lewis number, Le, is defined as:

$$Le = \frac{\alpha_{eff}}{D_{eff}} \tag{4.6}$$

where α_{eff} is the effective thermal diffusivity of the water vapor in the fabric and D_{eff} is the diffusivity of the gas phase in the fabric.

The effective thermal diffusivity of the water vapor in the fabric, α_{eff}, is defined as:

$$\alpha_{eff} = \frac{k_{eff}}{\rho_v (c_p)_v} \tag{4.7}$$

where k_{eff} is the effective thermal conductivity of the fabric.

The effective thermal conductivity of the fabric, k_{eff}, which is originally given by Progelhof et al. [17], is calculated as (Gibson [4]):

$$k_{eff} = k_g \left\{ \frac{[1+(\varepsilon_l + \varepsilon_b + \varepsilon_f)]k_s + \varepsilon_g k_g}{\varepsilon_g k_s + [1+(\varepsilon_l + \varepsilon_b + \varepsilon_f)]k_g} \right\} \tag{4.8}$$

where ε_f is the volume fraction of the fiber, ε_g is the volume fraction of the gas phase, k_g is the thermal conductivity of the gas phase, and k_s is the thermal conductivity of the solid phase.

The thermal conductivity of the gas phase, k_g, can be calculated as:

$$k_g = \left(\frac{k_v \rho_v + k_a \rho_a}{\rho_v + \rho_a} \right) \tag{4.9}$$

where k_v is the thermal conductivity of the saturated water vapor and k_a is the thermal conductivity of the dry air.

The thermal conductivity of the solid phase, k_s, can be calculated as:

$$k_s = \left(\frac{k_l \rho_l \varepsilon_l + k_b \rho_b \varepsilon_b + k_f \rho_f \varepsilon_f}{\rho_l \varepsilon_l + \rho_b \varepsilon_b + \rho_f \varepsilon_f} \right) \tag{4.10}$$

where ρ_l is the density of the free liquid water, ρ_f is the density of the dry fiber, k_l is the thermal conductivity of the free liquid water, k_b is the thermal conductivity of the bound water, and k_f is the thermal conductivity of the dry solid.

The effective diffusivity of the gas phase in the fabric, D_{eff}, is defined in Gibson's work [4] as:

$$D_{eff} = \frac{D_a \varepsilon_g}{\tau} \tag{4.11}$$

where D_a is the diffusivity of the water vapor in the air and τ is the fabric tortuosity. The tortuosity of the fabric is the degree of bending or twist of the passage of moisture diffusion due to the bending or twist of fibers in the fibrous insulation. It normally changes between 1.0 and 1.2 (Fan and Wen [18]), depending on the fiber arrangement.

The diffusivity of the water vapor in the air, D_a, is calculated in Gibson [5] as:

$$D_a = 2.23 \times 10^{-5} \left(\frac{T}{273.15} \right)^{1.75} \tag{4.12}$$

where T is the temperature.

The specific surface area per unit volume, a_s, is given in Le et al. [5] as:

$$a_s = \frac{4\varepsilon_s}{d_f} \tag{4.13}$$

where ε_s is the volume fraction of the solid phase and d_f is the average fiber diameter.

The volume fraction of the solid phase can be expressed in terms of the volume fractions of dry fiber and bound water as:

$$\varepsilon_s = \varepsilon_f + \varepsilon_b \tag{4.14}$$

The critical value of the liquid fraction at which the liquid phase becomes mobile, ε_l^{cr}, according to Kaviany and Mittal [19], is assumed to be:

$$\varepsilon_l^{cr} = 0.1\varepsilon_g \tag{4.15}$$

The equilibrium fiber regain at the fiber surface, $R_{f,eq}$, which is a function of the relative humidity, is originally obtained by Lotens and Havenith [20] and then modified by Gibson [4] as:

$$R_{f,eq} = 0.578 \cdot \phi \cdot R_{f,\phi=0.65}\left[\frac{1}{(0.321+\phi)} + \frac{1}{(1.262-\phi)}\right] \tag{4.16}$$

where $R_{f,\phi=0.65}$ is the fiber regain at 65% relative humidity and ϕ is the relative humidity.

The relative humidity, ϕ, is defined as:

$$\phi = \frac{P_v}{P_{sat}} \tag{4.17}$$

where P_v is the partial pressure of the water vapor and P_{sat} is the saturation vapor pressure, which is a function of T only.

The saturation vapor pressure, P_{sat}, is given in Gibson [4] as:

$$P_{sat} = 614.3\exp\left\{17.06\left[\frac{(T-273.15)}{(T-40.25)}\right]\right\} \tag{4.18}$$

The instantaneous fiber regain, R_f, is defined in Morton and Hearle [21] as:

$$R_f = \frac{\varepsilon_b \rho_b}{\varepsilon_f \rho_f} \tag{4.19}$$

The regain difference is the driving force for the mass transfer between the fiber and the vapor. The mass transfer rate of the gaseous phase to the solid phase, $\dot{m}_{gs}$, is given in Le et al. [5] as:

$$\dot{m}_{gs} = \frac{8D_f \rho_f}{d_f^2}\left(R_{f,eq} - R_f\right) \tag{4.20}$$

where D_f is the effective diffusivity of the bound water in the solid phase.

The liquid phase accounts for the condensed water that may accumulate on the fiber surface. If moisture content is sufficiently high, all three phases of water may co-exist. In that case, liquid water does not get absorbed into the fiber and does not re-evaporate into the gaseous phase. The continuity equation for the free liquid phase is expressed as:

$$\frac{\partial}{\partial t}\left(\rho_l \varepsilon_l\right)+\frac{\partial}{\partial x}\left(\rho_l v_l\right)=-\dot{m}_{ls}+\dot{m}_{gl} \tag{4.21}$$

where x is the linear coordinate across the fabric, v_l is the volume average velocity of the free liquid water, and $\dot{m}_{gl}$ is the rate of mass transfer from the gaseous phase to the liquid phase.

The filtration velocity of the free liquid water, v_l, is calculated in Gibson [4] as:

$$v_l=-\frac{K_l}{\mu_l}\frac{\partial}{\partial x}\left[\left(P_a+P_v\right)-P_c\right] \tag{4.22}$$

where K_l is the Darcian permeability to the liquid phase, μ_l is the viscosity of the liquid phase, P_a is the partial pressure of the air, and P_c is the capillary pressure.

The liquid permeability, K_l, is a function of the saturation given in Gibson's work [4] as:

$$K_l=\begin{cases}0; & s<s_{ir}\\ K_{l,sat}\left\{1-\cos\left[\dfrac{\pi}{2}\dfrac{s-s_{ir}}{(1-s_{ir})}\right]\right\}; & s\geq s_{ir}\end{cases} \tag{4.23}$$

where $K_{l,sat}$ is the Darcian permeability when the porous medium is fully saturated, s is the saturation, and s_{ir} is the irreducible saturation, which is the saturation at which the flow of the liquid phase becomes discontinuous. Below the irreducible saturation, the relative permeability falls to zero and the liquid migration ceases due to the loss of continuity in the

liquid phase. Above the irreducible saturation, the relative permeability increases in a sinusoidal manner with increasing the relative saturation.

The saturation, s, is defined in terms of volume fractions (Gibson [4]) as:

$$s = \left[\frac{\varepsilon_l}{\varepsilon_l + \varepsilon_g} \right] \tag{4.24}$$

An empirical equation for the capillary pressure, P_c, obtained by Stanish et al. [22], as a function of the saturation, is given by:

$$P_c = a \cdot s^b \tag{4.25}$$

where a and b are empirical constants, which depend on the structure of the fabric.

The condensation-evaporation rates, $\dot{m}_{gl}$, are driven by the difference in vapor density between that in the gaseous phase and that at the condensing surface; these rates are given in Le et al. [5] as:

$$\dot{m}_{gl,cond} = h_m a_s \left[\rho_v - \rho_{v,sat} \right] \tag{4.26}$$

for condensation, and

$$\dot{m}_{gl,evap} = h_m a_s \frac{\varepsilon_l}{\varepsilon_l^{cr}} \left[\rho_v - \rho_{v,sat} \right] \tag{4.27}$$

for evaporation, where $\rho_{v,sat}$ is the density of the water vapor in the saturated state.

For the gaseous phase, the dry air does not exchange mass with the fiber; therefore, only the water vapor is considered in the mass balance equation. The continuity equation for the gaseous phase is expressed as:

$$\frac{\partial}{\partial t}\left(\rho_v \varepsilon_g \right) = -\dot{m}_{gs} - \dot{m}_{gl} + \frac{\partial}{\partial x}\left(D_{eff} \frac{\partial \rho_v}{\partial x} \right) \tag{4.28}$$

The thermal equilibrium is assumed. The combined thermal energy equation for all phases is expressed as:

$$\left(\rho c_p\right)_{eff}\frac{\partial T}{\partial t}+\left(\rho c_p\right)_l v_l\frac{\partial T}{\partial x}=\frac{\partial}{\partial x}\left(k_{eff}\frac{\partial T}{\partial x}\right)+\gamma\cdot q''_{rad,fl}e^{-\gamma x} + \Delta h_{vap}\left(\dot{m}_{gs}+\dot{m}_{gl}\right)+\Delta h_{diff}\left(\dot{m}_{ls}+\dot{m}_{gs}\right) \tag{4.29}$$

where ρ_{eff} is the effective density of the fabric, $\left(c_p\right)_{eff}$ is the effective specific heat of the fabric, $\left(c_p\right)_l$ is the specific heat of the free liquid water, Δh_{vap} is the heat of evaporation per unit mass, Δh_{diff} is the differential heat of absorption per unit mass, γ is the radiative extinction coefficient of the fabric, and $q''_{rad,fl}$ is the incident radiation heat flux from the flame onto the outer surface of the fabric.

The effective density of the fabric, ρ_{eff}, can be calculated as:

$$\rho_{eff}=\varepsilon_l\rho_l+\varepsilon_b\rho_b+\varepsilon_f\rho_f+\varepsilon_g(\rho_v+\rho_a) \tag{4.30}$$

The effective specific heat of the fabric, $\left(c_p\right)_{eff}$, is given by the following equation:

$$\left(c_p\right)_{eff}=\frac{\varepsilon_l\rho_l(c_p)_l+\varepsilon_b\rho_b(c_p)_b+\varepsilon_f\rho_f(c_p)_f+\varepsilon_g[\rho_v(c_p)_v+\rho_a(c_p)_a]}{\rho_{eff}} \tag{4.31}$$

where $\left(c_p\right)_b$ is the specific heat of the bound water and $\left(c_p\right)_f$ is the specific heat of the dry solid fiber.

The enthalpy of evaporation per unit mass, Δh_{vap}, can be calculated, according to Gibson [4], as:

$$\Delta h_{vap}=2.792\times10^6-160T-3.43T^2 \tag{4.32}$$

The enthalpy of absorption per unit mass, Δh_{diff}, is given (Gibson [4]) as:

$$\Delta h_{diff} = 1.95 \times 10^5 (1-\phi) \times \left[\frac{1}{(0.2+\phi)} + \frac{1}{(1.05-\phi)} \right] \tag{4.33}$$

The radiative extinction coefficient, γ, that characterizes the decrease of thermal radiation as it penetrates deeper into the fabric, is given in Torvi [8] as:

$$\gamma = \frac{-\ln(\tilde{\tau})}{L_{fab}} \tag{4.34}$$

where $\tilde{\tau}$ is the transmissivity of the fabric and L_{fab} is the fabric thickness. It is assumed that the radiation penetrates through the outer layer of the fabric only.

The incident radiation heat flux coming from the flame to the fabric, $q''_{rad,fl}$, is found in Torvi [8] as:

$$q''_{rad,fl} = \sigma \tilde{\varepsilon}_{fl} (T_{fl}^4 - T_{fab}^4\big|_{x=0}) - \sigma \tilde{\varepsilon}_{fab} F_{fab-amb} (1-\tilde{\varepsilon}_{fl}) (T_{fab}^4\big|_{x=0} - T_{amb}^4) \tag{4.35}$$

where σ is the Stefan-Boltzman constant, $\tilde{\varepsilon}_{fl}$ is the emissivity of the flame, T_{fl} is the temperature of the flame, $T_{fab}\big|_{x=0}$ is the temperature at the outside surface of the fabric, $\tilde{\varepsilon}_{fab}$ is the emissivity of the fabric, $F_{fab-amb}$ is the view factor accounting for the geometry of the fabric with respect to the ambient, and T_{amb} is the temperature of the ambient air.

It is assumed that the flame is uniform (there is no variation of flame intensity along the vertical direction). This assumption makes the problem one-dimensional; therefore, the view factor, $F_{fab-amb}$, is set to unity.

The volume fraction constraint can be expressed as:

$$\varepsilon_g + \varepsilon_l + \varepsilon_b + \varepsilon_f = 1 \tag{4.36}$$

It is also assumed that all gaseous phase species must obey the thermodynamic relations of the ideal gas. These can be written as:

$$P_a = P_g - P_v \tag{4.37}$$

$$P_a = \rho_a \frac{R_u}{M_{w,a}} T \tag{4.38}$$

$$P_v = \rho_v \frac{R_u}{M_{w,v}} T \tag{4.39}$$

where P_g is the total gas pressure, R_u is the universal gas constant, $M_{w,a}$ is the molecular weight of the air, and $M_{w,v}$ is the molecular weight of the water vapor.

Full details of the heat transfer model in the living tissue, natural convection in the air gap between the fabric and the human skin, and tissue burn injury model are given in Chitrphiromsri and Kuznetsov [11]. According to the Pennes' model [12], heat transfer in the living tissue can be modeled utilizing the following equation:

$$(\rho c_p)_{tissue} \frac{\partial T}{\partial t} = \nabla \cdot (k_{tissue} \nabla T) + (\rho c_p)_{blood} \omega_{blood} (T_{arterial} - T) \tag{4.40}$$

where ρ_{tissue} is the density of the living tissue, $(c_p)_{tissue}$ is the specific heat of the living tissue, k_{tissue} is the thermal conductivity of the living tissue, ρ_{blood} is the density of the blood, $(c_p)_{blood}$ is the specific heat of the blood, ω_{blood} is the blood perfusion, and $T_{arterial}$ is the arterial temperature.

It is assumed that conduction heat flux at the outer surface of the fabric is negligibly small compared to the sum of convection and radiation fluxes. This is because of the small thermal conductivity of the air and very large intensity of the flame. The boundary conditions at the outside surface of the fabric are

$$-k_{eff}\left.\frac{\partial T}{\partial x}\right|_{x=0} = \left(q''_{conv,fl} + q''_{rad,fl}\right)_{x=0} \tag{4.41}$$

$$h_{m,amb}(\rho_{v,amb} - \rho_{v,x=0}) = -D_{eff}\left.\frac{\partial \rho_v}{\partial x}\right|_{x=0} \tag{4.42}$$

$$v_l\big|_{x=0} = 0 \tag{4.43}$$

where $q''_{conv,fl}$ is the convective heat flux from the flame to the outer surface of the fabric, $h_{m,amb}$ is the convective mass transfer coefficient of the water vapor between the outside fabric surface and the ambient, and $\rho_{v,amb}$ is the density of water vapor in the ambient.

The radiation and convection heat fluxes can be found according to Torvi [8] as:

$$(q''_{conv,fl} + q''_{rad,fl})_{x=0} = h_{c,fl}(T_{fl} - T_{fab}\big|_{x=0}) \tag{4.44}$$

where $h_{c,fl}$ is the overall equivalent heat transfer coefficient between the flame and the outer surface of the fabric.

The boundary conditions at the inside surface of the fabric are

$$-k_{eff}\left.\frac{\partial T}{\partial x}\right|_{x=L_{fab}} = q''_{rad,airgap} + q''_{cond/conv,airgap} \tag{4.45}$$

$$h_{m,airgap}(\rho_{v,x=L_{fab}} - \rho_{v,airgap}) = -D_{eff}\left.\frac{\partial \rho_v}{\partial x}\right|_{x=L_{fab}} \tag{4.46}$$

$$v_l\big|_{x=L_{fab}} = 0 \tag{4.47}$$

where $q''_{rad,airgap}$ is the heat flux by radiation from the fabric to the human skin across the air gap, $q''_{cond/conv,airgap}$ is the heat flux by conduction/convection from the fabric to the human skin across the air gap, $h_{m,airgap}$ is the convective mass transfer coefficient of the water vapor

between the inner surface of the fabric and the air gap, and $\rho_{v,airgap}$ is the density of the water vapor in the air gap.

The heat flux by radiation from the inside surface of the fabric to the human skin across the air gap is given in Torvi [8] as:

$$q''_{rad,airgap} = \frac{\sigma\left({T_{fab}}^4\Big|_{x=L_{fab}} - {T_{skin}}^4\Big|_{x=L_{fab}+L_{airgap}} \right)}{\left(\frac{A_{skin}}{A_{fab}} \left(\frac{1-\widetilde{\varepsilon}_{fab}}{\widetilde{\varepsilon}_{fab}} + \frac{1}{F_{fab-skin}} \right) + \frac{1-\widetilde{\varepsilon}_{skin}}{\widetilde{\varepsilon}_{skin}} \right)} \tag{4.48}$$

where $T_{fab}\Big|_{x=L_{fab}}$ is the temperature of the inside surface of the fabric, $T_{skin}\Big|_{x=L_{fab}+L_{airgap}}$ is the temperature of the outside surface of the human skin, L_{airgap} is the thickness of the air gap, A_{skin} is the surface area of the human skin, A_{fab} is the area of the inner fabric surface, $F_{fab-skin}$ is the view factor accounting for the geometry of the inner fabric surface with respect to the human skin (set to unity because the model is one-dimensional), and $\widetilde{\varepsilon}_{skin}$ is the emissivity of the human skin.

The heat flux by conduction/convection from the inner fabric surface to the human skin across the air gap is given in Torvi [8] as:

$$q''_{cond/conv,airgap} = h_{c,airgap}(T_{fab}\Big|_{x=L_{fab}} - T_{skin}\Big|_{x=L_{fab}+L_{airgap}}) \tag{4.49}$$

where $h_{c,airgap}$ is the overall equivalent heat transfer coefficient due to conduction and natural convection in the air gap.

The convective heat transfer coefficient due to conduction and natural convection in the air gap, $h_{c,airgap}$, can be found as:

$$h_{c,airgap} = Nu \frac{k_{airgap}}{L_{airgap}} \tag{4.50}$$

where Nu is the Nusselt number and k_{airgap} is the thermal conductivity of the air in the air gap.

The Nusselt number correlations for the air in a long vertical enclosure heated from one side are given as:

$$Nu = \begin{cases} 1.0 & , Ra \le 1713 \\ 0.112 Ra^{0.294} & , Ra > 1713 \end{cases} \tag{4.51}$$

Here Ra is the Rayleigh number defined as:

$$Ra = \frac{g\beta_a L_{airgap}^3 \left[T_{fab}\Big|_{x=L_{fab}} - T_{skin}\Big|_{x=L_{fab}+L_{airgap}}\right]}{\alpha_a \nu_a} \tag{4.52}$$

where g is the gravitational acceleration, β_a is the thermal expansion coefficient of the dry air in the air gap, α_a is the thermal diffusivity of the dry air in the air gap, and ν_a is the kinematic viscosity of the dry air in the air gap.

The boundary conditions for the skin are

$$-k_{tissue} \left.\frac{\partial T}{\partial x}\right|_{x=L_{fab}+L_{airgap}} = q''_{rad,airgap} + q''_{cond/conv,airgap} \tag{4.53}$$

$$T\Big|_{x=L_{fab}+L_{airgap}+L_{skin}} = T_{arterial} \tag{4.54}$$

where L_{skin} is the thickness of the human skin.

4.3. NUMERICAL PROCEDURE

The implicit finite difference method was used to solve the governing equations (4.1), (4.21), (4.28), (4.29), and (4.40). The rates of the phase change of the moisture are computed by using equations (4.2), (4.20), (4.26), and (4.27). It is assumed that at $t = 0$ the textile assembly is in thermal and phase equilibrium with the moist air surrounding it:

$$T(x, t = 0) = T_0(x) \tag{4.55}$$

$$\phi(x, t = 0) = \phi_0(x) \tag{4.56}$$

$$R_f(x, t = 0) = R_{f,0}(x) \tag{4.57}$$

$$s(x, t = 0) = s_0(x) \tag{4.58}$$

where T_0 is the initial temperature, ϕ_0 is the initial relative humidity, $R_{f,0}$ is the initial fiber regain, and s_0 is the initial saturation.

In computations, at each time step and at each position, changes in the temperature of the fabric and the tissue are calculated by equations (4.29) and (4.40), respectively. The volume fraction of the bound water is evaluated by equation (4.1), the volume fraction of the free liquid by equation (4.21), the volume fraction of the gas phase by equation (4.36), and the vapor density by equation (4.28). At each time step, temperature profiles in multiple layers of skin are obtained. Henriques and Moritz's burn criterion [13] is used to predict the tissue burn injury. The maximum durations of the flash fire exposure before the human skin can get the second and third degree burns are computed.

4.4. NUMERICAL RESULTS AND DISCUSSION

The first case is the investigation of transport phenomena in the fabric and living tissue for the duration of the flash fire exposure of 4 seconds with the nominal thickness of the air gap of 0.00635 m (1/4"), which is the standard thickness in the thermal protective performance (TPP) test for the firefighter garment. After the fire is off, computations continue until the time reaches 60 seconds. The numerical values of the various physical parameters of the fabric are given in Table 4-1, those of the human skin and blood are summarized in Table 4-2, and radiation parameters are given in Table 4-3. The initial parameters and the thermo-physical/geometrical properties of the flame, the ambient air, and the air gap are listed in Table 4-4. The *x*-coordinate in Figs. 4-2 to 4-5 shows the distance from the outer surface of the fabric, which is exposed to fire.

Table 4-1 Thermo-physical/geometrical properties of the fabric

Property	Outer Shell: Kombat™ 7.5 oz/yd^2	Moisture Barrier: ComfortZone™	Thermal Liner: Aralite®
ρ_f [kg m^{-3}]	1384	1295	1380
$(c_p)_f$ [J kg^{-1} K^{-1}]	1420	1325	1200
k_f [W m^{-1} K^{-1}]	0.179	0.144	0.130
L_{fab} [m]	0.56×10^{-3}	0.73×10^{-3}	1.66×10^{-3}
ε_f	0.334	0.186	0.115
$R_{f,\phi=0.65}$	0.084	0.038	0.045
τ	1.50	1.25	1.00
D_f [m^2 s^{-1}]	6.0×10^{-14}	6.0×10^{-14}	6.0×10^{-14}
d_f [m]	1.6×10^{-5}	1.6×10^{-5}	1.6×10^{-5}
a [Pa]	1.0×10^{4}	1.0×10^{4}	1.0×10^{4}
b	-0.61	-0.61	-0.61
$K_{l,sat}$ [m^2]	5.0×10^{-16}	5.0×10^{-16}	5.0×10^{-16}
s_{ir}	0.1	0.1	0.1
γ_{ls} [kg m^{-3}]	5.0×10^{-4}	5.0×10^{-4}	5.0×10^{-4}

Table 4-2 Thermo-physical/geometrical properties of the human skin and blood

Property	Epidermis	Dermis	Subcutaneous	Blood
ρ [kg m^{-3}]	1200	1200	1000	1060
c_p [J kg^{-1} K^{-1}]	3600	3400	3060	3770
k [W m^{-1} K^{-1}]	0.255	0.523	0.167	-
L [m]	8×10^{-5}	2×10^{-3}	1×10^{-2}	-
ω_{blood} [m^3 s^{-1} m^{-3}]	-	-	-	1.25×10^{-3}
$T_{arterial}$ [°C]	-	-	-	37.0
$T_{skin}\big\|_{x=L_{fab}+L_{airgap}}$ [°C]	34.0	-	-	-

Table 4-3 Radiation parameters

Property	Fabric	Flame	Skin
$\widetilde{\varepsilon}$	0.9	0.02	0.94
$\widetilde{\tau}$	0.01	-	-

Table 4-4 The initial parameters and the thermo-physical/geometrical properties of the flame, the ambient air, and the air gap

$T_{fab,0}$ [°C]	40.0
$\phi_{fab,0}$	0.65
s_0	0.10
$\phi_{airgap,0}$	0.65
ϕ_{amb}	0.65
T_{fl} [°C]	1000
T_{amb} [°C]	30.0
$h_{c,fl}$ [W m^{-2} K^{-1}]	120.0
$h_{m,amb}$ [m s^{-1}]	0.021
L_{airgap} [m]	6.35×10^{-3}
P_g [N m^{-2}]	1.01325×10^5
h_c [W m^{-2} K^{-1}]	2.88

Figure 4-2(a) depicts the temperature distributions in the fabric at different moments of time. While the garment is exposed to fire, the temperature at the outer surface of the fabric

increases very fast and the temperature at the inner surface of the fabric increases slowly. During the cool-down period (after the fire is off), the temperature at the outer surface of the fabric reduces very fast and the temperature at the inner surface of the fabric decreases slowly. Figure 4-2(b) displays the temperature distributions in the human skin and tissue at different moments of time. According to Tables 4-1 and 4-4, the epidermis skin layer begins at a distance of 0.0093 m from the outer surface of the fabric. Because of the energy accumulated within the fabric and the air gap during the fire exposure, the skin temperature keeps increasing even when the fire is off. This may result in skin burns even after the flash fire exposure.

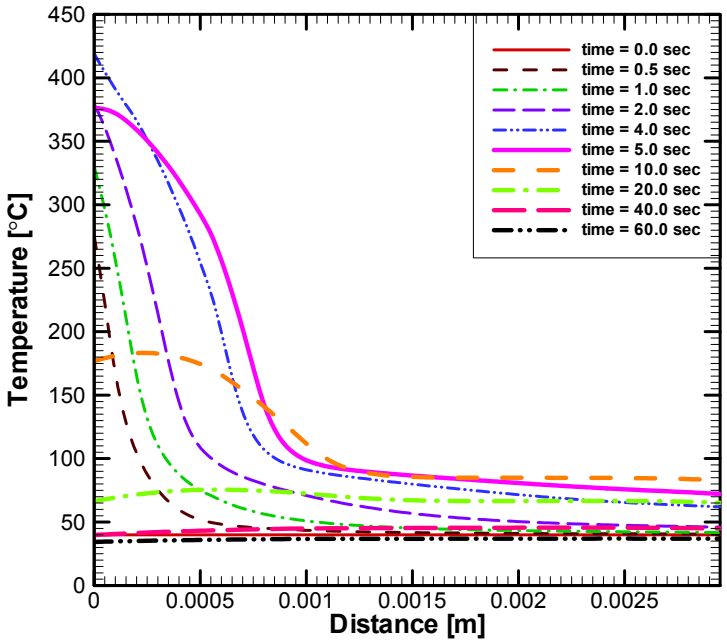

(a)

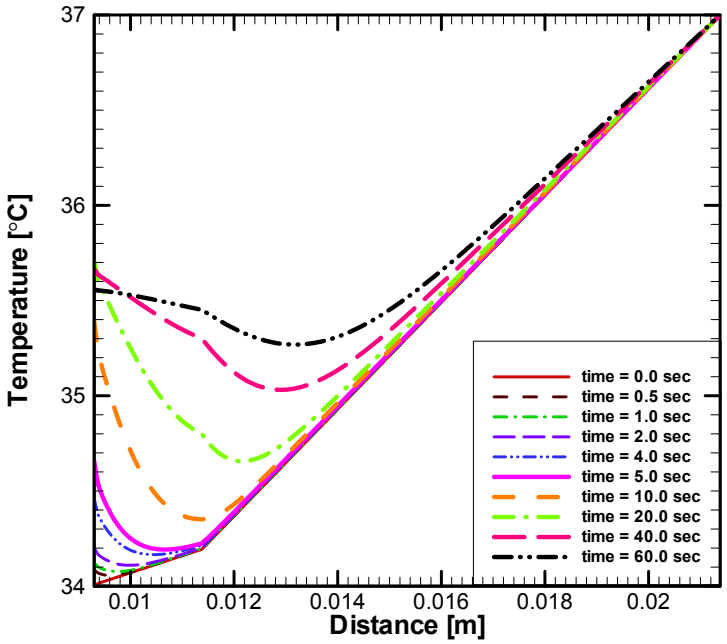

(b)

Figure 4-2 (a) Temperature distributions in the fabric at different moments of time, (b) Temperature distributions in the human skin and tissue at different moments of time

Figures 4-3(a), (b), and (c) show the distributions of the volume fraction of the bound water, free liquid water, and gas phase in the fabric at different moments of time, respectively. The temperature increases when the fabric is exposed to the flash fire, which causes evaporation of the free liquid water. Thus, the volume fractions of free liquid water decrease in the outer fabric layer. However, the evaporation of the free liquid water also results in increasing of the relative humidity close to saturation. Since the relative humidity increases, therefore, the fiber can absorb more bound water resulting in increasing of the volume fraction of the bound water. As the temperature increases, the volume fraction of the gas phase increases. This is because the free liquid evaporates into the gas phase. In addition, the free liquid water

is pushed away from the outer fabric layer to the inner fabric layer because of the temperature gradient and the capillary pressure gradient. Therefore, the volume fraction of the free liquid water increases in the inner fabric layer.

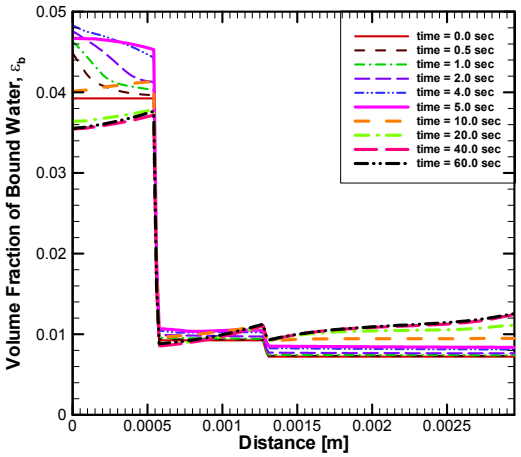

(a)

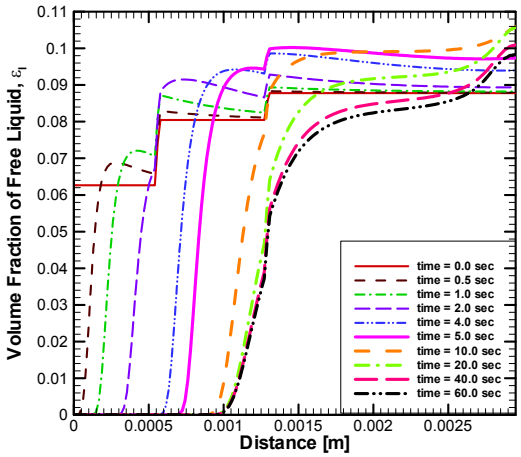

(b)

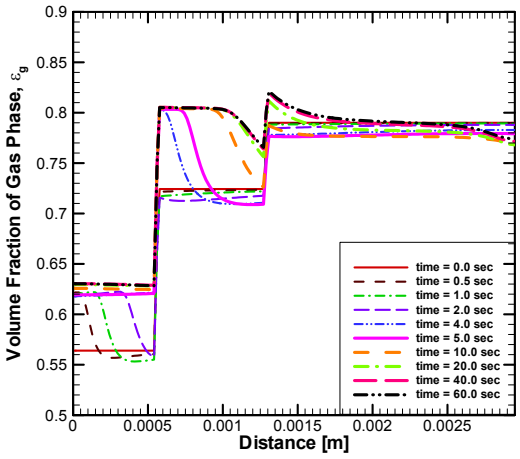

(c)

Figure 4-3 (a) Distributions of the volume fraction of the bound water in the fabric at different moments of time, (b) Distributions of the volume fraction of the free liquid water in the fabric at different moments of time, (c) Distributions of the volume fraction of the gas phase in the fabric at different moments of time

Figure 4-4(a) depicts distributions of the vapor density in the fabric at different moments of time. The vapor density increases because the temperature increases and causes the evaporation of the free liquid water. Figure 4-4(b) shows distributions of the relative humidity in the fabric at different moments of time. The relative humidity near the outer surface of the garment drops very fast when it is exposed to the flash fire. This means that the moisture evaporates very fast during the exposure. After the temperatures at the outer and the inner surfaces of the fabric become sufficiently low, the relative humidity starts growing back to its initial distribution. Figure 4-4(c) displays the distributions of the fiber regain in the fabric at different moments of time. At the initial state, the garment is assumed to be in thermal and phase equilibrium. The equilibrium fiber regain decreases in the outer fabric layer because the relative humidity decreases but the fiber regain increases in the inner fabric layer as the relative humidity increases. Moreover, the bound water evaporates in the outer layer of the garment, which decreases the fiber regain. Figure 4-4(d) illustrates the distributions of the saturation of the free liquid water in the fabric at different moments of time. The saturation of the free liquid water is the ratio of the volume occupied by the free liquid water to the total volume of voids in the control volume. Therefore, the behavior of this parameter is similar to that of the volume fraction of the free liquid. When the temperature increases, the saturation of the free liquid decreases. The temperature gradient and the capillary pressure will force the free liquid water to move away from the outer shell to the moisture barrier (cf. Fig. 4-1(a)). Therefore, the saturation of the free liquid water increases in the inner fabric layer during the exposure.

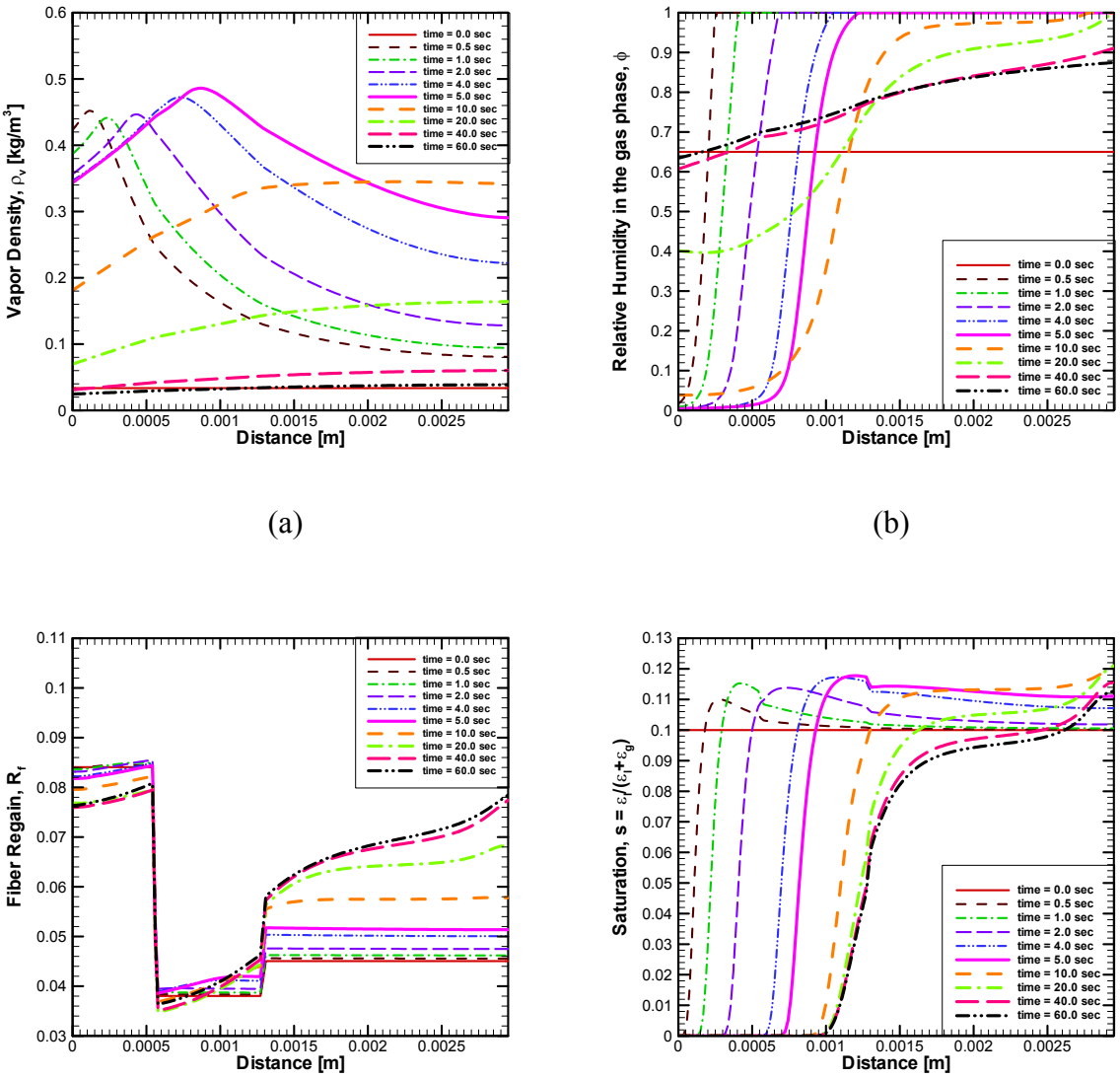

(a) (b)

(c) (d)

Figure 4-4 (a) Distributions of the vapor density in the fabric at different moments of time, (b) Distributions of the relative humidity in the fabric at different moments of time, (c) Distributions of the fiber regain in the fabric at different moments of time, (d) Distributions of the saturation of the free liquid water in the fabric at different moments of time

Figures 4-5(a), (b), (c), and (d) show the distributions of the effective density of the fabric, effective specific heat of the fabric, effective volumetric capacity of the fabric, and effective

thermal conductivity of the fabric at different moments of time, respectively. The effective density of the fabric near the outer surface reduces rapidly as the temperature rises. During the flash fire exposure, the effective density of the fabric in the outer layer near the interface between the outer shell and the moisture barrier is higher than that near the outer surface because the free liquid moves from the outer layer to the inner layer. The effective volumetric heat capacity of the fabric, which is the product of the effective density and the effective specific heat of the fabric, represents the energy absorbed by the fabric during the processes. The effective volumetric heat capacity near the outer surface decreases rapidly when the amounts of the free liquid and bound water become small or when these phases completely vanish because the effective specific heat of the fabric also decreases rapidly near the outer fabric surface as the volume fraction of the gas phase becomes large. The effective thermal conductivity of the fabric increases during the fire exposure, which results in poor thermal protective performance. Thus, the moisture content and its distribution significantly affect the thermal protective performance of the firefighter clothing.

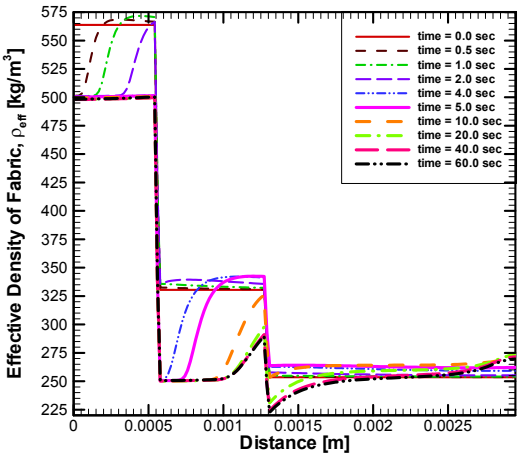

(a)

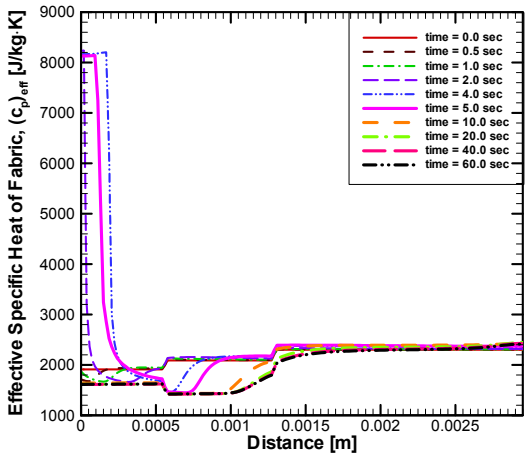

(b)

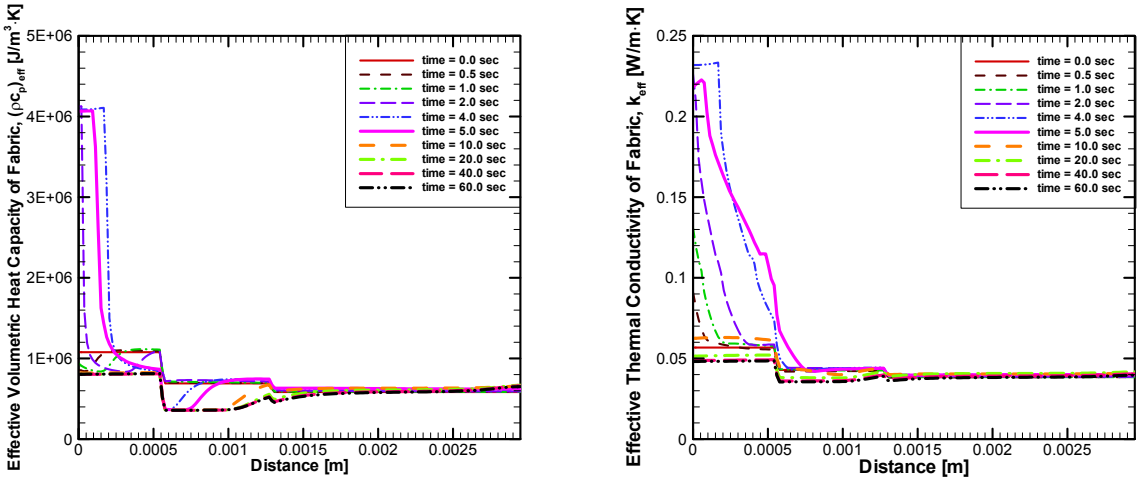

(c) (d)

Figure 4-5 (a) Distributions of the effective density of the fabric at different moments of time, (b) Distributions of the effective specific heat of the fabric at different moments of time, (c) Distributions of the effective volumetric capacity of the fabric at different moments of time, (d) Distributions of the effective thermal conductivity of the fabric at different moments of time

Figure 4-6 shows the calculated fabric weight per unit area, vapor density in the air gap, and relative humidity in the air gap versus time. The fabric weight decreases because the fabric loses moisture that vaporizes into the ambient and the air gap. The vapor density in the air gap increases because the air gap gains moisture from the fabric. Therefore, the relative humidity of the gas phase in the air gap increases close to saturation as the moisture content in the air gap increases until the temperature of the air in the air gap starts decreasing during the cool-down period then the vapor density in the air gap reduces.

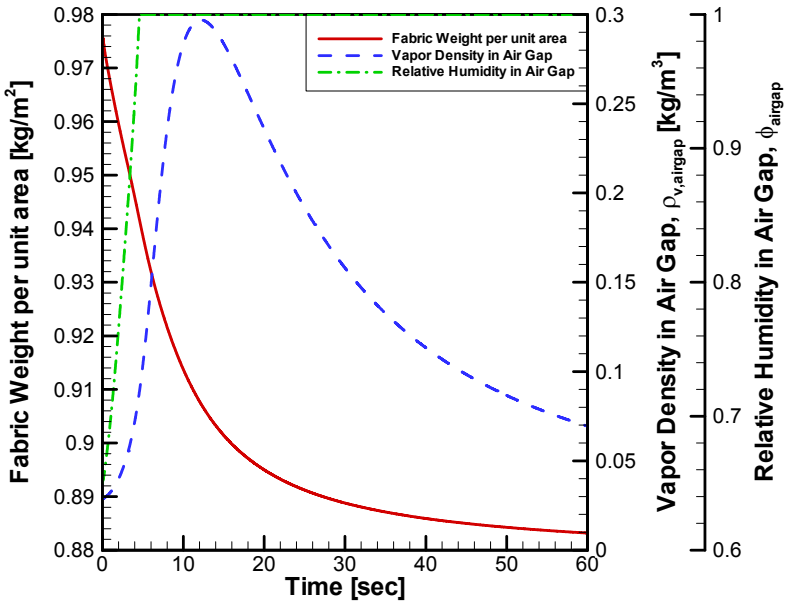

Figure 4-6 Calculated fabric weight per unit area, vapor density in the air gap, and relative humidity in the air gap versus time

Figures 4-7(a) and (b) display the maximum durations of the flash fire exposure before getting second and third degree burns at different locations on the human body. As the initial saturation of the free liquid water in the fabric increases, the maximum durations of flash fire exposure before getting second and third degree burns also increase because the transferred energy during the processes is absorbed by the free liquid water stored in the fabric. The maximum durations of flash fire exposure before getting second and third degree burns increase quickly when the air gap thickness increases until it reaches the critical thickness at approximately 6 mm, after that the durations increase only slightly with further increase of the air gap thickness. The outcomes of the TPP test with the nominal air gap thickness of 6.35 mm is also shown in the Figures 4-7(a) and (b) for the reference purpose. TPP test is a standard thermal protective performance test for the firefighter garment. Figure 4-7 shows

that TPP test does not give the full picture of garment protective performance because it does not account for the variation of the gap thickness depending on the location on the body.

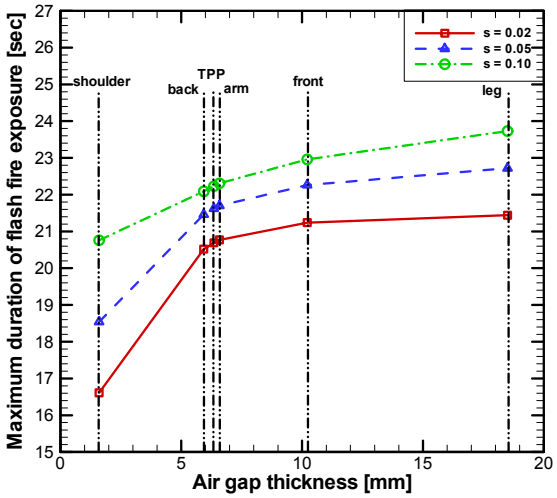

(a)

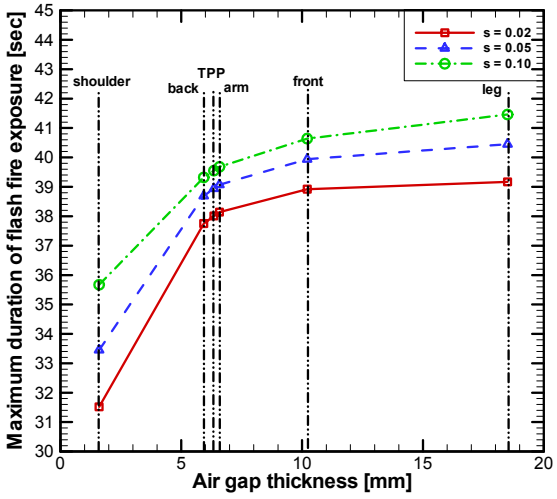

(b)

Figure 4-7 (a) Maximum durations of the flash fire exposure before getting second degree burns at different locations on the human body, (b) Maximum durations of the flash fire exposure before getting third degree burns at different locations on the human body

4.5. CONCLUSIONS

The numerical study of transient heat and moisture transport in firefighter protective clothing under high intensity thermal exposure is carried out. A comprehensive model of heat and moisture transport is developed. This model can be used to predict thermal response and thermal protective performance of the fabric. The distributions of temperature and fiber regain in the fabric and the human skin during flash fire exposure are obtained. At different locations on the human body, the maximum durations of flash fire exposure before getting second and third degree burns can also be predicted for various amounts of the free liquid water in the fabric.

ACKNOWLEDGEMENTS

The support provided by the National Textile Center is gratefully acknowledged. Helpful discussions with Profs. R. L. Barker, H. Hamouda, and Drs. D. B. Thomson and G. Song are greatly appreciated.

REFERENCES

1 K. Vafai, "Characterization of thermal performance of fibrous insulations subject to a humid environment", *J. Thermophysics Heat Transfer*, vol. **7**, pp. 187-192, 1993.

2 K. Vafai and M. Sözen, "A comparative analysis of multiphase transport models in porous media", *Ann. Rev. Heat Transfer*, vol. 3, pp. 145-162, 1990.

3 K. Vafai and S. Whitaker, "Simultaneous heat and mass transfer accompanied by phase change in porous insulation", *J. Heat Transfer*, vol. 108, pp. 132-140, 1986.

4 P. W. Gibson, “Multiphase heat and mass transfer through hygroscopic porous media with applications to clothing materials”, *Technical Report Natick/TR-97/005*, U.S. Army Natick Research, Development, and Engineering Center, Natick, MA, 1996.

5 C. V. Le, N. G. Ly, and R. Postle, “Heat and mass transfer in the condensing flow of steam through an absorbing fibrous medium”, *Int. J. Heat Mass Transfer*, vol. 38, pp. 81-89, 1995.

6 K. Vafai and S. Sarkar, “Condensation effects in a fibrous insulation slab”, *J. Heat Transfer*, vol. 108, pp. 667-675, 1986.

7 M. Sözen and K. Vafai, “Analysis of the non-thermal equilibrium condensing flow of a gas through a packed bed”, *Int. J. Heat Mass Transfer*, vol. 33, pp. 1247-1261, 1990.

8 D. A. Torvi, “Heat transfer in thin fibrous materials under high heat flux conditions”, *Ph.D. Thesis, University of Alberta*, Edmonton, Alberta, Canada, 1997.

9 K. Prasad, W. Twilley, and J. R. Lawson, “Thermal performance of fire fighter’s protective clothing I: Numerical study of transient heat and water vapor transfer”, *Technical Report NISTIR 6681*, Fire Research Division, Building and Fire Research Laboratory, National Institute of Standards and Technology, Gaithersburg, MD, 2002.

10 J. Barry, R. Hill, P. Brasser, M. Sobera, C. Kleijn, and P. Gibson, “Computational fluid dynamics modeling of fabric systems for intelligent garment design”, *MRS Bull.*, vol. 28, pp. 568-573, 2003.

11 P. Chitrphiromsri and A. V. Kuznetsov, “Modeling heat and moisture transport in firefighter protective clothing during flash fire exposure”, *Heat and Mass Transfer*, accepted for publication, 2004.

12 H. H. Pennes, “Analysis of tissue and arterial blood temperatures in resting human forearm”, *J. Appl. Physiol.*, vol. 1, pp. 93-122, 1948.

13 F. C. Jr. Henriques and A. R. Moritz, “Studies of thermal injuries I: The conduction of heat to and through skin and the temperatures attained therein. A theoretical and experimental investigation”, *Am. J. Pathol.*, vol. 23, pp. 531-549, 1947.

14 S. Whitaker, “Simultaneous heat, mass, and momentum transfer in porous media: A theory of drying”, *Adv. Heat Transfer*, vol. 13, pp. 119-203, 1977.

15 J. P. Holman, *Heat Transfer*, McGraw-Hill, Inc., New York, NY, 2002.

16 E. L. Cussler, *Diffusion Mass Transfer in Fluid Systems*, 2nd Ed., Cambridge University Press, Cambridge, MA, 1997.

17 R. C. Progelhof, J. L. Throne, and R. R. Ruetsch, “Methods for predicting the thermal conductivity of composite systems: a review”, *Polym. Eng. Sci.*, vol. 16, pp. 615-625, 1976.

18 J. Fan and X. Wen, “Modeling heat and moisture transfer through fibrous insulation with phase change and mobile condensates”, *Int. J. Heat Mass Transfer*, vol. 45, pp. 4045-4055, 2002.

19 M. Kaviany and M. Mittal, “Funicular state in drying of a porous slab”, *Int. J. Heat Mass Transfer*, vol. 30, pp. 1407-1418, 1987.

20 W. A. Lotens and G. Havenith, “Effects of moisture absorption in clothing on the human heat balance”, *Ergonomics*, vol. 38, pp. 1092-1113, 1994.

21 W. Morton and J. Hearle, *Physical Properties of Textile Fibres*, The Textile Institute, Manchester, UK, 1993.

22 M. A. Stanish, G. S. Schajer, and F. Kayihan, “A mathematical model of drying for hygroscopic porous media”, *AIChE J.*, vol. 32, pp. 1301-1311, 1986.

PART THREE:

APPLICATIONS

5. INVESTIGATION OF FEASIBILITY OF DEVELOPING INTELLIGENT FIREFIGHTER PROTECTIVE GARMENTS BASED ON THE UTILIZATION OF A WATER-INJECTION SYSTEM

ABSTRACT

This chapter develops a new approach to designing and creating a prototype of an intelligent firefighter thermal protective garment. During the flash fire exposure, this intelligent garment will absorb a significant amount of the incident heat flux due to evaporation of the injected water, thus limiting the temperature increase and the total heat flux to the firefighter's skin. A comprehensive mathematical model of heat and mass transport in the fabric layer during the flash fire exposure is suggested and numerically implemented using a finite volume technique. A computational investigation is performed to optimize the performance of this novel garment system in terms of the activation temperature and the necessary amount of injected water.

NOMENCLATURE

a empirical coefficient for the capillary pressure defined in Eq. (5.15) [Pa]

a_s specific surface area per unit volume [m^{-1}]

b empirical constant for the capillary pressure defined in Eq. (5.15)

c_p specific heat at constant pressure [J kg^{-1} K^{-1}]

D_{v-a} diffusivity of the water vapor in the air [m^2 s^{-1}]

D_{eff} effective diffusivity of the gas phase in the fabric [m^2 s^{-1}]

D_{b-f} diffusivity of the bound water in the solid fiber [m^2 s^{-1}]

d_f average fiber diameter [m]

g gravitational acceleration [9.81 m s^{-2}]

h_c convective heat transfer coefficient [W m^{-2} K^{-1}]

h_m convective mass transfer coefficient of the water vapor [m s^{-1}]

K Darcian permeability coefficient [m^2]

k thermal conductivity [W m^{-1} K^{-1}]

L thickness [m]

Le Lewis number, $Le = \alpha_{eff} / D_{eff}$

M_w molecular weight [kg $kmol^{-1}$]

$\dot{m}_{inject}$ volumetric mass transfer rate of the water injection into the fabric [kg m^{-3} s^{-1}]

$\dot{m}_{l-b}$ volumetric mass transfer rate from the free liquid water to the bound water [kg $m^{-3}s^{-1}$]

$\dot{m}_{v-b}$ volumetric mass transfer rate from the water vapor to the bound water [kg m^{-3} s^{-1}]

$\dot{m}_{v-l}$ volumetric mass transfer rate from the water vapor to the free liquid water [kg m^{-3} s^{-1}]

Nu Nusselt number, $Nu = h_c L / k$

p pressure [Pa]

$q''_{cond/conv,airgap}$ heat flux by conduction/convection from the inner surface of the fabric to the human skin across the air gap [W m^{-2}]

$q''_{conv,fl}$ convective heat flux from the flame to the outer surface of the fabric [W m^{-2}]

$q''_{rad,airgap}$ heat flux by radiation from the inner surface of the fabric to the human skin across the air gap [W m^{-2}]

$q''_{rad,fl}$ incident radiation heat flux from the flame onto the outer fabric surface [W m^{-2}]

R_f fiber regain

R_u universal gas constant [8.315×10^3 J $kmol^{-1}$ K^{-1}]

Ra Rayleigh number, $Ra = g\beta\Delta TL^3 / \alpha\nu$

s saturation of the pores in the fabric by the liquid, defined in Eq. (5.14)

T temperature [K]

t time [s]

v velocity [m s^{-1}]

x linear coordinate across the fabric [m]

Greek symbols

α thermal diffusivity [m^2 s^{-1}]

β thermal expansion coefficient [K^{-1}]

Δh_{trans} enthalpy of transition from the bound water to the free liquid water [J kg^{-1}]

Δh_{vap} enthalpy of evaporation per unit mass [J kg^{-1}]

ε volume fraction

$\tilde{\varepsilon}$ emissivity

ϕ relative humidity

γ radiative extinction coefficient of the fabric [m^{-1}]

γ_{l-b} proportionality constant related to the rate of absorption of the free liquid water by a fiber [kg m^{-3}]

κ_z Kozeny factor given in Eq. (5.18)

μ dynamic viscosity [kg m^{-1} s^{-1}]

ν kinematic viscosity [m^2 s^{-1}]

ρ density [kg m^{-3}]

σ Stefan-Boltzman constant [5.670×10^{-8} W m^{-2} K^{-4}]

τ fabric tortuosity

$\widetilde{\tau}$ transmissivity of the fabric

ω_{blo} blood perfusion [0.00125 m^3 s^{-1} m^{-3} tissue]

Subscripts

0 initial state

a dry air

act activation

airgap air gap

amb ambient air

art arterial

b bound water

blo blood

c capillary

cond condensation

eff effective

eq equilibrium

evap evaporation

f dry fiber

fab fabric

fl flame

g gas phase

ir irreducible

l free liquid water

s solid phase

sat saturation

skin skin

tiss tissue

v water vapor

Superscript

cr critical

5.1. INTRODUCTION

Traditional textile materials used in multi-layer thermal protective garments rely on the thermal properties of the fabric and the entrapment of insulating air layers to resist heat flux from flash fire exposures in order to protect firefighters from burn injuries. To improve the level of heat flux resistance of thermal protective garments, this research evaluates the

feasibility of developing a novel garment system, which incorporates knowledge and technologies that actively raise thermal resistance in the presence of intensive heat exposure.

A considerable amount of research (Kaska and Chen [1]; Colvin and Mulligan [2]) is conducted on thermal management for textile fibers and composite materials by utilizing microencapsulated phase change materials (PCMs). The encapsulated PCMs can be microscopically suspended or embedded into fibers inside the textile material to produce a garment with passive insulation and regenerative thermal protection. Thus, phase change materials (PCMs) have been used as thermal control materials because of the high latent heat of phase change, which permits high thermal storage as well as high moisture transport between the capsules (Colvin and Bryant [3]; Colvin et al. [4]). Pause [5] suggested a new heat protective garment with a phase change material that is capable of absorbing large quantities of latent heat within a certain temperature range. This feature can be utilized to create new protective garments offering significantly improved protection against conductive and radiant heat. Hayes et al. [6] proposed a mathematical model for an encapsulated phase change material placed in a conductive media by adopting a macroscopic view of the entire system, using the amount of released latent heat from the PCM determined by the temperature difference between the capsules and the conducting media, and incorporating this term into a standard heat conduction equation.

Chitrphiromsri and Kuznetsov [7, 8] performed investigations of heat and moisture transport in multi-layer protective clothing under high intensity thermal radiation. Their investigations accounted for the moisture transport in all three possible phases, which are the bound water, free liquid water, and water vapor. They showed that the amount of moisture affects the

thermal protective performance of the fabric system. As the amount of the free liquid water increases, the exposure time before getting a burn injury also increases.

While traditional textile materials used in thermal protective garments rely on a passive insulation mechanism to protect the firefighter, intelligent garment will provide active protection. For the intelligent garment investigated in this research, the liquid water will be injected in the outer layer of the garment through a capillary net; the injection process will be activated by a temperature sensor embedded in the outer fabric layer. During the flash fire exposure, the injected water will evaporate resulting in large absorption of heat thus limiting the temperature increase in the outer fabric layer. Therefore, the outer layer of fabric will provide an active thermal barrier and act as a thermal buffer against the high heat flux associated with flash fire exposure. The inner layers of this garment system will still work in a traditional way and provide efficient insulation due to their small thermal conductivity. Therefore, the new turnout system augments the outer layer, to provide an active protection against flash fire exposures upon the activation temperature by injecting water, while the remaining inner layers continue to provide conventional protection based on their traditional insulation properties.

5.2. STATEMENT OF THE PROBLEM

Figure 5-1 displays a schematic diagram of a problem. A multiple layer protective turnout gear is composed of three different fabric layers, which are the outer shell, the moisture barrier, and the thermal liner. The injected water is uniformly distributed over the outer shell through a capillary system composed of thin perforated tubes, which is controlled by an automated electrical circuit activated by a temperature sensor. The garment can be

considered as a porous medium saturated with a mixture of multi-phase water, as described in Chitrphiromsri and Kuznetsov [8]. The air gap between the garment and the human skin usually exists; this gap assists in enhancing insulation properties of the garment. The human skin can be divided into three different layers, which are the epidermis, the dermis, and the subcutaneous, respectively, counting from the external to the internal tissues. Full details of the tissue model are given in Pennes [9], and the details of the three-layer skin model are given in Torvi and Dale [10].

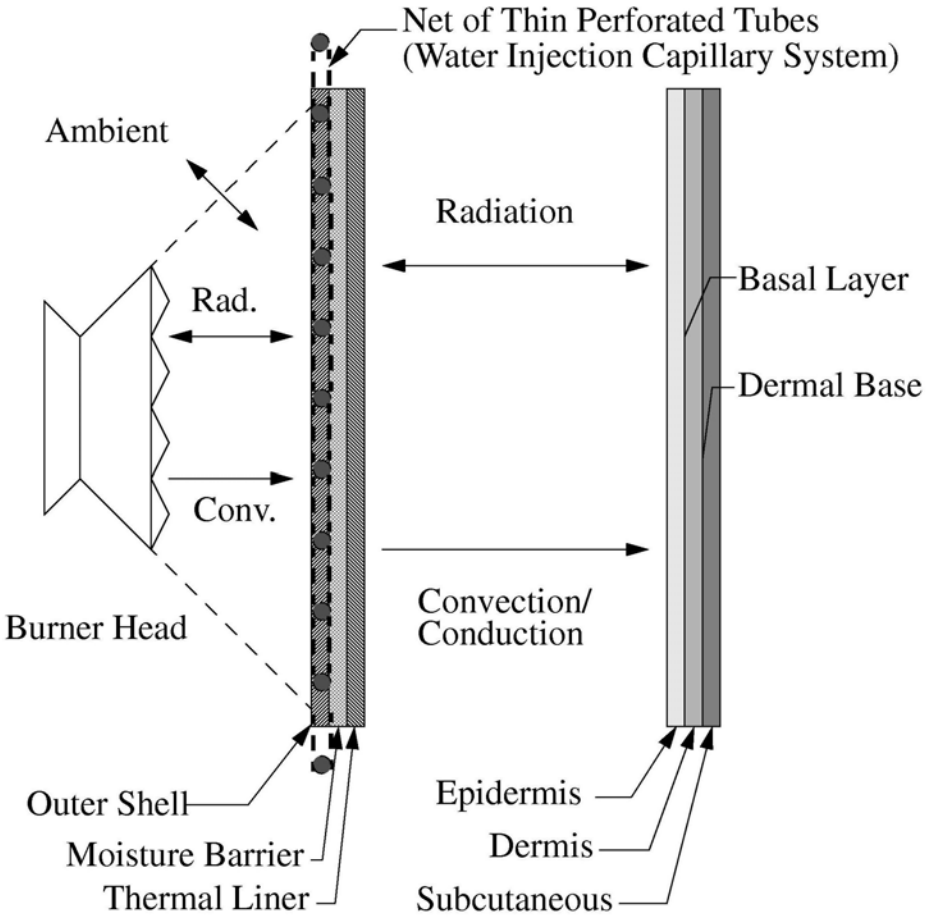

Figure 5-1 Schematic diagram of heat and mass transport in the human skin, the air gap, and the firefighter's intelligent thermal protective garment with the water injection

5.3. MATHEMATICAL FORMULATION

The mathematical formulation in this work uses the method of local volume averaging [11]. The transport processes are assumed to be one-dimensional. Local thermal and phase equilibrium is also assumed.

5.3.1. MASS BALANCE EQUATIONS

Our assumptions lead to the following set of differential equations expressing mass balances of the bound water, free liquid water, and water vapor, respectively:

$$\frac{\partial}{\partial t}\left(\rho_b \varepsilon_b\right) = \dot{m}_{l-b} + \dot{m}_{v-b} \tag{5.1}$$

$$\frac{\partial}{\partial t}\left(\rho_l \varepsilon_l\right) + \frac{\partial}{\partial x}\left(\rho_l v_l\right) = -\dot{m}_{l-b} + \dot{m}_{v-l} + \dot{m}_{inject} \tag{5.2}$$

$$\frac{\partial}{\partial t}\left(\rho_v \varepsilon_g\right) + \frac{\partial}{\partial x}\left(\rho_v v_g\right) = -\dot{m}_{v-b} - \dot{m}_{v-l} + \frac{\partial}{\partial x}\left(D_{eff}\frac{\partial \rho_v}{\partial x}\right) \tag{5.3}$$

where t is the time, x is the linear coordinate across the fabric, ρ_b is the density of the bound water, ρ_l is the density of the free liquid water, ρ_v is the density of the water vapor, ε_b is the volume fraction of the bound water, ε_l is the volume fraction of the free liquid water, ε_g is the volume fraction of the gas phase, v_l is the volume average velocity of the free liquid water, v_g is the volume average velocity of the gas phase, D_{eff} is the effective diffusivity of the gas phase in the fabric, $\dot{m}_{l-b}$ is the volumetric rate of mass transfer from the free liquid water to the bound water, $\dot{m}_{v-b}$ is the volumetric rate of mass transfer from the water vapor to the bound water, $\dot{m}_{v-l}$ is the volumetric rate of mass transfer from the water

vapor to the free liquid water, and $\dot{m}_{inject}$ is the volumetric mass transfer rate of the water injection.

The volume fraction constraint can be expressed as (Gibson [12]):

$$\varepsilon_g + \varepsilon_l + \varepsilon_b + \varepsilon_f = 1 \tag{5.4}$$

where ε_f is the volume fraction of the fiber.

5.3.2. HEAT BALANCE EQUATIONS

By assuming that the fiber and the moisture have locally the same temperature, the combined thermal energy equation for the solid, liquid, and gas phases in the fabric can be express as:

$$\begin{aligned}\left(\rho c_p\right)_{eff}\frac{\partial T}{\partial t} + \left[\left(\rho c_p\right)_l v_l + \left(\rho c_p\right)_g v_g\right]\frac{\partial T}{\partial x} = {} & \frac{\partial}{\partial x}\left(k_{eff}\frac{\partial T}{\partial x}\right) + \gamma \cdot q''_{rad,fl} e^{-\gamma x} \\ & + \dot{m}_{v-b}\left(\Delta h_{vap} + \Delta h_{trans}\right) \\ & + \dot{m}_{v-l}\Delta h_{vap} + \dot{m}_{l-b}\Delta h_{trans}\end{aligned} \tag{5.5}$$

where T is the temperature, ρ_{eff} is the effective density of the fabric, $\left(c_p\right)_{eff}$ is the effective specific heat of the fabric, $\left(c_p\right)_l$ is the specific heat of the free liquid water, ρ_g is the density of the gas phase, $\left(c_p\right)_g$ is the specific heat of the gas phase, k_{eff} is the effective thermal conductivity of the fabric, γ is the radiative extinction coefficient of the fabric, $q''_{rad,fl}$ is the incident radiation heat flux from the flame onto the outer surface of the fabric, Δh_{vap} is the heat of evaporation of moisture per unit mass, and Δh_{trans} is the differential heat of absorption of moisture into the fiber per unit mass.

Heat transfer in the living tissue can be modeled utilizing the bioheat equation given in Pennes [9] as:

$$(\rho c_p)_{tiss}\frac{\partial T}{\partial t}=\frac{\partial}{\partial x}\left(k_{tiss}\frac{\partial T}{\partial x}\right)+(\rho c_p)_{blo}\omega_{blo}(T_{art}-T) \tag{5.6}$$

where ρ_{tiss} is the density of the living tissue, $(c_p)_{tiss}$ is the specific heat of the living tissue, k_{tiss} is the thermal conductivity of the living tissue, ρ_{blo} is the density of the blood, $(c_p)_{blo}$ is the blood specific heat, ω_{blo} is the blood perfusion, and T_{art} is the arterial temperature.

5.3.3. MASS TRANSFER RATES

Transport and phase change processes in the fabric are illustrated in Figure 5-2 (cf. Le et al. [13]).

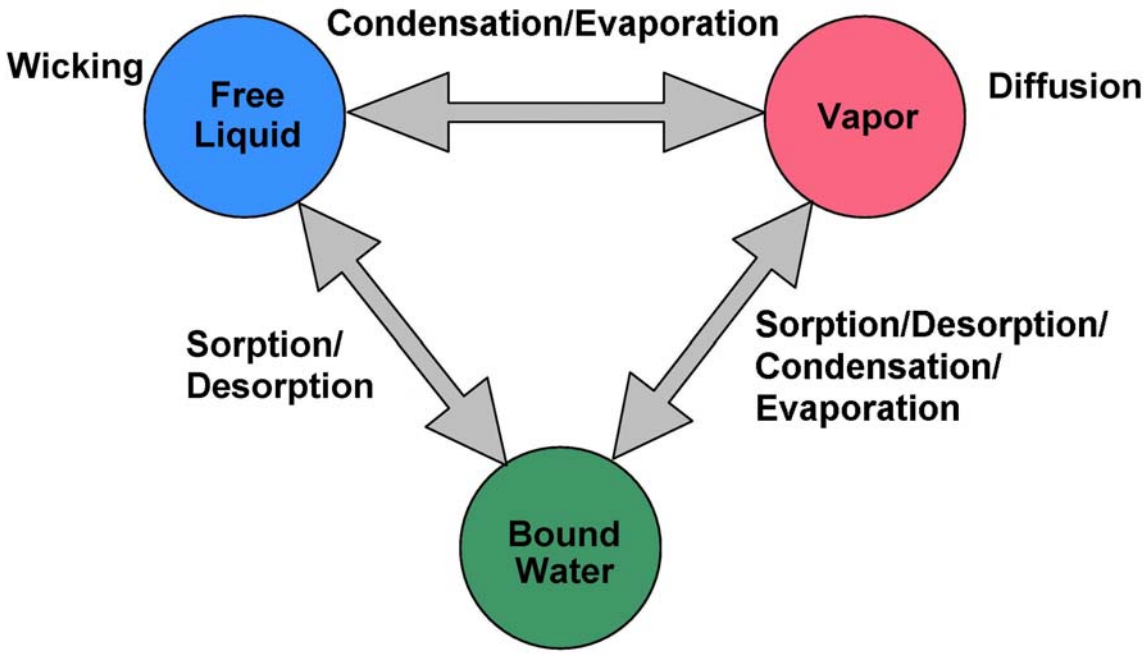

Figure 5-2 Transport and phase change processes in the fabric

Relative humidity of the air in the pores of the fabric determines the equilibrium regain in the fiber. The mass transfer rate of absorption of the free liquid water to the fibers is given as:

$$\dot{m}_{l-b} = h_m a_s \gamma_{l-b} \frac{\varepsilon_l}{\varepsilon_l^{cr}} \left(\frac{R_{f,eq}}{R_f} - 1 \right) \tag{5.7}$$

where h_m is the convective mass transfer coefficient of the water vapor to the air, a_s is the specific surface area per unit volume of the fabric, γ_{l-b} is a proportionality constant related to the rate of absorption of the free liquid water by a fiber, ε_l^{cr} is the critical volume fraction of the liquid water at which the liquid phase becomes mobile, $R_{f,eq}$ is the equilibrium fiber regain at the fiber surface, and R_f is the instantaneous fiber regain.

The rate of mass transfer between the fiber and the water vapor is obtained by assuming that the driving force is the difference of the two regains, as suggested in [13]:

$$\dot{m}_{v-b} = \frac{8 D_{b-f} \rho_f}{d_f^2} \left(R_{f,eq} - R_f \right) \tag{5.8}$$

where D_{b-f} is the effective diffusivity of the bound water in the solid phase, ρ_f is the density of the dry fiber, and d_f is the average fiber diameter.

Condensation-evaporation rates are driven by the difference in vapor density between that in the gas phase and that at the condensing surface. The rate of condensation is given by:

$$\dot{m}_{v-l,cond} = h_m a_s \left[\rho_v - \rho_{v,sat} \right] \tag{5.9}$$

where $\rho_{v,sat}$ is the density of the water vapor in the saturated state.

The rate of evaporation is given by:

$$\dot{m}_{v-l,evap} = h_m a_s \frac{\varepsilon_l}{\varepsilon_l^{cr}} \left[\rho_v - \rho_{v,sat} \right] \tag{5.10}$$

Equation (5.10) is based on a model suggested in [13], according to which the mass transfer rate by evaporation from the free liquid phase to the vapor phase is proportional to the normalized volume fraction of the liquid phase.

The water injection system is activated by the temperature sensor embedded in the outer fabric layer, near the fabric surface. This system will uniformly inject water into the outer layer of the garment when the temperature at the outer surface of the garment rises above the activation temperature. The rate of water injection is given as:

$$\dot{m}_{inject} = \begin{cases} 0, & T_{fab}\big|_{x=0} < T_{act} \\ \dot{m}_{inject}, & T_{fab}\big|_{x=0} \geq T_{act} \end{cases} \tag{5.11}$$

where $T_{fab}\big|_{x=0}$ is the temperature at the outer surface of the fabric and T_{act} is the activation temperature.

5.3.4. Momentum Balances for the Liquid and Gas Phases

The liquid phase is driven by the capillary pressure gradient, which is a function of the fraction of the void space occupied by the liquid. Liquid present in a porous material may be either in a pendular state or in a continuous state. If the liquid is in a pendular state, there is no liquid flow since the liquid does not form a continuous phase and it is present as discrete drops or regions, which are disconnected from each other. There may be significant capillary pressure present, but until the volume fraction of liquid rises to a critical level to form a continuous phase, there will be no liquid flow. This implies that there is a critical saturation

level, which liquid volume fraction must reach before liquid motion begins. Thus, the filtration velocity of the free liquid water is calculated as:

$$v_l = -\frac{s \cdot K_l}{\mu_l}\frac{\partial}{\partial x}\left[\left(p_a + p_v\right) - p_c\right] \qquad (5.12)$$

where K_l is the Darcian permeability of the fabric to the liquid phase for a single phase flow, μ_l is the viscosity of the liquid phase, p_a is the partial pressure of the air, p_v is the partial pressure of the water vapor, and p_c is the capillary pressure.

The liquid permeability, which is a function of the saturation of the pores in the fabric by the liquid, is given in Gibson [12] as:

$$K_l = \begin{cases} 0; & s < s_{ir} \\ K_{l,sat}\left\{1 - \cos\left[\dfrac{\pi}{2}\dfrac{s - s_{ir}}{(1 - s_{ir})}\right]\right\}; & s \geq s_{ir} \end{cases} \qquad (5.13)$$

where $K_{l,sat}$ is the Darcian permeability at which the porous medium is fully saturated, s is the saturation of the pores in the fabric by the liquid, and s_{ir} is the irreducible saturation, which is the saturation of the pores by the liquid at which the flow of the liquid phase stops. Below the irreducible saturation, the relative permeability falls to zero and the liquid migration ceases because of the loss of continuity in the liquid phase. Above the irreducible saturation, the relative permeability increases in a sinusoidal manner, as the relative saturation of the pores by the liquid increases.

The saturation of the pores in the fabric by the liquid, s, is defined in terms of the relative value of the volume fractions of the liquid and gas phases as:

$$s = \left[\frac{\varepsilon_l}{\varepsilon_l + \varepsilon_g} \right] \tag{5.14}$$

The capillary pressure is obtained from the following empirical correlation:

$$p_c = a \cdot s^b \tag{5.15}$$

where a and b are empirical constants, which depend on the structure of the fabric.

The pressure gradient of the gas phase causes the steam to flow and displace air as it penetrates into the fabric. The velocity of steam-flow through the fabric is small and the flow can be assumed to be of Darcian type. The convective velocity of the flow depends on the permeability of the fabric, which changes as the steaming progresses, and is calculated as:

$$v_g = -\frac{(1-s) \cdot K_g}{\mu_g} \frac{\partial}{\partial x} \left[p_a + p_v \right] \tag{5.16}$$

where K_g is the Darcian permeability of the fabric to the gas phase (for a single-phase flow) and μ_g is the viscosity of the gas phase.

The fabric permeability to the gas phase is calculated from the Kozeny-Carman equation [14] as:

$$K_g = \frac{\varepsilon_g^3}{\kappa_z a_s^2 (1-\varepsilon_g)^2} \tag{5.17}$$

where κ_z is the Kozeny factor. In a bed of fiber with a circular cross-section, this value is given by Labrecque's empirical relation [15] as:

$$\kappa_z = 5.0 + \exp[14(\varepsilon_g - 0.8)] \tag{5.18}$$

5.3.5. *PHYSICAL AND THERMAL RELATIONS*

Effective physical properties of the fabric can be approximated by the following linear correlations. The effective density of the fabric can be calculated as:

$$\rho_{eff} = \varepsilon_l \rho_l + \varepsilon_b \rho_b + \varepsilon_f \rho_f + \varepsilon_g (\rho_v + \rho_a) \tag{5.19}$$

where ρ_a is the density of the dry air.

The effective specific heat of the fabric is given by the following equation:

$$\left(c_p\right)_{eff} = \frac{\varepsilon_l \rho_l (c_p)_l + \varepsilon_b \rho_b (c_p)_b + \varepsilon_f \rho_f (c_p)_f + \varepsilon_g [\rho_v (c_p)_v + \rho_a (c_p)_a]}{\rho_{eff}} \tag{5.20}$$

where $\left(c_p\right)_b$ is the specific heat of the bound water, $\left(c_p\right)_f$ is the specific heat of the dry solid fiber, $\left(c_p\right)_v$ is the specific heat of the water vapor, and $\left(c_p\right)_a$ is the specific heat of the dry air.

The effective thermal conductivity of the fabric is calculated as:

$$k_{eff} = k_g \left\{ \frac{[1 + (\varepsilon_l + \varepsilon_b + \varepsilon_f)]k_s + \varepsilon_g k_g}{\varepsilon_g k_s + [1 + (\varepsilon_l + \varepsilon_b + \varepsilon_f)]k_g} \right\} \tag{5.21}$$

where k_g is the thermal conductivity of the gas phase and k_s is the thermal conductivity of the solid phase.

The thermal conductivity of the gas phase can be calculated as:

$$k_g = \left(\frac{k_v \rho_v + k_a \rho_a}{\rho_v + \rho_a} \right) \tag{5.22}$$

where k_v is the thermal conductivity of the saturated water vapor and k_a is the thermal conductivity of the dry air.

The thermal conductivity of the solid phase, k_s, can be calculated as:

$$k_s = \left(\frac{k_l \rho_l \varepsilon_l + k_b \rho_b \varepsilon_b + k_f \rho_f \varepsilon_f}{\rho_l \varepsilon_l + \rho_b \varepsilon_b + \rho_f \varepsilon_f} \right) \tag{5.23}$$

where k_l is the thermal conductivity of the free liquid water, k_b is the thermal conductivity of the bound water, and k_f is the thermal conductivity of the dry solid.

The total pressure of the gas phase is the summation of the partial pressure of the dry air and the partial pressure of the water vapor. All gas phase species are assumed to obey the thermodynamic relations of the ideal gas. The equations of state for the dry air and water vapor can be written as:

$$p_a = p_g - p_v \tag{5.24}$$

$$p_a = \rho_a \frac{R_u}{M_{w,a}} T \tag{5.25}$$

$$p_v = \rho_v \frac{R_u}{M_{w,v}} T \tag{5.26}$$

where p_g is the total gas pressure, R_u is the universal gas constant, $M_{w,a}$ is the molecular weight of air, and $M_{w,v}$ is the molecular weight of the water vapor.

The densities of the dry air and water vapor in the air gap between the inner surface of the fabric and the surface of the skin are calculated by balancing the mass fluxes of the dry air and vapor transported in/out by convection at the inner surface of the fabric, respectively. The partial pressures of both the dry air and water vapor in the air gap are also assumed to obey the ideal gas equation of state. In addition, as in Le at al. [13], the total gas pressure in the garment is assumed to change linearly with the distance from the outer surface of the fabric to the inner surface of the fabric:

$$p_g = p_{g,amb} + \frac{(p_{g,airgap} - p_{g,amb})}{L_{fab}} x \tag{5.27}$$

where $p_{g,amb}$ is the total gas pressure in the ambient surrounding the outer surface of the fabric, $p_{g,airgap}$ is the total gas pressure in the air gap between the inner surface of fabric and the surface of the skin, and L_{fab} is the total fabric thickness.

The relative humidity, ϕ, is defined as:

$$\phi = \frac{p_v}{p_{sat}} \tag{5.28}$$

where p_{sat} is the saturation vapor pressure, which is a function of T only.

The instantaneous fiber regain is defined as:

$$R_f = \frac{\varepsilon_b \rho_b}{\varepsilon_f \rho_f} \tag{5.29}$$

The convective mass transfer coefficient of the water vapor to the air can be related to the convective heat transfer coefficient by utilizing the Chilton-Colburn analogy [16], as:

$$h_m = \frac{h_c}{\left(\rho c_p\right)_g Le^{\frac{2}{3}}} \tag{5.30}$$

where h_c is the convective heat transfer coefficient and Le is the Lewis number.

The density of the gas phase can be calculated as:

$$\rho_g = \rho_v + \rho_a \tag{5.31}$$

The specific heat of the gas phase is given as:

$$\left(c_p\right)_g = \frac{\left[\rho_v \left(c_p\right)_v + \rho_a \left(c_p\right)_a\right]}{\rho_g} \tag{5.32}$$

The Lewis number is defined as:

$$Le = \frac{\alpha_{eff}}{D_{eff}} \tag{5.33}$$

where α_{eff} is the effective thermal diffusivity of the water vapor in the fabric, which is defined as:

$$\alpha_{eff} = \frac{k_{eff}}{\rho_v (c_p)_v} \tag{5.34}$$

The effective diffusivity of the gas phase in the fabric is given by:

$$D_{eff} = \frac{D_{v-a}\varepsilon_g}{\tau} \tag{5.35}$$

where D_{v-a} is the diffusivity of the water vapor in the air and τ is the fabric tortuosity which depends on the fiber structure arrangement.

The diffusivity of the water vapor in the air can be calculated as a function of temperature (Gibson [12]):

$$D_{v-a} = 2.23 \times 10^{-5} \left(\frac{T}{273.15} \right)^{1.75} \tag{5.36}$$

The specific surface area per unit volume is defined as:

$$a_s = \frac{4\varepsilon_s}{d_f} \tag{5.37}$$

where ε_s is the volume fraction of the solid phase.

The volume fraction of the solid phase, which is the summation of the volume fractions of dry fiber and bound water, can be expressed as:

$$\varepsilon_s = \varepsilon_f + \varepsilon_b \tag{5.38}$$

The critical value of the liquid fraction when the liquid phase becomes mobile, is assumed to be:

$$\varepsilon_l^{cr} = 0.1\varepsilon_g \tag{5.39}$$

The equilibrium fiber regain at the fiber surface, which is a function of the relative humidity, is given in Gibson [12] as:

$$R_{f,eq} = 0.578 \cdot \phi \cdot R_{f,\phi=0.65}\left[\frac{1}{(0.321+\phi)} + \frac{1}{(1.262-\phi)}\right] \tag{5.40}$$

where $R_{f,\phi=0.65}$ is the fiber regain at 65% relative humidity.

The saturation vapor pressure is given by:

$$p_{sat} = 614.3\exp\left\{17.06\left[\frac{(T-273.15)}{(T-40.25)}\right]\right\} \tag{5.41}$$

The enthalpy of evaporation of the water per unit mass, which is a function of the temperature only, can be calculated as:

$$\Delta h_{vap} = 2.792\times10^6 - 160T - 3.43T^2 \tag{5.42}$$

The enthalpy of transition (per unit mass) from the free liquid water to the bound water when the free liquid water is absorbed by the fiber, which is a function of the relative humidity only, is given by:

$$\Delta h_{trans} = 1.95\times10^5(1-\phi)\times\left[\frac{1}{(0.2+\phi)} + \frac{1}{(1.05-\phi)}\right] \tag{5.43}$$

The radiative extinction coefficient that characterizes the decrease of thermal radiation as it penetrates deeper into the fabric, is given by:

$$\gamma = \frac{-\ln(\tilde{\tau})}{L_{fab}} \tag{5.44}$$

where $\tilde{\tau}$ is the transmissivity of the fabric.

5.3.6. BOUNDARY CONDITIONS

The intensity of the flame is very high and the thermal conductivity of the air is small; therefore, it can be assumed that the convective and radiative heat fluxes at the outer surface of the garment are dominant and the conduction is negligibly small compared to those. Therefore, the boundary conditions at the outer surface of the garment are:

$$-k_{eff}\left.\frac{\partial T}{\partial x}\right|_{x=0} = q''_{conv,fl} + q''_{rad,fl} + h_{m,amb}(\rho_{v,amb} - \rho_v\big|_{x=0})\Delta h_{vap} \tag{5.45}$$

$$h_{m,amb}(\rho_{v,amb} - \rho_{v,x=0}) = -D_{eff}\left.\frac{\partial \rho_v}{\partial x}\right|_{x=0} \tag{5.46}$$

$$v_l\big|_{x=0} = 0 \tag{5.47}$$

where $T\big|_{x=0}$ is the temperature at the outer surface of the fabric, $q''_{conv,fl}$ is the convective heat flux from the flame to the outer surface of the fabric, $h_{m,amb}$ is the convective mass transfer coefficient of the water vapor between the outer fabric surface and the ambient, $\rho_v\big|_{x=0}$ is the density of water vapor at the outer surface of the fabric, $\rho_{v,amb}$ is the density of water vapor in the ambient, and $v_l\big|_{x=0}$ is the velocity of liquid water at the outer surface of the fabric.

The boundary conditions at the inner surface of the fabric are:

$$-k_{eff}\left.\frac{\partial T}{\partial x}\right|_{x=L_{fab}} = q''_{rad,airgap} + q''_{cond/conv,airgap} + h_{m,airgap}(\rho_v\big|_{x=L_{fab}} - \rho_{v,airgap})\Delta h_{vap} \tag{5.48}$$

$$h_{m,airgap}(\rho_{v,x=L_{fab}} - \rho_{v,airgap}) = -D_{eff}\left.\frac{\partial \rho_v}{\partial x}\right|_{x=L_{fab}} \tag{5.49}$$

$$v_l\big|_{x=L_{fab}} = 0 \tag{5.50}$$

where $T\big|_{x=L_{fab}}$ is the temperature at the inner surface of the fabric, $q''_{rad,airgap}$ is the heat flux by radiation from the fabric to the human skin across the air gap, $q''_{cond/conv,airgap}$ is the heat flux by conduction/convection from the fabric to the human skin across the air gap, $h_{m,airgap}$ is the convective mass transfer coefficient of the water vapor between the inner surface of the fabric and the air gap, $\rho_v\big|_{x=L_{fab}}$ is the density of water vapor at the outer surface of the fabric, $\rho_{v,airgap}$ is the density of the water vapor in the air gap, and $v_l\big|_{x=L_{fab}}$ is the velocity of liquid water at the inner surface of the fabric.

The boundary conditions for the human skin are

$$-k_{tiss}\left.\frac{\partial T}{\partial x}\right|_{x=L_{fab}+L_{airgap}} = q''_{rad,airgap} + q''_{cond/conv,airgap} \tag{5.51}$$

$$T\big|_{x=L_{fab}+L_{airgap}+L_{skin}} = T_{art} \tag{5.52}$$

where L_{airgap} is the thickness of the air gap and L_{skin} is the combined thickness of all three layers of the human skin.

The incident radiation heat flux coming from the flame to the fabric is found in Torvi [17] as:

$$q''_{rad,fl} = \sigma\,\widetilde{\varepsilon}_{fl}(T_{fl}^4 - T_{fab}^4\big|_{x=0}) - \sigma\,\widetilde{\varepsilon}_{fab}(1-\widetilde{\varepsilon}_{fl})(T_{fab}^4\big|_{x=0} - T_{amb}^4) \tag{5.53}$$

where σ is the Stefan-Boltzman constant, $\widetilde{\varepsilon}_{fl}$ is the emissivity of the flame, T_{fl} is the temperature of the flame, $\widetilde{\varepsilon}_{fab}$ is the emissivity of the fabric, and T_{amb} is the temperature of the ambient air.

The radiation and convection heat fluxes at the outer surface of the fabric can be calculated as:

$$q''_{conv,fl} + q''_{rad,fl} = h_{c,fl}(T_{fl} - T_{fab}\big|_{x=0}) \tag{5.54}$$

where $h_{c,fl}$ is the overall equivalent heat transfer coefficient between the flame and the outer surface of the fabric.

The heat flux by radiation from the inner surface of the fabric to the human skin across the air gap is given in Torvi [17] as:

$$q''_{rad,airgap} = \frac{\sigma\left({T_{fab}}^4\big|_{x=L_{fab}} - {T_{skin}}^4\big|_{x=L_{fab}+L_{airgap}} \right)}{\left(\frac{1}{\widetilde{\varepsilon}_{fab}} + \frac{1-\widetilde{\varepsilon}_{skin}}{\widetilde{\varepsilon}_{skin}} \right)} \tag{5.55}$$

where $T_{fab}\big|_{x=L_{fab}}$ is the temperature of the inner surface of the fabric, $T_{skin}\big|_{x=L_{fab}+L_{airgap}}$ is the temperature of the outer surface of the human skin, and $\widetilde{\varepsilon}_{skin}$ is the emissivity of the human skin.

The heat flux by conduction/convection from the inner fabric surface to the human skin across the air gap is given as:

$$q''_{cond/conv,airgap} = h_{c,airgap}(T_{fab}\big|_{x=L_{fab}} - T_{skin}\big|_{x=L_{fab}+L_{airgap}}) \tag{5.56}$$

where $h_{c,airgap}$ is the overall equivalent heat transfer coefficient due to conduction and natural convection in the air gap.

The convective heat transfer coefficient due to conduction and natural convection in the air gap can be found as:

$$h_{c,airgap} = Nu \frac{k_{airgap}}{L_{airgap}} \tag{5.57}$$

where Nu is the Nusselt number and k_{airgap} is the thermal conductivity of the air in the air gap.

The Nusselt number correlation for the air in a long vertical enclosure heated from one side is given by Catton [18] as:

$$Nu = \begin{cases} 1.0 & , Ra \le 1713 \\ 0.112 Ra^{0.294} & , Ra > 1713 \end{cases} \tag{5.58}$$

where Ra is the Rayleigh number, which is defined as:

$$Ra = \frac{g\beta_a L_{airgap}^3 \left[T_{fab}\big|_{x=L_{fab}} - T_{skin}\big|_{x=L_{fab}+L_{airgap}} \right]}{\alpha_a \nu_a} \tag{5.59}$$

where g is the gravitational acceleration, β_a is the thermal expansion coefficient of the air in the air gap, α_a is the thermal diffusivity of the air in the air gap, and ν_a is the kinematic viscosity of the air in the air gap.

5.4. NUMERICAL PROCEDURE

All numerical simulations are carried out using a finite-volume method (FVM). The Lower-Upper triangular matrix (LU) decomposition solver for a non-symmetric matrix is used in conjunction with the iterative scheme to solve the system of fully implicit finite difference equations. Due to non-linearities in this system, the underrelaxation procedure is utilized in order to avoid the divergence of the iterative method. The value of the underrelaxation parameter is 0.1. The solution procedure is as follows. All variables are known at the initial state, then the program marches forward in given time increments. The new values of

variables are computed by solving iteratively the system of the algebraic equations until the changes in all variables become smaller than the convergence criterion, which is set to 10^{-6}.

5.5. RESULTS AND DISCUSSION

The nominal thickness of the air gap in the thermal protective performance (TPP) test [19] for the firefighter garment is used in this study. Numerical values of thermo-physical and geometrical properties of the fabric are listed in Table 5-1. Numerical values of thermo-physical/geometrical properties of the human skin and blood, which are given by Torvi and Dale [10], are tabulated in Table 5-2. The radiation parameters, which are given by Torvi [17], are listed in Table 5-3. The initial parameters, the water-injection parameters, and the thermo-physical and geometrical properties of the flame, the ambient air, and the air gap are summarized in Table 5-4. The origination point of the x-axis is chosen at the outer surface of the garment, which is exposed to the flash fire and the ambient air (cf. Fig 5-1). The x-axis is directed towards the human skin. Accounting for the thickness of the fabric layers and the air gap, the epidermis skin layer begins at a distance of 0.0093 m from the outer surface of the garment.

Table 5-1 Thermo-physical and geometrical properties of the fabric

Property	Outer Shell: Kombat™ 7.5 oz/yd^2	Moisture Barrier: ComfortZone™	Thermal Liner: Aralite®	Refs.
ρ_f [kg m^{-3}]	1384	1295	1380	-
$(c_p)_f$ [J kg^{-1} K^{-1}]	1420	1325	1200	-
k_f [W m^{-1} K^{-1}]	0.179	0.144	0.130	-
L_{fab} [m]	0.56×10^{-3}	0.73×10^{-3}	1.66×10^{-3}	-
ε_f	0.334	0.186	0.115	-
$R_{f,\phi=0.65}$	0.084	0.038	0.045	-
τ	1.50	1.25	1.00	-
D_{b-f} [m^2 s^{-1}]	6.0×10^{-14}	6.0×10^{-14}	6.0×10^{-14}	[13]
d_f [m]	1.6×10^{-5}	1.6×10^{-5}	1.6×10^{-5}	[13]
a [Pa]	1.0×10^{4}	1.0×10^{4}	1.0×10^{4}	[12]
b	-0.61	-0.61	-0.61	[12]
$K_{l,sat}$ [m^2]	5.0×10^{-16}	5.0×10^{-16}	5.0×10^{-16}	[12]
s_{ir}	0.1	0.1	0.1	[12]
γ_{ls} [kg m^{-3}]	5.0×10^{-4}	5.0×10^{-4}	5.0×10^{-4}	[13]

Table 5-2 Thermo-physical/ geometrical properties of the human skin and blood

Property	Epidermis	Dermis	Subcutaneous	Blood
ρ [kg m^{-3}]	1200	1200	1000	1060
c_p [J kg^{-1} K^{-1}]	3600	3400	3060	3770
k [W m^{-1} K^{-1}]	0.255	0.523	0.167	-
L [m]	8×10^{-5}	2×10^{-3}	1×10^{-2}	-
ω_{blo} [m^3 s^{-1} m^{-3}]	-	-	-	1.25×10^{-3}
T_{art} [°C]	-	-	-	37.0
$T_{skin}\big\|_{x=L_{fab}+L_{airgap}}$ [°C]	34.0	-	-	-

Table 5-3 Radiation parameters

Property	Fabric	Flame	Skin
$\tilde{\varepsilon}$	0.9	0.02	0.94
$\tilde{\tau}$	0.01	-	-

Table 5-4 The initial parameters, the water-injection parameters and the thermo-physical and geometrical properties of the flame, the ambient air, and the air gap

$T_{fab,0}$ [°C]	40.0
$\phi_{fab,0}$	0.65
s_0	0.01
$\phi_{airgap,0}$	0.65
ϕ_{amb}	0.65
T_{fl} [°C]	1000.0
T_{amb} [°C]	30.0
$h_{c,fl}$ [W m^{-2} K^{-1}]	120.0
$h_{m,amb}$ [m s^{-1}]	1.2
L_{airgap} [m]	6.35×10^{-3}
$p_{g,0}$ [N m^{-2}]	1.01325×10^{5}
h_c [W m^{-2} K^{-1}]	2.88
T_{act} [°C]	50.0
$\dot{m}_{inject}$ [kg m^{-3} s^{-1}]	20.0

When the temperature rises above the activation temperature, the water-injection system is activated by the temperature sensor to uniformly inject water into the outer layer of the garment. Because of the cooling that results from evaporation of the injected water, the intelligent thermal protective garment system can potentially lead to a significant improvement in the thermal protective performance during an intense heat exposure by limiting the temperature rise in the outer fabric layer. However, there is one potential danger that can lead to a worsening of the protective performance. The injected water, which evaporates during the flash fire exposure, may diffuse and/or convect from the outer fabric layer to the inner fabric layer due to a high temperature gradient in the fabric, which may result in a temperature rise in the inner fabric layer and at the skin surface. One way of solving this problem is using a moisture barrier between the outer and inner layers of the

fabric, which has a low permeability to the vapor phase. Also, in order to improve the thermal protective performance, the rate of water injection and the activation temperature must be carefully determined for each specific garment. Figure 5-3 illustrates the influence of the rate of water injection and the activation temperature. The details of the method used to compute the maximum durations of the flash fire exposure before getting a 2nd degree burn is given in Chitrphiromsri and Kuznetsov [7]. For the case considered in this paper, in which the initial volumetric content of the liquid water in the fabric is 1% (with respect to the volume of the voids in the fabric) and the flame temperature is 1000°C, the best protective performance is obtained by choosing the rate of the water injection equal to or greater than 20.0 kg/m^3·s and the activation temperature equal to or less than 100°C. Figure 5-3 shows that by using water injection, it is possible to increase the duration of flash fire exposure before getting a 2nd degree burn from approximately 23 seconds (without the water injection) to almost 32 seconds (the curve corresponding to the activation temperature of 50°C and the water injection rate of 20 $\mathrm{kg\,m^{-3}s^{-1}}$, which is almost a 40% improvement of performance.

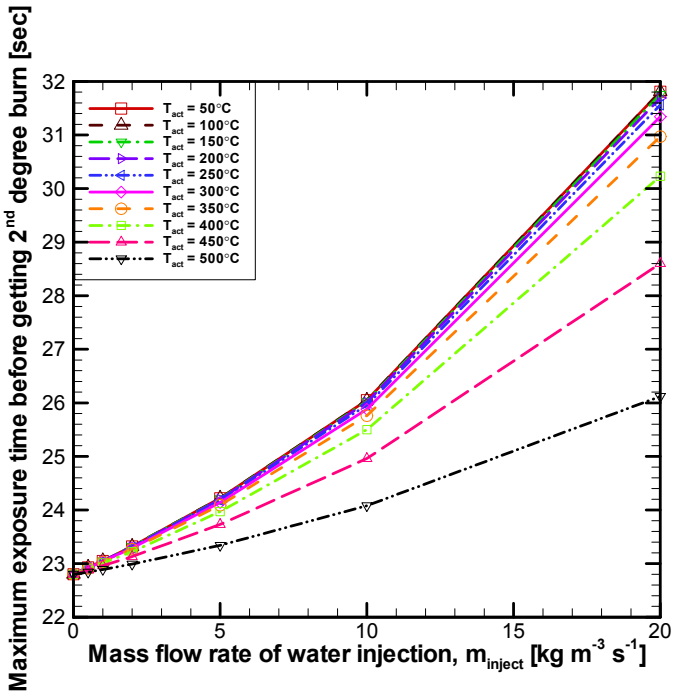

Figure 5-3 Plots of the maximum durations of the flash fire exposure before getting 2nd degree burns versus the rates of water injection at different activation temperatures

To get better insight into the mechanisms by which the intelligent thermal protective system improves the performance of the garment, transport phenomena in the garment with the water injection system are investigated for the duration of the flash fire exposure of 4 seconds. The total duration of computations is 60 seconds, which accounts for both burning (4 seconds) and cool-down (56 seconds) periods of the process. Figure 5-4(a) shows temperature distributions in the garment at different moments of time. Temperature distributions in the human skin at different moments of time are displayed in Figure 5-4(b). The fabric temperature rises rapidly in the outer layer during the flash fire exposure. Even when the fire is off, the skin temperature keeps raising because of the energy accumulated within the fabric and the air gap during the exposure. This may cause tissue damage even after the 4 seconds of the flash fire exposure.

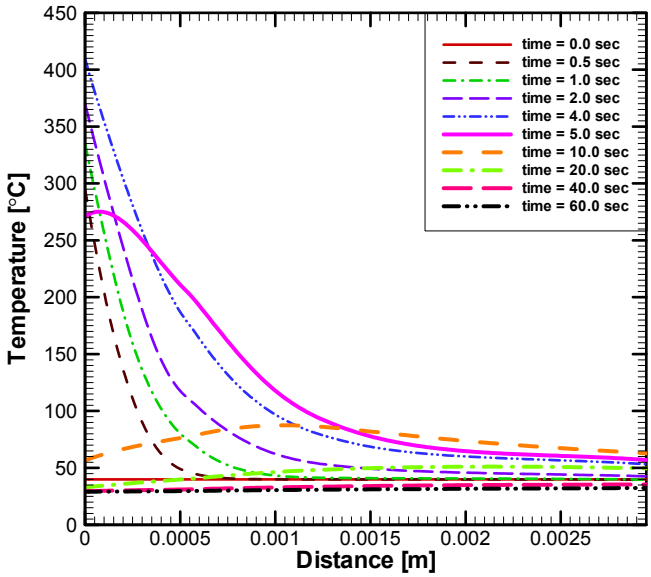

(a)

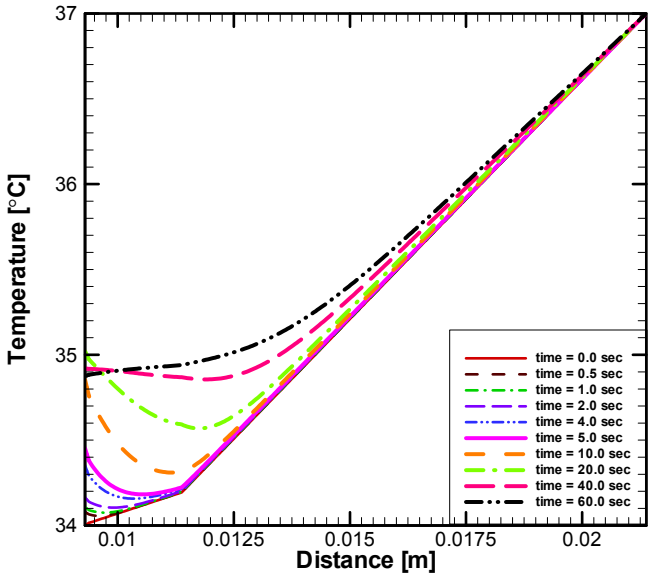

(b)

Figure 5-4 (a) Temperature distributions in the fabric at different moments of time, (b) Temperature distributions in the human skin and tissue at different moments of time

Figures 5-5 and 5-6 illustrate the basic mechanisms of moisture transport and phase change during the flash fire exposure and cool-down periods. Figures 5-5(a), (b), and (c) show distributions of the volume fraction of the bound water, free liquid, and gas phase in the garment at different moments of time, respectively.

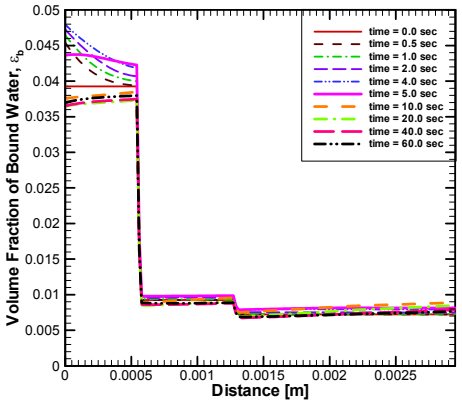

(a)

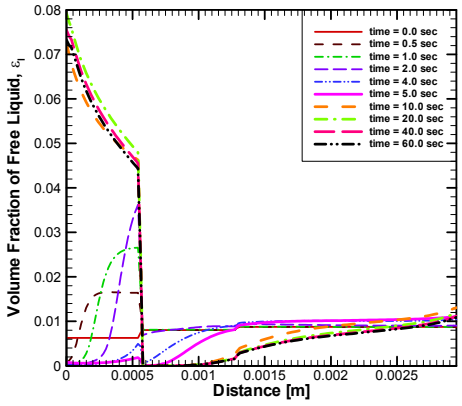

(b)

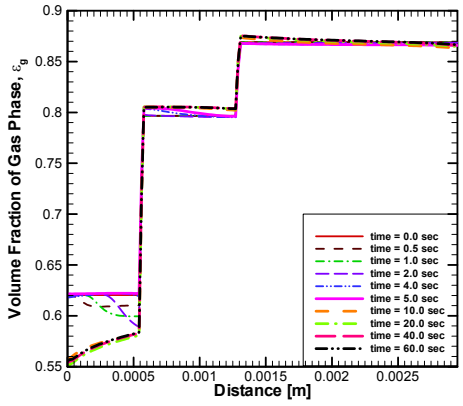

(c)

Figure 5-5 (a) Distributions of the volume fraction of the bound water in the fabric at different moments of time, (b) Distributions of the volume fraction of the free liquid water in the fabric at different moments of time, (c) Distributions of the volume fraction of the gas phase in the fabric at different moments of time

Figure 5-6(a) displays the distribution of the vapor density in the fabric at different moments of time. Figure 5-6(b) shows the distribution of the relative humidity of the gas phase in the fabric at different moments of time. Figure 5-6(c) shows the distribution of the fiber regain in the fabric at different moments of time, which depends on the relative humidity and the sorption capacity of the fiber. Figure 5-6(d) displays the saturation of the pores by the liquid water in the fabric at different moments of time. The volume fractions of the bound water and free liquid water in the outer shell increase during the flash fire exposure because of the water injected in the outer shell; however, those in the moisture barrier and thermal liner decrease because the temperature rise causes the desorption and evaporation of the moisture which initially was present in the fabric as a bound and free liquid water, respectively. Consequently, the volume fraction of the gas phase in the outer shell decreases but that in the latter fabric layers increases. Moreover, the vapor density also increases because of that. The relative humidity in the outer layer of the garment drops very fast when it is exposed to the flash fire. Therefore, the moisture in the outer fabric layer evaporates very fast during the exposure. As the vapor density increases, the relative humidity in the inner layer of the garment increases and becomes close to saturation. The fabric is assumed to be in the thermal and phase equilibrium at the initial state. During the fire exposure, the decrease of relative humidity in the outer fabric layer causes a decrease of fiber regain in the outer fabric layer; however, the behavior of relative humidity and fiber regain is opposite to that in the inner fabric layer. The saturation of the free liquid is defined as the ratio of the volume occupied by the liquid water to the total volume of the voids in the control volume. The temperature gradient and the capillary pressure force the free water to migrate. Therefore, the saturation of the free water has the same behavior as the volume fraction of the free liquid.

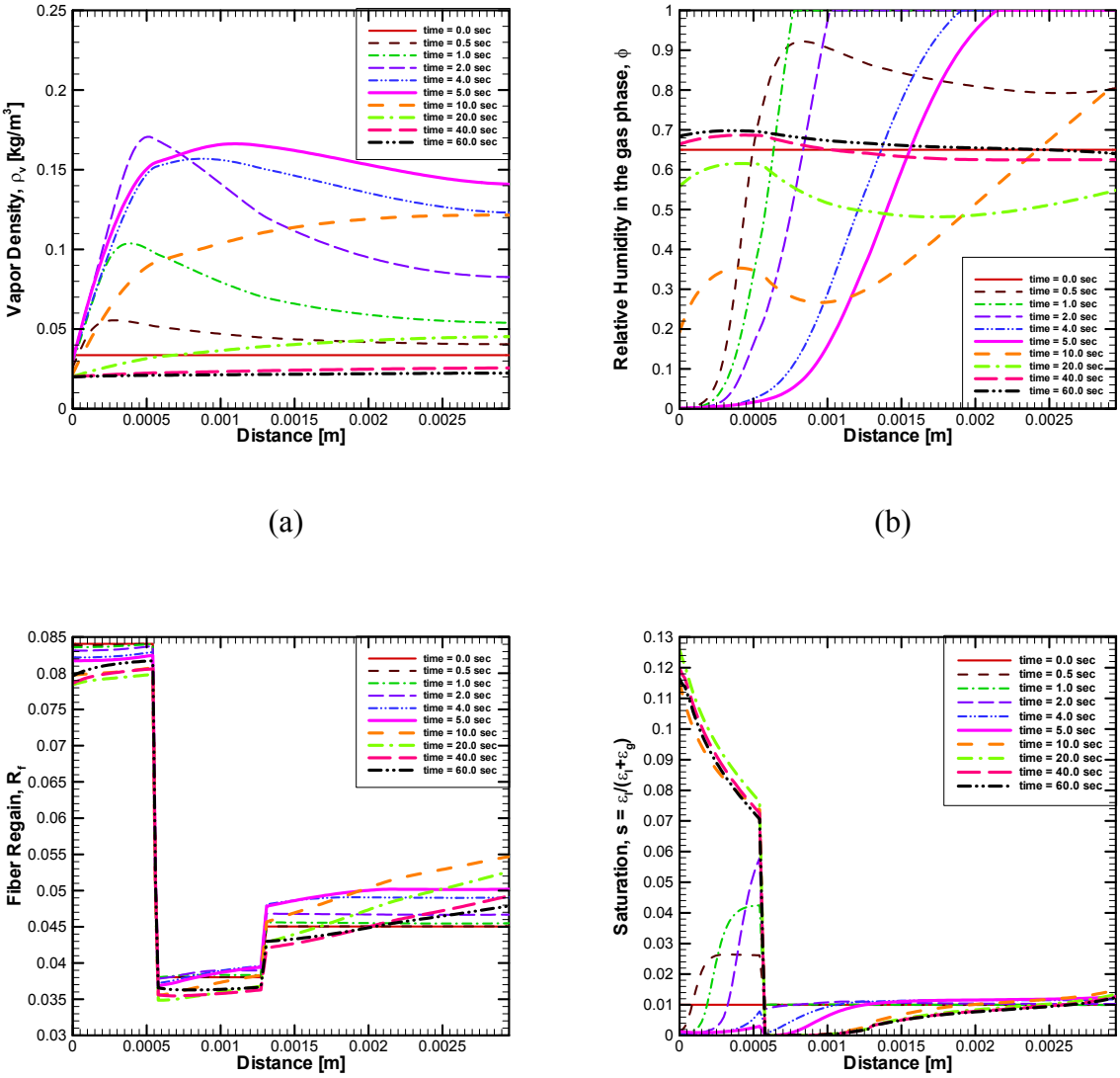

(a) (b)

(c) (d)

Figure 5-6 (a) Distributions of the vapor density in the fabric at different moments of time, (b) Distributions of the relative humidity in the fabric at different moments of time, (c) Distributions of the fiber regain in the fabric at different moments of time, (d) Distributions of the saturation of the free liquid water in the fabric at different moments of time

The effective volumetric heat capacity of the fabric is shown in Figure 5-7(a). Figure 5-7(b) shows the effective thermal conductivity of the fabric. These parameters represent the energy absorbed by the fabric and the thermal insulation/conduction of the fabric, respectively. The effective volumetric heat capacity of the fabric decreases because the amounts of the free liquid and bound water become small. Because of the injection of the liquid water in the outer fabric layer, the effective thermal conductivity of the fabric increases during the flash fire exposure, and this results in worsening the insulation properties of the fabric. On the other hand, evaporation of the water from the outer surface of the fabric results in cooling, which positively impacts the protective behavior of the garment. This means that the amount of the injected water must be selected very carefully; if the system injects more water than the amount that can evaporate from the outer fabric surface, the moisture content in the outer fabric layer will increase and the protective performance of the garment will get worse.

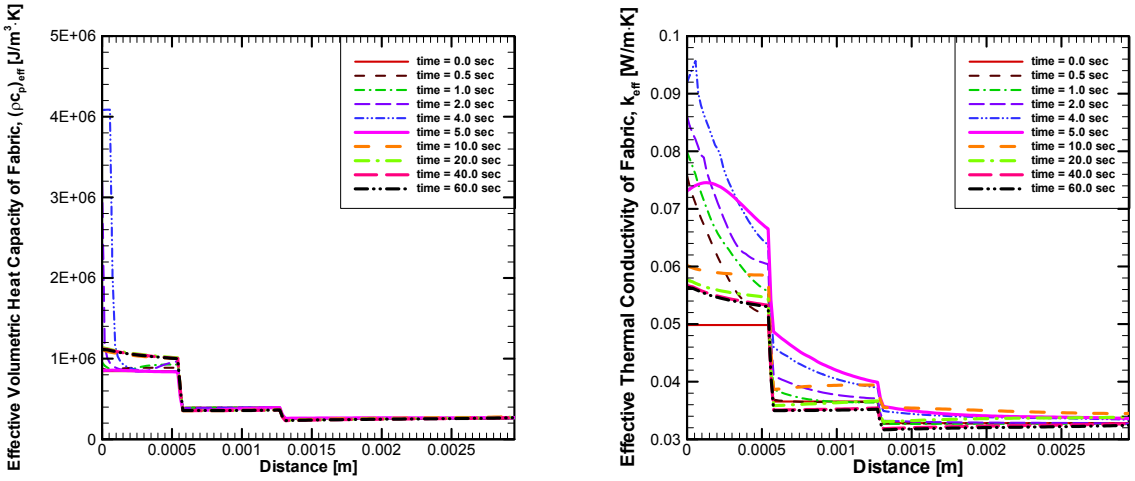

(a) (b)

Figure 5-7 (a) Distributions of the effective volumetric capacity of the fabric at different moments of time, (b) Distributions of the effective thermal conductivity of the fabric at different moments of time

Figure 5-8 shows the calculated fabric weight per unit area, vapor density in the air gap, and relative humidity in the air gap versus time. This figure shows that the garment gains moisture from the water-injection and then loses moisture, which vaporizes into the air gap. First, the amount moisture in the air gap increases until its density becomes close to saturation, and then it decreases during the cool-down period, as the temperature and pressure decrease.

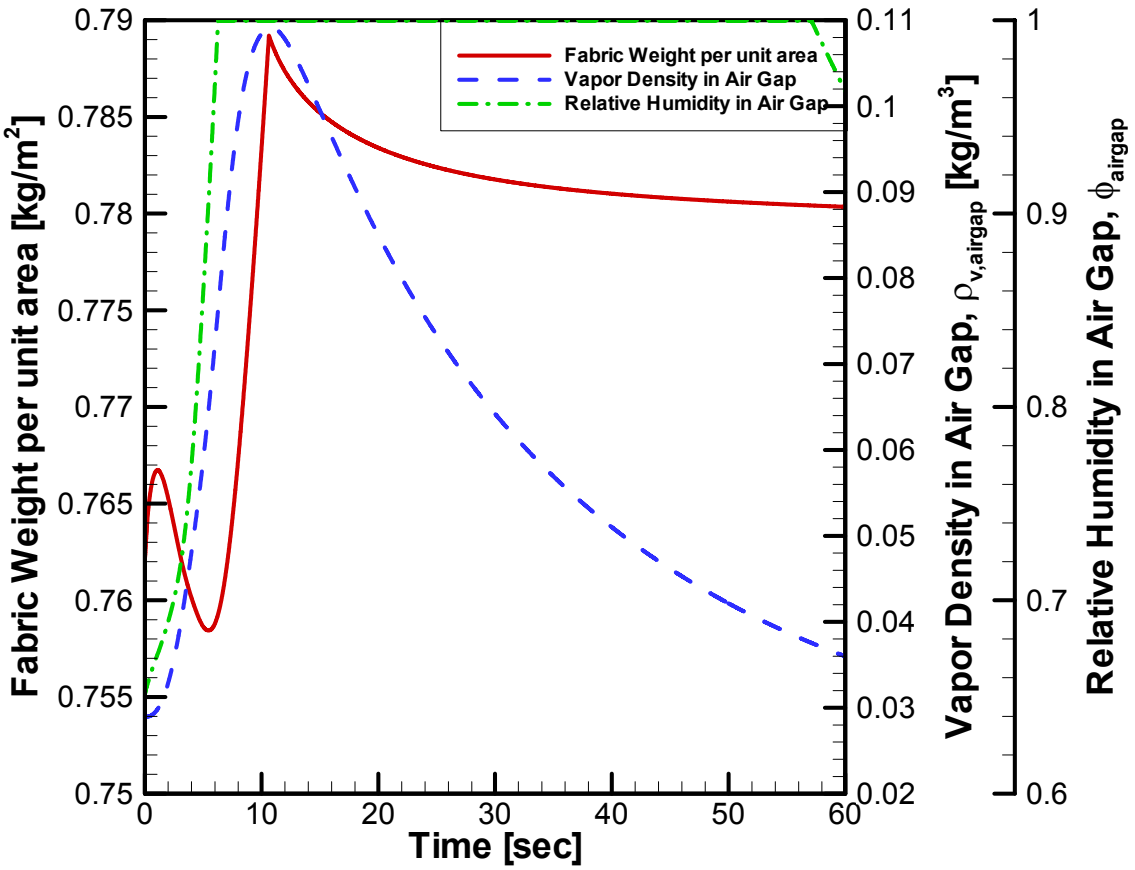

Figure 5-8 Calculated fabric weight per unit area, vapor density in the air gap, and relative humidity in the air gap versus time

5.6. CONCLUSIONS

A numerical investigation of an intelligent firefighter protective garment that incorporates a water-injection system is performed. This intelligent thermal protective garment system shows a potential for significant improvement in the thermal insulation under the intense heat exposure by limiting the temperature rise in the outer layer of the fabric and the total heat flux to the skin. However, in order to optimize the performance of this innovative garment system, the activation temperature and the amount of injected water must be carefully considered for any specific fabric and exposure conditions.

ACKNOWLEDGEMENTS

This work was supported by a grant from the National Textile Center, University Research Consortium, project F01-NS50.

REFERENCES

1 K. E. Kaska and M. M. Chen, "Improvement of the performance of solar energy of waste heat utilization systems using phase change slurry as enhanced heat transfer storage fluid", *J. Solar Energy Eng.*, vol. 107, pp. 229-236, 1985.

2 D. P. Colvin and J. C. Mulligan, "Microencapsulated phase change materials for storage of heat", *NASA Tech Briefs*, July, 1989.

3 D. P. Colvin and Y. G. Bryant, "Protective clothing containing encapsulated phase change materials", *ASME-IMECE, HTD-Vol. 362, BED-Vol. 40*, pp. 123-132, 1998.

4 D. P. Colvin, L. J. Hayes, Y. G. Bryant, and D. R. Myers, "Thermal analysis of PCM cooling garments", *ASME HTD-Vol. 268, Advances in Bioheat and Mass Transfer*, 1993.

5 B. H. Pause, "New heat protective garment with phase change material", *Performance of Protective Clothing: Issues and Priorities for the 21st Century: Seventh Volume, ASTM STP 1386*, 2000.

6 L. J. Hayes, E. H. Wissler, and D. P. Colvin, "A model for encapsulated phase change material in a conductive media", Paper Number: a0162626, *Cell and Tissue Engineering V: Heat and Mass Transfer, Bioengineering Conference*, Big Sky, MT, June 16-20, 1999.

7 P. Chitrphiromsri and A. V. Kuznetsov, "Modeling heat and moisture transport in firefighter protective clothing during flash fire exposure", *Heat and Mass Transfer*, accepted for publication, 2004.

8 P. Chitrphiromsri and A. V. Kuznetsov, "A Porous medium model for investigating transient heat and moisture transport in firefighter protective clothing under high intensity thermal exposure", *J. Porous Media*, accepted for publication, 2004.

9 H. H. Pennes, "Analysis of tissue and arterial blood temperatures in resting human forearm", *J. Applied Physiology*, vol. 1, pp. 93-122, 1948.

10 D. A. Torvi and J. D. Dale, "A finite element model of skin subjected to flash fire", *J. Biomech. Eng.*, vol. 116, pp. 250-256, 1994.

11 S. Whitaker, *The Method of Volume Averaging, (Theories and Applications of Transport in Porous Media, Vol. 13)*, Kluwer Academic Publishers, Dordrecht, 1999.

12 P. W. Gibson, "Multiphase heat and mass transfer through hygroscopic porous media with applications to clothing materials", *Technical Report Natick/TR-97/005*, U.S. Army Natick Research, Development, and Engineering Center, Natick, MA, 1996.

13 C. V. Le, N. G. Ly, and R. Postle "Heat and moisture transfer in textile assemblies, Part I: Steaming of wool, cotton, nylon, and polyester fabric beds", *Textile Res. J.*, vol. 65 (4), pp. 203-212, 1995.

14 P. C. Carman, *Flow of Gases through Porous Media*, Academic Press, New York, NY, 1956.

15 R. P. Labrecque, "An investigation of the effects of fibre cross sectional shape on the resistance to the flow of fluids through fibre mats", *Ph.D. Thesis, Lawrence University*, Appleton, WI, 1967.

16 E. L. Cussler, *Diffusion Mass Transfer in Fluid Systems*, 2nd Ed., Cambridge University Press, Cambridge, MA, 1997.

17 D. A. Torvi, "Heat transfer in thin fibrous materials under high heat flux conditions", *Ph.D. Thesis, University of Alberta*, Edmonton, Alberta, Canada, 1997.

18 I. Catton, "Natural convection in enclosures", *Proceeding of the 6th International Heat Transfer Conference*, Toronto, vol. 6, pp. 13-31, 1978.

19 American Society for Testing and Materials, *ASTM D 4108-87, Standard Test Method for Thermal Protective Performance of Materials for Clothing by Open-Flame Method*, West Conshohocken, PA, 1987.

6. CONCLUSIONS

Prediction of protective garment performance in preventing and minimizing tissue burns from the incident radiant and convection heat flux is investigated. Intense heat exposure induces fundamental changes in fabric thermal properties that produce nonlinear thermal characteristics. A model that predicts the thermal protective performance of the protective garments in the intense heat exposures is developed by taking into account the effects of the complex nonlinear dynamic changes in the thermal properties of the garment to simulate the basic mechanism of the transient heat transfer through the protective clothing, air gap, and human skin in the intense thermal environments.

6.1. REMARKS ON HEAT TRANSFER MODEL

The basic heat transfer through the fabric, air gap, and skin is modeled in Chapter 2. This model incorporates characteristics of the simulated flash fire generated in the Pyroman® chamber (which are the flame temperature and heat transfer coefficient between the flame and the fabric) and the heat induced changes in fabric thermo-physical properties (which are the density, specific heat, and thermal conductivity). In addition, the air gap distribution between the manikin body and protective garment is obtained by using three-dimensional body scanning technology to superimpose the data between a dressed manikin and an undressed manikin. The model is validated using an instrumented manikin fire test system. The model is capable of predicting heat transfer through protective clothing and resulting human skin damages in flash fire conditions with a good accuracy.

6.2. REMARKS ON HEAT AND MOISTURE TRANSPORT MODEL (BOUND WATER)

The effect of coupled heat and moisture transport on the protective performance of the garment under the high intense heat exposure is investigated numerically in Chapter 3. The model prediction is in good agreement with experimental data of a multi-layer protective garment subjected to a high intensity flash fire exposure in Thermal Protective Performance (TPP), ASTM D 4108-87, test configuration. Moreover, the duration of exposure during which the garment protects the firefighter from getting the second and third degree burns from the flash fire exposure is also predicted.

6.3. REMARKS ON HEAT AND MOISTURE TRANSPORT MODEL (FREE WATER)

The comprehensive model for accounting for all possible phases of moisture in the multi-layer fabric assemblies during the flash fire exposure is developed in Chapter 4. This model accounts for changes in thermal-physical and transport properties of fabric due to the presence of moisture. The energy associated with the phase change of the moisture such as evaporation, condensation, desorption, and absorption plays the important factor in thermal protective performance of the firefighter garment. Consequently, the temperature and the total heat flux to skin are significantly influenced by the amount of moisture and the distribution of the moisture in the protective clothing. Wet fabrics normally can absorb more heat than dry fabrics. However, if the right amount of free water is introduced to the fabric, and this free water continuously evaporates from the outer surface of the fabric during the heat exposure. This evaporation can create cooling effect sufficient to protect the firefighter from the flash fire exposure. Additionally, at different locations on the human body, the

maximum durations of flash fire exposure before getting second and third degree burns can also be predicted for various amounts of the free liquid water in the fabric.

6.4. REMARKS ON HEAT AND MOISTURE TRANSPORT MODEL (INJECTED WATER)

Feasibility of developing intelligent firefighter protective garments based on the utilization of a water-injection system is investigated in Chapter 5. The outer layer of this innovative garment is injected with water through a capillary net of thin perforated tubes. The injection process can be activated by a temperature sensor embedded in the outer layer of the garment. This intelligent garment will absorb a significant amount of the incident heat flux due to evaporation of the injected water, thus limiting the temperature rise in the outer layer of the garment and the total heat flux to the firefighter's skin. Therefore, this novel thermal protective garment system shows significant improvement in the thermal insulation under the intense heat exposure. However, there is one potential danger that can lead to worsening of the protective performance. The injected water, which evaporates during the flash fire exposure, may diffuse and/or convect from the outer fabric layer to the inner fabric layer due to a high temperature gradient in the fabric. This happens if the amount of free liquid water injected to the garment exceeds the amount of water vapor at the outer surface of the garment that can convect to the ambient. This may result in a temperature rise in the inner fabric layer and at the skin surface. One way of lessening this problem is using a moisture barrier between the outer and inner layers of the fabric, which has a low permeability to the vapor phase. Also, in order to improve the thermal protective performance, the activation

temperature and necessary amount of the injected water must be carefully considered for any specific garment and exposure conditions.

6.5. RECOMMENDATIONS FOR FUTURE WORK

The validation of modeling of heat and moisture transport (free liquid water) is interesting to investigate. It is also interesting to design and test an intelligent protective garment with the water injection system, in which the temperature sensor and the capillary net of the perforated tubes are embedded into the outer layer of the garment. Finally, the alternative non-toxic medium for absorbing the incident heat, which has lighter weight, higher specific heat and lower heat conductivity than the water, is very interesting to investigate.